OC6 Phase II: Verification of an Advanced Soil-Structure Interaction Model for Offshore Wind Turbines

Journal:	*Wind Energy*
Manuscript ID	WE-21-0062.R2
Wiley - Manuscript type:	Research Article
Date Submitted by the Author:	12-Oct-2021
Complete List of Authors:	Bergua Archeli, Roger; National Renewable Energy Laboratory, Robertson, Amy; National Renewable Energy Laboratory, Jonkman, Jason; NREL, NWTC; Platt, Andy; National Renewable Energy Laboratory Page, Ana; Norwegian Geotechnical Institute Qvist, Jacob; 4Subsea Amet, Ervin; Bureau Veritas Group Cai, Zhisong; China General Certification Huali, Han; CSIC Haizhuang Windpower Co., Ltd. Beardsell, Alec; DNV GL Shi, Wei; Dalian University of Technology Galván, Josean; eureka! Bachynski, Erin E.; Norwegian University of Science and Technology, Marine Technology McKinnon, Gill; Orcina Harnois, Violette; PRINCIPIA Bonnet, Paul; Siemens Industry Software Suja-Thauvin, Loup; Simis AS Melchior Hansen, Anders; DTU Mendikoa Alonso, Iñigo; TECNALIA Research & Innovation Aristondo, Ander; TECNALIA Research & Innovation Battistella, Tommaso; Universidad de Cantabria Guanche, Raúl; Universidad de Cantabria, Instituto de Hidráulica Ambiental de Cantabria Schünemann, Paul; Universität Rostock Fakultät für Maschinenbau und Schiffstechnik Thanh Dam, Pham; University of Ulsan Trubat, Pau; Universitat Politècnica de Catalunya Alarcón, Daniel; Universitat Politècnica de Catalunya Haudin, Florence; Vulcain Engineering Nguyen, Minh Quan ; Vulcain Engineering Goveas, Akhilesh; WyndTek BV
Keywords:	Offshore wind, monopile, soil-structure interaction, macro-element, hysteretic damping, OC6

OC6 Phase II: Verification of an Advanced Soil-Structure Interaction Model for Offshore Wind Turbines

Roger Bergua,* ***Amy Robertson***, ***Jason Jonkman***, ***Andy Platt***—National Renewable Energy Laboratory, United States
Ana Page—Norwegian Geotechnical Institute**,** Norway
Jacob Qvist—4Subsea**,** Norway
Ervin Amet—Bureau Veritas, France
Zhisong Cai—China General Certification Center, China
Han Huali—CSIC Haizhuang Windpower Co., Ltd., China
Alec Beardsell—DNV GL, United Kingdom
Wei Shi—Dalian University of Technology, China
Josean Galván—eureka!, Spain
Erin Bachynski-Polić—Norwegian University of Science and Technology, Norway
Gill McKinnon—Orcina, United Kingdom
Violette Harnois—PRINCIPIA, France
Paul Bonnet—Siemens Industry Software, Spain
Loup Suja-Thauvin—Simis AS, Norway
Anders Melchior Hansen—Technical University of Denmark, Denmark
Iñigo Mendikoa Alonso, Ander Aristondo—Tecnalia, Spain
Tommaso Battistella, Raúl Guanche—Universidad de Cantabria, Spain
Paul Schünemann—University of Rostock, Germany
Pham Thanh Dam—University of Ulsan, Korea
Pau Trubat, Daniel Alarcón—Universitat Politècnica de Catalunya, Spain
Florence Haudin, Minh Quan Nguyen—Vulcain Engineering, France
Akhilesh Goveas—WyndTek, The Netherlands

*Corresponding author. E-mail address: roger.bergua@nrel.gov
Tel: +1-303-384-7960
15013 Denver West Parkway, Golden, CO 80401, United States.

Abstract

This paper provides a summary of the work done within the OC6 Phase II project, which was focused on the implementation and verification of an advanced soil-structure interaction model for offshore wind system design and analysis. The soil-structure interaction model comes from the REDWIN project, and uses an elasto-plastic, macro-element model with kinematic hardening, which captures the stiffness and damping characteristics of offshore wind foundations more accurately than more traditional and simplified soil-structure interaction modeling approaches. Participants in the OC6 project integrated this macro-element capability to coupled aero-hydro-servo-elastic offshore wind turbine modeling tools and verified the implementation by comparing simulation results across the modeling tools for an example monopile design. The simulation results were also compared to more traditional soil-structure interaction modeling approaches like apparent fixity, coupled springs, and distributed springs models. The macro-element approach resulted in smaller overall loading in the system due to both shifts in the system frequencies and increased energy dissipation. No validation work was performed, but the macro-element approach has shown increased accuracy within the REDWIN project, resulting in decreased uncertainty in

the design. For the monopile design investigated here, that implies a less conservative and thus more cost-effective offshore wind design.

Keywords

Offshore wind, monopile, soil-structure interaction, macro-element, hysteretic damping, OC6

1 Introduction

As the wind industry moves to increasingly larger offshore wind turbines (OWTs) to lower cost, the associated support structures must similarly increase in size. One of the main challenges in designing fixed-bottom systems with large support structures is accurately representing the soil-structure interaction (SSI). The soil reaction is dependent on the foundation movement, and the foundation movement is dependent on the soil reaction. Thus, the SSI directly affects the dynamic response of the OWT system.

The foundation models traditionally used in integrated analysis of OWTs are simplistic and based on several assumptions. Most engineering tools model the foundation according to one of the following approaches: apparent fixity (AF), coupled springs (CS), or distributed springs (DS). The Norwegian Geotechnical Institute (NGI) has developed new macro-element models [1] for the soil-structure interaction in offshore wind turbines that address some of the limitations in these previous models, allowing for a more accurate assessment of the dynamic response for OWTs. This development was done as part of the REDWIN (REDucing cost of offshore WINd by integrated structural and geotechnical design) project [1].

The OC6 (Offshore Code Comparison Collaboration, Continued, with Correlation and unCertainty) Phase II project focuses on integrating the new REDWIN SSI modeling capability into coupled aero-hydro-servo-elastic modeling tools used to design offshore wind systems and verifying the new capability. OC6 is part of an ongoing effort under Wind Task 30 of the International Energy Agency (IEA) to verify and validate OWT modeling tools, which originated back in 2005 with the foundational OC3 project (Offshore Code Comparison Collaboration). In the current extension, OC6 is focused on examining specific physical phenomena that are not well represented in present modeling approaches and have a significant impact on their ability to accurately represent OWT loads and performance.

To verify the integration of the new REDWIN SSI capability, participants in OC6 Phase II modeled a monopile offshore wind system examined in the WAS-XL (Wave loads And Soil support for eXtra Large monopiles) project [2]; ran a series of simulations, including wind and wave loading; and compared the resulting system loads across different modeling tools. The resulting system loads were also compared to more traditional SSI modeling approaches to assess the level of difference that the macro-element modeling approach has on the global loads of the system. This paper summarizes the work of the OC6 Phase II project, including findings on the improvements the REDWIN model provides.

The organization of the remainder of the paper is as follows. Section 2 summarizes the different soil-structure interaction models considered in the project, including the new REDWIN model. Section 3 provides a definition of the example model that was used to verify the implementation of the new SSI modeling capability. Section 4 provides a description of the active participants

involved in OC6 Phase II and the modeling approach used. Section 5 then summarizes the load cases that were performed for the verification study. Finally, Sections 6 and 7 provide some example results from the project and the conclusions drawn.

The modeling information and simulation results from this project will be made available to the public by the end of 2021 through the U.S. Department of Energy Data Archive and Portal, https://a2e.energy.gov/projects/oc6.

2 Soil-Structure Interaction Models

In this section, an overview of the traditional methods for modeling SSI is given, and then the new REDWIN modeling capability is introduced.

2.1 Traditional Methods

The traditional approaches presently used within the offshore wind industry to model SSI rely on the AF, CS, or DS methods. The AF method assumes that the substructure is fixed (cantilevered, without surrounding soil) at a depth below the original seabed, with a fixity depth and beam properties determined such that it matches the same lateral displacement and rotation at the seabed as the one resulting from the pile embedded in the true soil profile. The fixity depth and beam properties are dependent on the beam theory used (e.g., Euler-Bernoulli or Timoshenko). However, due to the nonlinear nature of the actual foundation, the response can only be identical under a particular set of conditions. The damping properties of the beams used in the AF method can also be modified to account for the energy dissipation provided by the soil-structure interaction. Using the same structural damping as for the substructure may result in an underestimation of the fatigue lifetime.

The CS approach replaces the soil with one linear stiffness matrix located at the seabed that accounts for the six rigid-body degrees of freedom (DOFs) (or fewer) of the base of the monopile. This approach can reproduce the same results as the AF model and can be extended with a viscous damping matrix to account for the energy dissipated by the foundation.

The DS approach is the most sophisticated of the three approaches and can be considered the current practice in the wind industry to model soil-pile interaction. This approach was originally developed by the oil and gas industry and it is recommended in many offshore design standards (e.g., Det Norske Veritas (DNV) [3] and the American Petroleum Institute (API) [4]). The method is based on the Winkler modeling approach. It employs uncoupled nonlinear springs represented by *p*-*y* curves to support the pile along the embedded depth. These springs relate the local lateral soil resistance (p) to the local lateral displacement of the pile (y). This relationship is commonly specified as semiempirical functions based on experimental tests. This approach characterizes four monopile DOFs (radial and bending directions). The vertical and torsional DOFs are usually fixed at the monopile base. It is also possible to add *t*-*z* curves in the vertical direction and torsional springs to define the six DOFs. Dashpot elements in parallel with the springs could be included to account for the foundation damping. This method was originally intended for static analysis, where the foundation response can be captured reasonably well with a nonlinear elastic curve, although the offshore wind industry takes advantage of the approach to perform dynamic analysis in situations where elastic models might not accurately capture the foundation response.

2.2 REDWIN Macro-Element

The primary objective of the REDWIN project [1] was to develop soil-foundation models that better account for key geotechnical issues such as stiffness, damping, drainage, and degradation. Three soil-foundation models were developed. The models cover the most common foundation types for OWTs and are intended to be used in integrated time-domain simulation tools, where the wind turbine structure itself is the main focus of the analysis.

REDWIN model 1 was developed primarily for piles that are intended to be analyzed by the traditional *p-y* approach. It can be used to model the distributed soil response along a monopile structure, a piled jacket, or the lumped response of a caisson foundation. REDWIN model 2 is a single macro-element intended for monopile foundations. The third model, REDWIN model 3, is a macro-element developed for shallow foundations such as gravity-based and caisson foundations (e.g., for suction bucket jackets).

OC6 Phase II focuses on verifying implementation of the REDWIN capability in participant modeling tools by investigating REDWIN model 2 to describe the response of a pile foundation supporting a monopile-based OWT. The REDWIN model 2 is an elasto-plastic macro-element model with kinematic hardening formulated within the multi-surface plasticity framework [5]. It reduces the foundation and surrounding soil to a set of linear and nonlinear load-displacement relationships in the six DOFs of the interface point (the seabed), separating the foundation and the rest of the structure (see Figure 1). It can represent the nonlinear hysteretic load-displacement response observed in experimental tests and in the field, including the coupled response between horizontal loads and bending moments. The model has been demonstrated to give good agreement with results from finite element analyses of the soil and monopile, results from large-scale pile tests, and results from full-scale field measurements of an OWT installed in the North Sea [5–7].

Aero-hydro-servo-elastic simulation tools are used during the design and certification of wind turbines [8]. During this process, thousands of load cases must be computed and analyzed. This requires these tools to be computationally efficient. In general, these simulation tools use relatively few DOFs, taking advantage of a combined modal and multibody dynamics formulation. Modeling the SSI in the time domain with a 3D finite-element model would require thousands of additional DOFs, which would substantially increase the simulation time of the aero-elastic solver. The REDWIN approach is a CPU efficient way to couple the SSI capability into these tools, using as few degrees of freedom as possible [1], leading to a minimal increase in computational time while providing higher fidelity than the traditional methods (AF, CS, or DS). The macro-element communicates with the wind turbine model through a DLL [dynamic link library] in a Windows environment or through a shared object in a Linux environment. In each calculation step, the OWT simulation tool provides the displacements and rotations at the seabed to the foundation model, which transfers back the computed forces and moments. The soil-foundation model is solved following an explicit integration algorithm with correction. The model also includes a sub-stepping algorithm, which should help the convergence when the input displacement and/or rotation increment is large.

The macro-element allows for an accurate representation of the foundation stiffness and hysteretic damping (see Figure 2) crucial to performing reliable fatigue analysis. It is important to note that aerodynamic damping provides the highest contribution to the overall system damping in the fore-aft direction when the wind turbine is operating, but the aerodynamic damping importance

decreases in idling and wind-wave misalignment situations, resulting in increased importance of soil damping [9,10].

Figure 2 illustrates how the macro-element model provides different stiffness values during loading (segment O-A-B and B-D), unloading (segment B-C and D-E), and reloading (segment C-B) conditions, as observed in pile tests [12]. The area of the loops described by the load-displacement trajectories is indicative of the energy dissipated. It is important to note that the macro-element provides foundation stiffness and energy dissipation independently of the applied loading frequency. The remaining displacement after the cycling loading (distance O-E) is due to the plastic nature of the system.

REDWIN model 2 requires two inputs from the user from which the macro-element behavior is derived: (1) the coefficients of the elastic stiffness matrix at the seabed, and (2) two load-displacement curves at the seabed from a nonlinear pushover analysis. In addition, a few numerical parameters must be specified. In OC6 Phase II, this information was supplied to the participants [13].

3 Verification Model Definition

To verify the integration of the REDWIN SSI approach into coupled OWT modeling tools, an example offshore wind system was modeled from the WAS-XL project [2]. WAS-XL is a project funded by the Norwegian Research Council that aims to reduce the uncertainties in large-diameter monopile design by improving hydrodynamic models for critical design loads and load history-consistent soil support modeling procedures.

Aerodynamic models are known to be an important source of differences in wind turbine code-to-code comparisons. In an effort to focus the verification work on the soil-structure interaction behavior, only the support structure was modeled, a lumped mass and inertia were used to represent the rotor-nacelle assembly (RNA), and time histories of lumped forces and moments were applied at the yaw bearing to represent rotor aerodynamics.

The global coordinate system used for defining the OWT design and outputting results is given in Figure 3. The x-axis of the global Cartesian coordinate system points downwind with respect to the main wind and wave direction. The z-axis points upwards and the y-axis forms a right-hand system.

3.1 Rotor-Nacelle Assembly

The RNA is modeled as a lumped mass and inertia at the location indicated in Table 1, which uses the standard wind turbine convention of Figure 3. The properties used can be considered representative of the ones from the IEA-10.0-198-RWT. This reference wind turbine (RWT) is a 10-MW, 198-m rotor diameter, direct-drive design developed as part of IEA Wind Task 37 [14].

On one hand, the products of inertia I_{xy} and I_{yz} equal to zero reported in Table 1 denote the symmetry about the XZ plane in the system. On the other hand, the product of inertia I_{xz} being different than 0 denotes that the X and Z principal axes of inertia have a different orientation than the global coordinate system (Figure 3).

3.2 Tower

The tower is based on the offshore DTU 10-MW wind turbine design [15]. The tower has a length of 105.63 m, a base outer diameter of 8.30 m with a thickness of 70 mm, and a top outer diameter of 5.50 m with a thickness of 30 mm. The tower base begins at an elevation of 40 m above the seabed (10 m above the mean sea level [MSL]). The water depth considered is 30 m.

3.3 Monopile

The monopile extends from the tower base with a constant outer diameter of 9 m, a constant thickness of 110 mm, and a penetration depth of 45 m, resulting in a length-to-diameter ratio of 5. The dimensions for the tower and monopile are included in Table 2, the material properties can be found in Table 3, and a schematic representation of the system can be seen in Figure 4. The outer diameter and wall thickness varies linearly between the elevations given in Table 2.

The material density used for the tower and monopile in Table 3 was increased from the default value of 7,850 kg/m^3 to account for mass of secondary structures not otherwise accounted for in the wall thickness. The eigenfrequencies of the system, assuming that the monopile is clamped at the seabed and there is no water, can be found in Table 4. The structural damping considered for the first bending mode—when the system is clamped at the seabed and the rigid RNA is placed atop the tower—is 0.5% critical damping. One percent critical damping is assumed for higher modes (e.g., second bending mode and torsion).

3.4 Soil-Structure Interaction

This section provides the inputs used for the REDWIN macro-element model 2 explained in section 2. The information provided in this section corresponds to the model used in the WAS-XL project [2]. The foundation model was calibrated by NGI [16]. Models for the AF, CS, and DS methods can be found in the project definition document [13].

The coefficients of the elastic stiffness matrix at the seabed used as an input for the REDWIN macro-element model 2 are provided in Eq. 1.

$$[K_{seabed\ 6x6}] = \begin{bmatrix} 6.336198E9 & 0 & 0 & 0 & -5.015421E10 & 0 \\ 0 & 6.336198E9 & 0 & 5.015421E10 & 0 & 0 \\ 0 & 0 & 1.119691E10 & 0 & 0 & 0 \\ 0 & 5.015421E10 & 0 & 8.111942E11 & 0 & 0 \\ -5.015421E10 & 0 & 0 & 0 & 8.111942E11 & 0 \\ 0 & 0 & 0 & 0 & 0 & 2.552673E11 \end{bmatrix} \quad (1)$$

The stiffness matrix in Eq. 1 accounts for the six DOFs at the seabed and is expressed according to the coordinate system shown in Figure 3. The stiffness matrix includes all diagonal coefficients (K_{11},K_{22}, K_{33}, K_{44}, K_{55}, K_{66}) and horizontal-rotational (K_{15},K_{24}, K_{42}, K_{51}) coupling coefficients. The vertical (K_{33}) and torsional (K_{66}) directions are uncoupled from the other DOFs. The coefficients are expressed according to the international system of units (N, m, rad). The stiffness matrix is symmetric, which denotes the reciprocity in the system.

The load-displacement curves used as input for the REDWIN macro-element model can also be found in the project definition document [13]. These values were obtained from a nonlinear pushover analyses performed with a quasi-static, three-dimensional FEA [finite-element analysis].

4 Participants and Modeling Approach

A total of 19 academic and industrial partners from 10 different countries actively participated in OC6 Phase II. Those actively involved are: the National Renewable Energy Laboratory (NREL, USA), 4Subsea (Norway), Bureau Veritas (BVEX, France), China General Certification Center (CGC, China), CSIC Haizhuang Windpower Co., Ltd (CSSC, China), DNV GL (United Kingdom), Dalian University of Technology (DUT, China), eureka! (Spain), Norwegian University of Science and Technology (NTNU, Norway), Orcina (United Kingdom), PRINCIPIA (France), Technical University of Denmark (DTU, Denmark), Tecnalia (Spain), Universidad de Cantabria (UC-IHC, Spain), University of Rostock (URO, Germany), University of Ulsan (UOU, Korea), Universitat Politècnica de Catalunya (UPC, Spain), Vulcain Engineering (France), and WyndTek (The Netherlands).

A list of the participants and the tools used in this study is provided in Table 5, which also shows the modeling approach employed.

As Table 5 shows, some participants decided to use more than one modeling approach and some used different codes. NREL used two different OpenFAST models (NREL 1 and NREL 2). NREL 1 models the tower by means of Euler-Bernoulli beams that account for the bending DOFs (ElastoDyn module) while NREL 2 models the tower by means of Timoshenko beams that account for axial, shear, bending, and torsion DOFs (SubDyn [17] module). A similar approach was adopted by eureka!. The EUREKA 1 model is equivalent to NREL 1 and EUREKA 2 is equivalent to NREL 2. The rest of the participants using OpenFAST adopted the same modeling approach as NREL 1.

There are three participants using the AF method: DUT 2, NREL 2, and WyndTek. The fixity depth and beam properties for this approach must be determined according to the beam theory used. NREL 2 and DUT 2 use Timoshenko beam elements and WyndTek uses Euler-Bernoulli beams. Accordingly, NREL 2 and DUT 2 use the AF properties specified in the project definition document [13], and WyndTek uses the properties corresponding to the improved AF method.

The participants modeling the SSI by means of the CS method use the stiffness matrix from Eq. 1 and the participants using the DS approach use 61 discrete nonlinear springs defined every 0.75 m along the monopile. Each spring is defined by 22 pairs of *p-y* points. The numerical values of these *p-y* curves are available in the project definition document [13].

The AF, CS, and DS approaches do not account for the SSI damping by default. To inform these methods, the equivalent SSI damping from the REDWIN approach was characterized at different loading levels by means of free-decay tests [13]. 4Subsea is the only participant using a traditional method (AF, CS, or DS) that includes damping for the SSI. 4Subsea includes viscous damping in the DS approach through dashpots with a constant damping coefficient in parallel with the springs. The damping coefficient is the same for all the dashpots and the same regardless of the loading condition. It is important to note that this viscous damping is proportional to the velocity while the hysteretic damping in the REDWIN approach is dependent on the displacement time history. The hysteretic damping of the REDWIN approach is also nonlinear; larger amplitudes translate into larger energy dissipated [13].

Some participants decided to use some built-in capabilities in their codes to study the system. For example, Orcina uses a nonlinear hysteretic stiffness model available in OrcaFlex. In this case, only the diagonal positions of the stiffness matrix are populated. The nonlinear horizontal (K_{11},K_{22}) and rotational (K_{44}, K_{55}) DOFs are defined according to the two load-displacement curves at the seabed from the nonlinear pushover analyses used as input for the REDWIN approach. The vertical (K_{33}) and torsional (K_{66}) DOFs are characterized based on the elastic stiffness matrix (see Eq. 1). Although this approach results in a hysteretic behavior in the horizontal and rotational DOFs, these directions are uncoupled because the stiffness matrix used does not include cross-coupling coefficients. To avoid this, the location of the stiffness matrix is placed at a point along the monopile longitudinal axis below the seabed that induces a coupling between the horizontal and rotational directions.

5 Verification Methodology

Similar to the OC3 [18], OC4 [19,20], and OC5 [21–25] projects, a stepwise verification procedure was performed in the OC6 Phase II project. The model complexity is increased one step at a time to facilitate the identification of modeling discrepancies introduced by different theories and/or model implementations in the various codes. Table 6 provides a summary of the simulations that are presented in section 6, including static simulations (1.X), eigenanalyses (2.X), wind-only simulations (3.X), wave-only simulations (4.X), and combined wind/wave simulations (5.X). The complete list of load cases studied can be found in the project definition document [13].

It is important to note that the responses from load cases that involve wind (i.e., load case 3.1 and load case 5.1) are used for verification purposes, but cannot be considered representative of a real wind turbine in operating conditions due to the lack of aerodynamic damping in the models used in this code-to-code verification.

6 Selected Results

In this section, a comprehensive overview of the studied load cases shown in Table 6 is presented and explained.

6.1 Static Simulations Results: Load Case 1.2

Load case 1.2 focus on ensuring that the structural model was implemented correctly by examining the static loads and deflections of the system with the gravity acceleration as the only external loading.

Figure 5 shows the tower-top (yaw bearing) displacement along the *x*-axis (fore-aft direction) under gravity-only conditions (load case 1.2). This displacement is the result of the overhanging weight of the RNA (see Table 1) and it is affected by the SSI stiffness. The dashed black line shows the average displacement from all participants and it can be used as a reference to compare the different solutions.

As Figure 5 shows, the linear SSI approaches (AF and CS) result in smaller tower-top displacements. These linear approaches were characterized based on the unloaded state (see Eq. 1) and behave slightly stiffer than the nonlinear SSI approaches. Interestingly, WyndTek AF using the improved AF method (Euler-Bernoulli beams) and NREL 2 AF using the AF method

(Timoshenko beams) produce the same displacement. The tower-top displacements for the DS approach are slightly bigger due to the nonlinearity of the *p-y* curves. Finally, the REDWIN shows slightly larger displacements than the DS approach because it accounts for the nonlinear stiffness and plasticity. Not all the simulation tools are able to perform a static analysis or gradually apply the gravity acceleration in a quasi-static fashion. Accordingly, some participants perform a transient analysis where the gravity acceleration is suddenly applied over the system at the beginning of the simulation. This results in an initial transient loading that can induce a small level of plasticity. Therefore, REDWIN solutions using an initial static computation or a gradual loading result in slightly smaller displacements closer to the DS approach.

6.2 Eigenanalysis Results: Load Case 2.3

Load case 2.3 furthers the examination of the structural model by assessing the system eigenfrequencies, damping values, and mode shapes. Figure 6 and Figure 7 show the system eigenfrequencies for the first and second bending modes in the fore-aft direction. These outputs are from load case 2.3, which includes foundation flexibility and still water conditions. For reference, the plots include a grey dashed line with the average result when the foundation is considered rigid (i.e., clamp at seabed) and there are no marine conditions (i.e., no water). These average results were obtained from the results provided by the participants in load case 2.1 (see the project definition document [13] for reference) and are aligned with the numerical values from Table 4. The black dashed line denotes the average solution when accounting for the foundation flexibility and marine conditions (i.e., still water).

As Figure 6 shows, the first bending mode drops around 10% in frequency due to the flexible foundation. The water does not have a significant impact for the first bending mode in this system. For the second bending mode (Figure 7), the drop in frequency is around 20% on average. The main reason for this drop in frequency is also the foundation flexibility, but the added mass from the still water is also noticeable. In the studied system and for all load cases, the monopile does not have water inside. Having the monopile filled with water would decrease these eigenfrequencies further.

There is a good agreement between participants for the first bending mode in the fore-aft direction. The linear approaches (AF and CS) behave slightly stiffer than the DS approach as expected and observed during the static analysis (i.e., load case 1.2). A similar trend can be observed in Figure 7 for the second bending mode. It is also interesting to note that in this second bending mode, the agreement between participants is not as good as for the first bending mode. One of the reasons for the dispersion in the eigenfrequencies between participants using the same SSI approach is the method used to extract the eigenproperties around the static equilibrium. Some simulation tools used by the participants include a linearization capability, while other participants without this functionality tried to obtain these properties from time-domain simulations (e.g., by means of a free-decay test or a broadband wind or wave excitation). For example, Figure 7 shows some significant differences between some of the participants using the REDWIN approach. However, when post-processing the time-domain results of load case 5.X in the frequency domain, these differences were not observed (see, e.g., Figure 18 and Figure 20). Extracting the eigenproperties of a model using the REDWIN approach can be challenging due to the nonlinear nature of the system.

Figure 8 shows the associated eigenvectors of the first and second bending modes in the fore-aft direction. The eigenvectors are normalized by their maximum amplitude to allow the comparison between participants.

As expected, the largest amplitude for the first bending mode is located at the tower-top. As seen in Figure 8, the agreement between the participants is very good regardless of the SSI approach used. For the second bending mode, the maximum amplitude occurs at about two-thirds of the support structure height. In this case, all the participants using the DS approach have slightly more deflections at the seabed (h = 0 m).

6.3 Wind-Only Simulations Results: Load Case 3.1

After analyzing the static cases and the eigenproperties of the system, the response under wind-only conditions was studied. The environmental conditions in load cases 3-5 are representative of a 30-m water depth site at the Norwegian Continental Shelf [10].

As noted in section 3, the computational models account for the support structure and a lumped mass and inertia for the RNA. The wind loading in the six DOFs for load cases 3.1 and 5.1 (see Table 6) was computed beforehand by NREL, and was applied as external force and moment time histories by participants at the yaw bearing (see the project definition document [13] for further details).

Load case 3.1 is a wind-only load case and considers a mean wind speed at hub height (V_{hub}) of 9.06 m/s. This wind speed is below the rated wind speed of 10.75 m/s [14] for the IEA-10.0-198-RWT. Under these conditions, the wind turbine is rotating at about 7.75 rpm. The aeroelastic model used to compute the externally applied loads did not include any rotor imbalance (e.g., no mass nor aerodynamic imbalance). Accordingly, the only excitations present in the computed loads correspond to the blade passing frequency (3P for a three-bladed wind turbine) and the corresponding harmonics (e.g., 6P and 9P), where P is the rotor speed.

The power spectral density (PSD) of the tower-top acceleration along the *x*-axis (fore-aft direction) is shown in Figure 9. The main excitations (i.e., 3P, 6P, and 9P) as well as the eigenfrequencies (i.e., first and second fore-aft bending modes) are also included with vertical dashed lines in the figure. The eigenfrequencies are marked according to the average solution from all participants in load case 2.3 (Figure 6 and Figure 7). It is important to note that load case 2.3 includes the marine conditions but load case 3.1 does not. However, the same vertical lines were used for the eigenfrequencies for an easier comparison against the results from load case 5.1.

Different line styles are used in the spectrum to compare the different approaches. The solutions using a linear SSI approach (AF or CS) are denoted with a dotted line, the ones using the DS approach are denoted with a dashed line, and the ones using the REDWIN approach are denoted with a solid line. In the legend, participants using different modeling approaches appear with the line style associated with its highest model fidelity used (REDWIN>DS>AF|CS).

For this loading condition, the 9P excitation is virtually at the same frequency as the second fore-aft bending mode. This resonance can lead to increased levels of structural activity at this frequency.

The agreement between participants for the first fore-aft bending mode eigenfrequency is very good with only some differences in terms of amplitude. For the second fore-aft bending mode, some differences in terms of frequency can be observed. The linear SSI approaches (AF and CS) show the stiffest behavior and the DS approach the softest. For this second bending mode, the DS approach also has the largest amplitude.

To more systematically compare the response between participants and modeling approaches, the PSD sum (Eq. 2) is computed based on the one-sided, unsmoothed, discrete power density functions.

$$S_{sum} = \sum_{i=j}^{k} S_{resp}(f_i)\Delta f \qquad (2)$$

where $S_{resp}(f_i)$ is the discrete PSD amplitude at frequency f_i, Δf is the frequency resolution, j and k are the indices of the first and last frequency of interest. This PSD sum is equivalent to the integral of the PSD for a given frequency range. For reference, the square root of this PSD sum is equivalent to the root mean square (RMS) for the frequency range of interest.

Two PSD sum magnitudes are computed to analyze the results in more detail: one for the frequency range between 0.2 and 0.3 Hz and the other between 1.0 and 1.5 Hz. These two frequency ranges are marked with two red rectangles in Figure 9 and can be considered indicative of the first and second fore-aft bending mode responses. Figure 10 shows the PSD sums for the different participants according to the SSI approach used. The *y*-axis scale for the first frequency range (0.2–0.3 Hz) is one order of magnitude higher than for the second frequency range (1.0–1.5 Hz) to highlight the relative importance of the first bending mode response compared to the second bending mode.

For the first fore-aft bending mode, the largest response corresponds to the linear SSI approaches. These linear approaches result in a slightly stiffer system, which places the first structural mode closer to the 3P excitation. The DS approach has a smaller response than the linear SSI approaches, but a larger response than the REDWIN due to the lack of damping. For the second fore-aft bending mode, the smallest response also corresponds to the REDWIN approach. 4Subsea also uses the DS approach, but it includes SSI damping. By including this damping, the response is the smallest of the DS solutions for the first and second fore-aft bending modes and is at a level that is quite similar to the REDWIN approach. The results across the REDWIN solutions are very similar, showing comparable trends for the remaining load cases.

Figure 11 shows the monopile fore-aft bending moment at the seabed and Figure 12 the associated PSD sums. The main difference in this case is the behavior at 0 Hz. This amplitude is indicative of the signal average; the mean fore-aft bending moment at the seabed in this case. This mean value is mainly driven by the aerodynamic thrust force acting over the system. For the acceleration, the mean value will always be zero.

6.4 Wave-Only Simulations Results: Load Case 4.2

Load case 4.2 analyzes the response of the system under irregular waves. Load case 4.2 is a wave-only load case. With a focus on the SSI model, a simple modeling approach was used for the hydrodynamic forces. Table 7 provides the settings that were used for the load cases that involve

marine conditions to try to replicate the same input loading across participants and simulation tools.

Figure 13 shows the wave elevation spectrum in load case 4.2. The peak-spectral wave frequency ($1/T_p$), as well as the first fore-aft bending mode are also included in the figure with vertical dashed lines. The frequency range between 0.1 and 0.5 Hz contains most of the energy in the wave spectrum. This wave-only condition can only excite the first bending mode of the structure.

Figure 14 and Figure 16 show the PSD of the tower-top acceleration along the x-axis and the monopile fore-aft bending moment at the seabed. Figure 15 and Figure 17 show the associated PSD sums for the frequency range between 0.2 and 0.3 Hz, representative of the first fore-aft bending mode response. The line styles, output locations, and post-processing in terms of PSD sums are the same as the one presented for the wind-only conditions. In this case, the largest response occurs for the DS approach and it is likely due to the slightly lower frequency compared to the other solutions. This lower frequency locates the structural mode in a region where the wave energy is higher. As already observed in the wind-only condition, 4Subsea also uses the DS approach but the response is more aligned with the REDWIN solution. For this participant, the first bending mode is slightly higher in terms of frequency than the other DS solutions (observed in Figure 14) and the SSI accounts for damping.

6.5 Combined Wind and Waves: Load Case 5.1

Load case 5.1 combines the wind conditions studied and presented in load case 3.1 with the Pierson-Moskowitz wave spectrum analyzed in load case 4.2. Figure 18 shows the PSD of the tower-top acceleration along the x-axis and Figure 19 the corresponding PSD sums. Figure 18 can be compared to the one from the wind-only condition (Figure 9). As it shows, the two main differences between the wind-only and the wind/wave conditions are the response amplitude for the first fore-aft bending mode and the slight frequency shift for the second fore-aft bending mode. The amplitude of the first fore-aft bending mode is higher due to the wave excitation. The drop in frequency for the second fore-aft bending mode is due to the added mass term from the water. The PSD sums for this load case are mainly the result of the superposition of the PSD sums from the wind-only and wave-only conditions.

Figure 20 shows the monopile fore-aft bending moment at the seabed and Figure 21 the associated PSD sums. Similar to the wind-only and wave-only conditions, the response of the REDWIN approach is the smallest for the first and second fore-aft bending modes. Also, the response of the DS with damping (4Subsea) is quite similar to the one from the REDWIN approach.

7 Conclusions

During the OC6 Phase II project, the REDWIN modeling capability was coupled to a variety of offshore wind modeling tools. The new capability was verified across different tools and against industry standard methods for an example monopile offshore wind system (DTU 10-MW wind turbine). Two linear (AF and CS) and two nonlinear (DS and REDWIN) soil-structure interaction approaches were used during this code-to-code verification.

The REDWIN macro-element approach differs from traditional methods in the inclusion of plasticity and hysteretic damping. It requires more elaborate inputs (e.g., stiffness matrix and load-

displacement curves at the seabed) to characterize the SSI. However, it models the hysteretic damping internally. This is a great advantage because the energy dissipated by the SSI is not easy to quantify and include in a numerical model. On the one hand, traditional methods have often employed a viscous damping matrix at the seabed or dashpot elements along the monopile with viscous damping. In these cases, the damping forces are proportional to the velocity. On the other hand, the hysteretic damping included in the REDWIN macro-element is dependent on the displacement trajectories. This hysteretic damping is inherently nonlinear: larger displacement loops result in more energy dissipated. The differences between these two damping approaches would be especially noticeable at high frequency ranges, where the displacements are relatively small, but the velocities are high. The proper characterization of this soil damping is especially important in idling and wind-wave misalignment conditions.

The support structure loads at the first and second bending mode are the smallest when using the REDWIN macro-element compared to the other modeling approaches, for all load cases analyzed. This would mean a lower fatigue estimate using the REDWIN model. Although no validation was done here to assess the accuracy of the REDWIN capability, this validation was achieved within the REDWIN project and the lower fatigue estimate would mean that OWT designs could remove some conservancy. The differences observed in the loads between the REDWIN and the traditional methods are mainly due to small differences in terms of system eigenfrequencies because of the foundation flexibility and the lack of damping defined in the traditional approaches.

Across the different tools that have integrated in the REDWIN modeling approach, very similar results were seen for all load cases. This verifies the accurate implementation of the REDWIN capability in these tools, making them ready for use in the design of future OWT systems.

Acknowledgments

The authors would like to thank the Norwegian Geotechnical Institute for their work in the REDWIN project to develop the capability being incorporated in OC6 Phase II and to provide the data to model the foundation as well as for their ongoing support. We would also like to thank the Norwegian University of Science and Technology for their support in developing the model for this project.

This work was authored in part by the National Renewable Energy Laboratory, operated by Alliance for Sustainable Energy, LLC, for the U.S. Department of Energy (DOE) under Contract No. DE-AC36-08GO28308. Funding provided by the U.S. Department of Energy Office of Energy Efficiency and Renewable Energy Wind Energy Technologies Office. The views expressed in the article do not necessarily represent the views of the DOE or the U.S. Government. The U.S. Government retains and the publisher, by accepting the article for publication, acknowledges that the U.S. Government retains a nonexclusive, paid-up, irrevocable, worldwide license to publish or reproduce the published form of this work, or allow others to do so, for U.S. Government purposes.

References

1. REDWIN (Reducing cost of offshore wind by integrated structural and geotechnical design). 3D Foundation Model Library. https://www.ngi.no/eng/Projects/REDWIN-reduce-wind-energy-cost/#Reports-and-publications. Accessed: 2020-03-23.

2. Velarde J, Bachynski EE. Design and fatigue analysis of monopile foundations to support the DTU 10 MW offshore wind turbine. *Energy Procedia*. 2017;137:3–13. https://doi.org/10.1016/j.egypro.2017.10.330.

3. DNV (Det Norske Veritas). DNV-OS-J101 - Design of Offshore Wind Turbine Structures. Oslo: Det Norske Veritas. 2014. https://rules.dnv.com/docs/pdf/dnvpm/codes/docs/2014-05/Os-J101.pdf.

4. API (American Petroleum Institute). RP 2A-WSD - Recommended Practice for Planning, Designing and Constructing Fixed Offshore Platforms. 2014. Washington, D.C.: American Petroleum Institute.

5. Page AM, Grimstad G, Eiksund GR, Jostad HP. A macro-element model for multidirectional cyclic lateral loading of monopiles in clay. *Comput Geotech*. 2019;106:314–326. https://doi.org/10.1016/j.compgeo.2018.11.007.

6. Page AM, Grimstad G, Eiksund GR, Jostad HP. A macro-element pile foundation model for integrated analyses of monopile-based offshore wind turbines. *Ocean Eng*. 2018;167:23–35. https://doi.org/10.1016/j.oceaneng.2018.08.019.

7. Page AM, Næss V, De Vaal JB, Eiksund GR, Nygaard TA. Impact of foundation modelling in offshore wind turbines: Comparison between simulations and field data. *Mar Struct.* 2019;64:379–400. https://doi.org/10.1016/j.marstruc.2018.11.010.

8. IEC (International Electrotechnical Commission). Wind energy generation systems – Part 3-1: Design requirements for offshore wind turbines. Geneva, Switzerland. 2019.

9. Malekjafarian A, Jalilvand S, Doherty P, Igoe D. Foundation damping for monopile supported offshore wind turbines: A review. *Mar Struct.* 2021;77:102937. https://doi.org/10.1016/j.marstruc.2021.102937.

10. Katsikogiannis G, Bachynski EE, Page AM. Fatigue sensitivity to foundation modelling in different operational states for the DTU 10MW monopile-based offshore wind turbine. *J Phys Conf Ser*. 2019;1356(1):012019. IOP Publishing. October. DOI:10.1088/1742-6596/1356/1/012019.

11. Page AM, Grimstad G, Eiksund GR, Jostad HP. A macro-element pile foundation model for integrated analyses of monopile-based offshore wind turbines. *Ocean Eng*. 2018;167:23–35. https://doi.org/10.1016/j.oceaneng.2018.08.019.

12. Byrne BW, McAdam R, Burd HJ, et al. New design methods for large diameter piles under lateral loading for offshore wind applications. In: *Frontiers in offshore geotechnics III*. 2015:705–710. 2015. June. DOI:10.1201/b18442-96.

13. Bergua R, Robertson A, Jonkman J, Platt A. Specification Document for Offshore Code Comparison Collaboration, Continued, with Correlation and unCertainty (OC6) Phase II: Verification of an Advanced Soil-Structure Interaction Model for Offshore Wind Turbines (NREL/TP-5000-79938). National Renewable Energy Laboratory (NREL), Golden, CO (United States). 2021. https://www.nrel.gov/docs/fy21osti/79938.pdf.

14. Bortolotti P, Canet Tarres H, Dykes KL, Merz K, Sethuraman L, Verelst D, Zahle F. IEA Wind TCP Task 37: Systems Engineering in Wind Energy-WP2. 1 Reference Wind Turbines. 2019. https://www.nrel.gov/docs/fy19osti/73492.pdf

15. Anaya-Lara O, Tande JO, Uhlen K, Merz K. Appendix. In: Anaya-Lara O, Tande JO, Uhlen K, Merz K, eds. *Offshore Wind Energy Technology*. 2020. https://doi.org/10.1002/9781119097808.app.

16. Sivasithamparam N, Misund B, Page A, Løkke A. Implementation of REDWIN models in OC6 [Offshore Code Comparison Collaboration, Continued, with Correlation and unCertainty] (Doc. 20190610-01-TN). 2020.

17. Damiani R, Jonkman J, Hayman G. SubDyn User's Guide and Theory Manual (NREL/TP-5000-63062). National Renewable Energy Laboratory (NREL), Golden, CO (United States). 2015. https://www.nrel.gov/wind/nwtc/assets/downloads/SubDyn/SubDyn_Manual.pdf.

18. Jonkman J, Musial W. Offshore Code Comparison Collaboration (OC3) for IEA Wind Task 23 Offshore Wind Technology and Deployment (NREL/TP-5000-48191). National Renewable Energy Laboratory (NREL), Golden, CO (United States). 2010. https://www.nrel.gov/docs/fy11osti/48191.pdf.

19. Popko W, Vorpahl F, Zuga A, et al. Offshore Code Comparison Collaboration Continuation (OC4), Phase I—Results of Coupled Simulations of an Offshore Wind Turbine with Jacket Support Structure (NREL/CP-5000-54124). National Renewable Energy Laboratory (NREL), Golden, CO (United States). 2012. https://www.nrel.gov/docs/fy12osti/54124.pdf.

20. Robertson A, Jonkman J, Musial W, Vorpahl F, Popko W. Offshore code comparison collaboration, continuation: Phase II results of a floating semisubmersible wind system (NREL/CP-5000-60600). National Renewable Energy Laboratory (NREL), Golden, CO (United States). 2013. https://www.nrel.gov/docs/fy14osti/60600.pdf.

21. Robertson AN, Wendt FF, Jonkman JM, et al. OC5 project phase I: Validation of hydrodynamic loading on a fixed cylinder (NREL/CP-5000-63567). National Renewable Energy Laboratory (NREL), Golden, CO (United States). 2015. https://www.nrel.gov/docs/fy15osti/63567.pdf.

22. Robertson AN, Wendt F, Jonkman JM, et al. OC5 Project Phase Ib: validation of hydrodynamic loading on a fixed, flexible cylinder for offshore wind applications (NREL/JA-5000-66648). National Renewable Energy Laboratory (NREL), Golden, CO (United States). 2016. https://doi.org/10.1016/j.egypro.2016.09.201.

23. Robertson AN, Wendt F, Jonkman JM, et al. OC5 project phase II: validation of global loads of the DeepCwind floating semisubmersible wind turbine. *Energy Procedia*. 2017;137:38–57. https://doi.org/10.1016/j.egypro.2017.10.333.

24. Robertson AN, Jonkman J, Wendt FF, et al. Verification of a Numerical Model of the Offshore Wind Turbine From the Alpha Ventus Wind Farm Within OC5 Phase III (NREL/CP-5000-70878). National Renewable Energy Laboratory (NREL), Golden, CO (United States). 2018. https://doi.org/10.1115/OMAE2018-77589.

25. Popko W, Robertson A, Jonkman J, et al. Validation of numerical models of the offshore wind turbine from the alpha ventus wind farm against full-scale measurements within OC5 Phase III. In: *ASME 2019 38th International Conference on Ocean, Offshore and Arctic Engineering*. American Society of Mechanical Engineers Digital Collection. 2019. May. https://doi.org/10.1115/OMAE2019-95429.

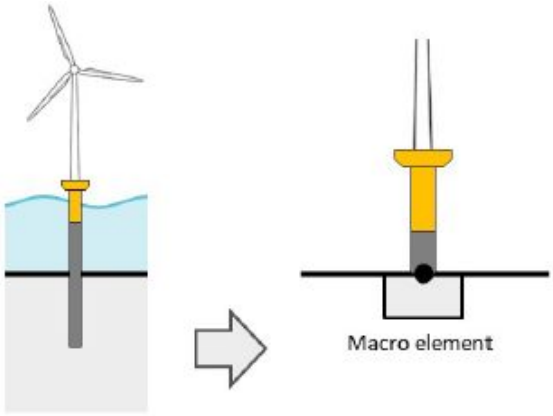

Figure 1. Illustration of the offshore wind turbine (left) and macro-element approach (right) [1]

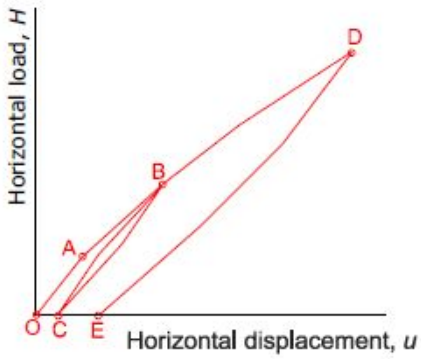

Figure 2. Nonlinear hysteretic pile foundation behavior [11]

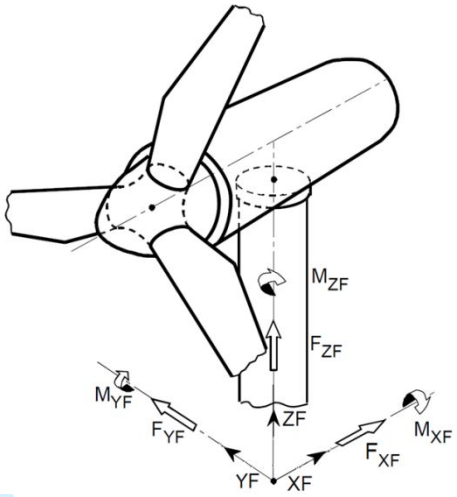

Figure 3. Global coordinate system

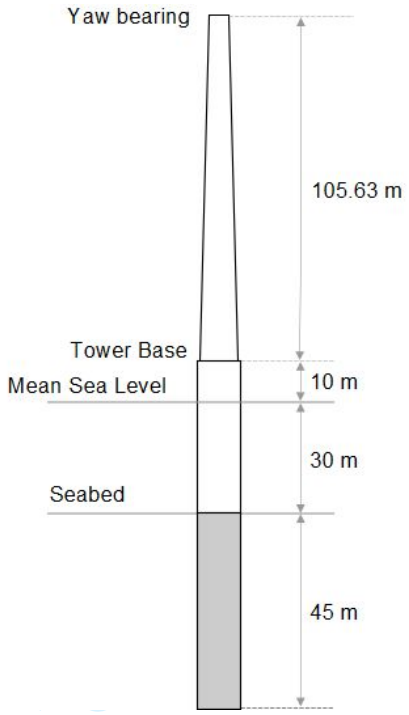

Figure 4. Schematic representation of the tower and monopile

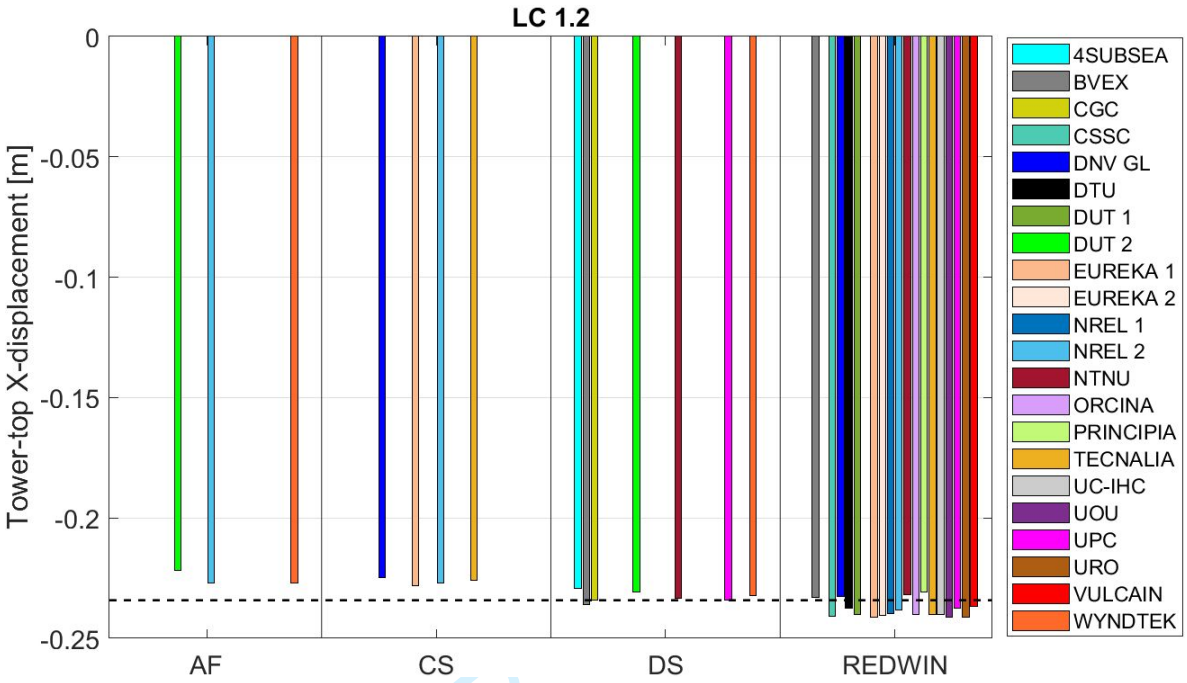

Figure 5. Tower-top X-displacement for gravity-only conditions in load case (LC) 1.2

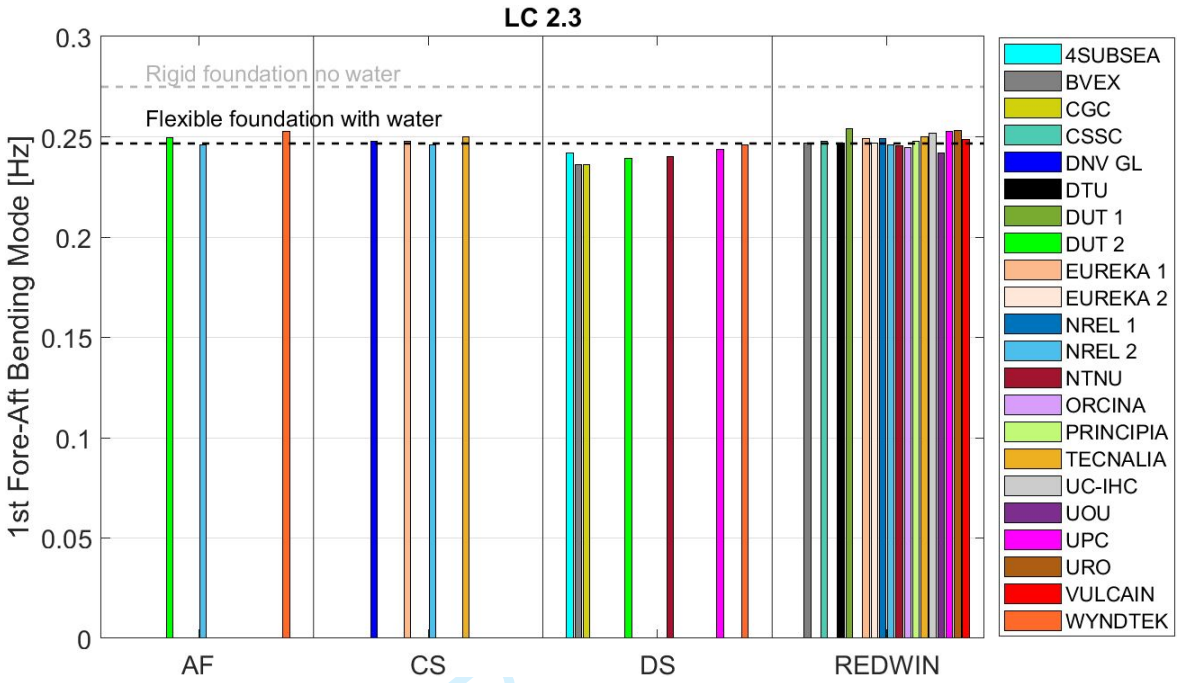

Figure 6. First fore-aft bending mode eigenfrequency depending on the soil-structure interaction approach in load case (LC) 2.3

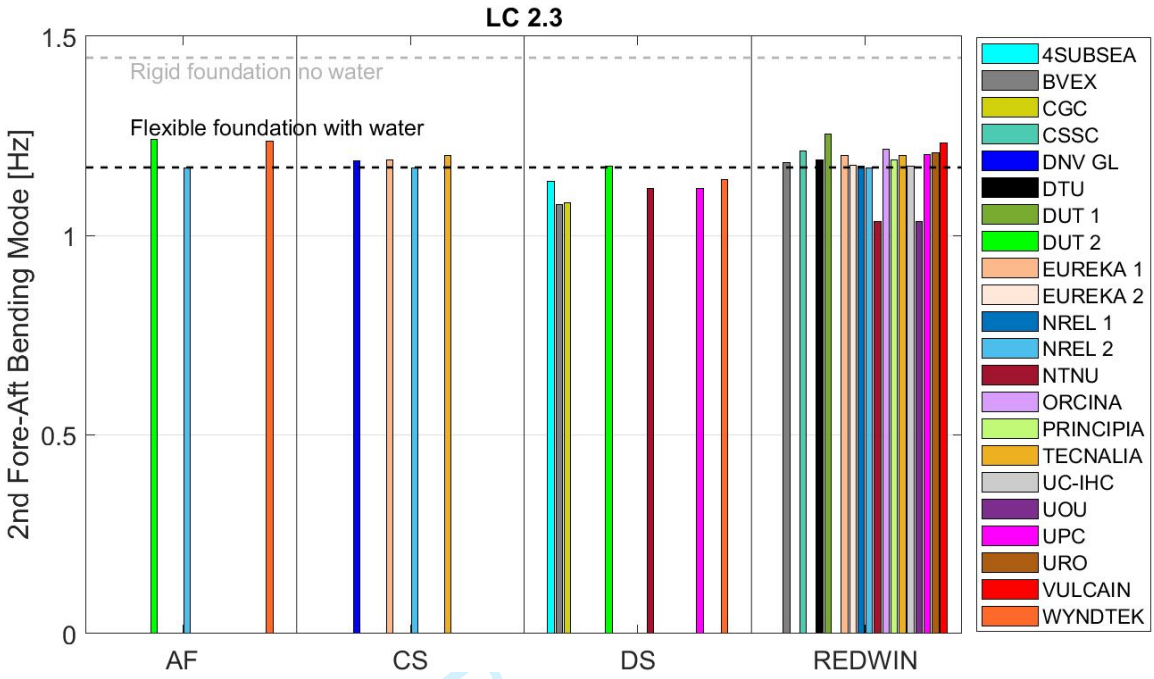

Figure 7. Second fore-aft bending mode eigenfrequency depending on the soil-structure interaction approach in load case (LC) 2.3

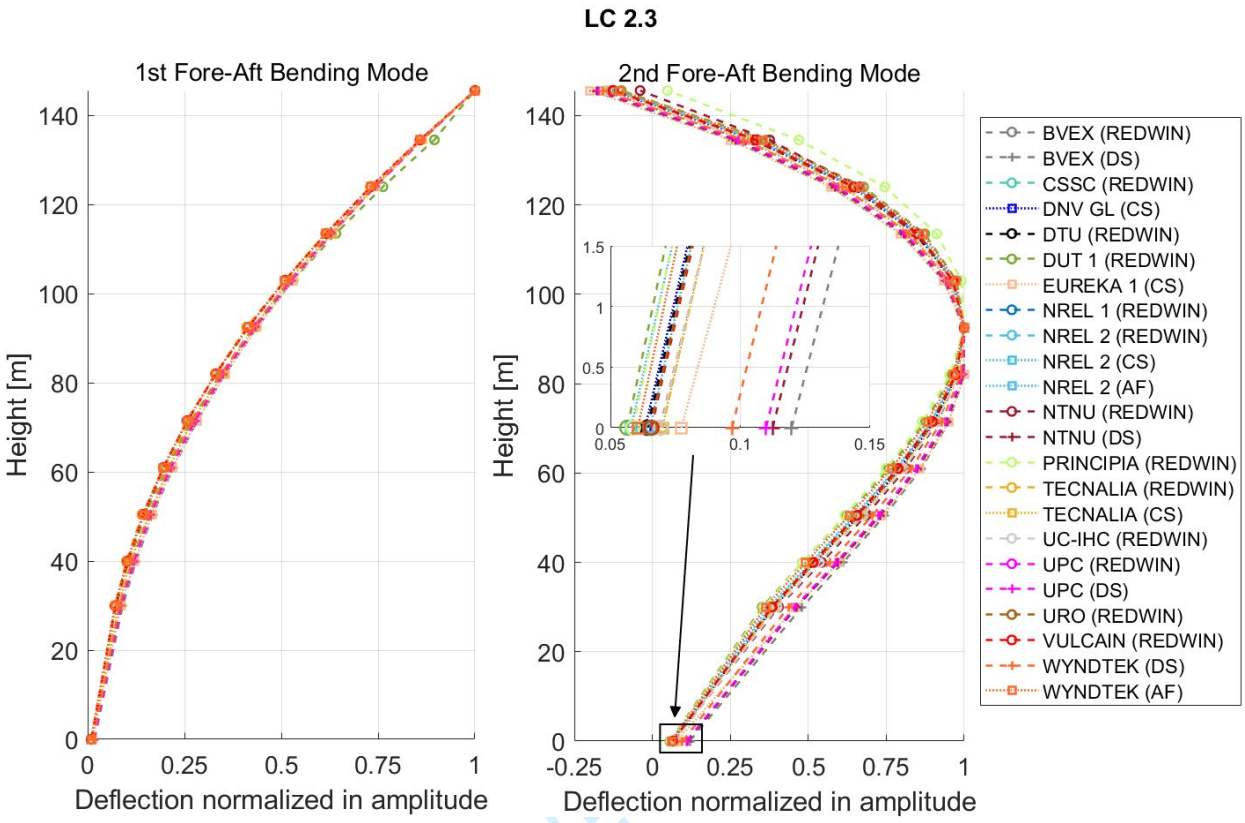

Figure 8. Eigenvectors of the first and second fore-aft bending modes in load case (LC) 2.3

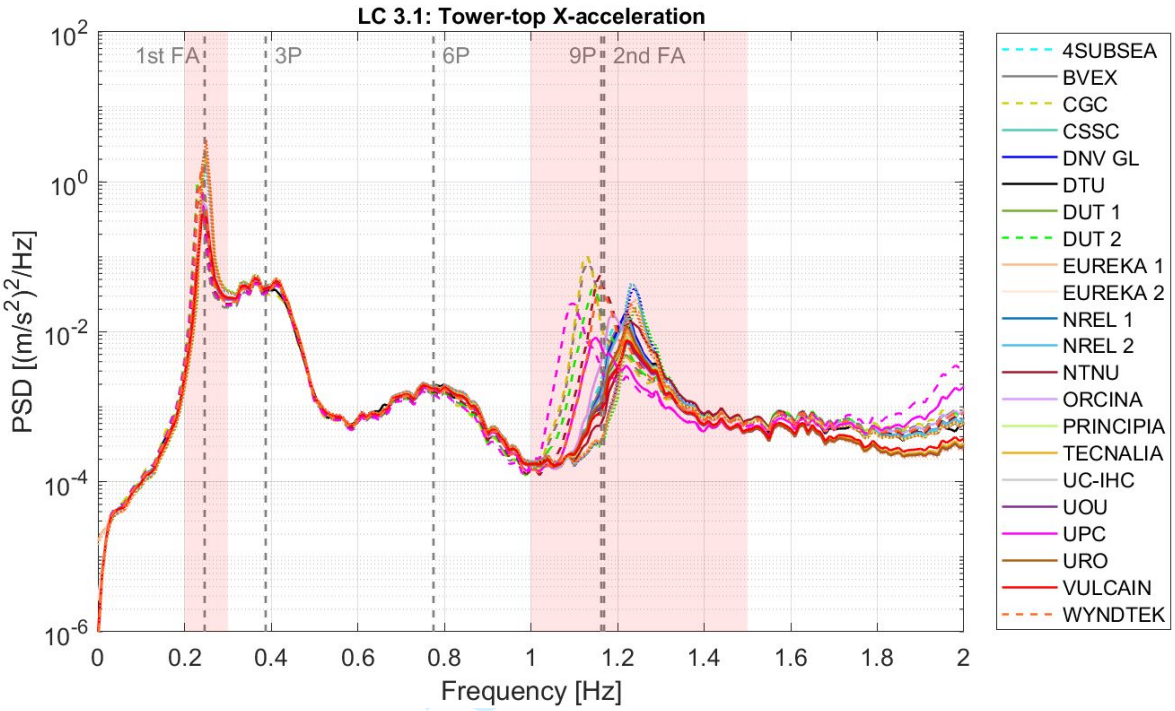

Figure 9. Power spectral density (PSD) of the tower-top X-acceleration in load case (LC) 3.1

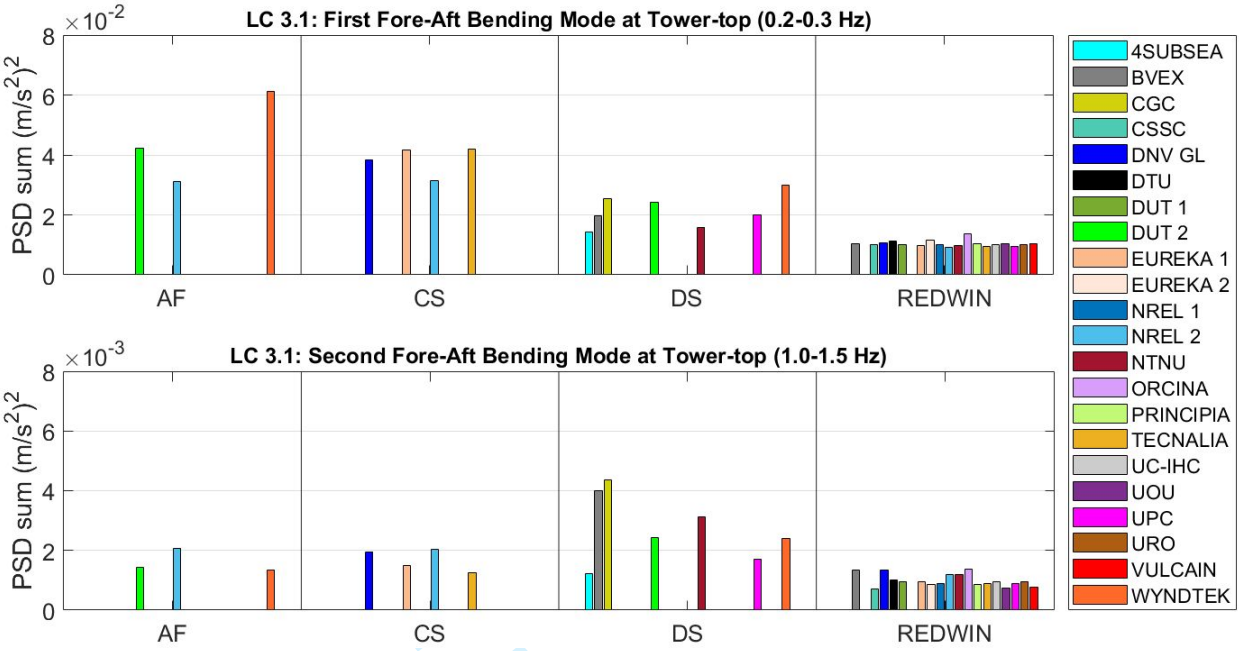

Figure 10. Power spectral density (PSD) sums of the tower-top X-acceleration in load case (LC) 3.1

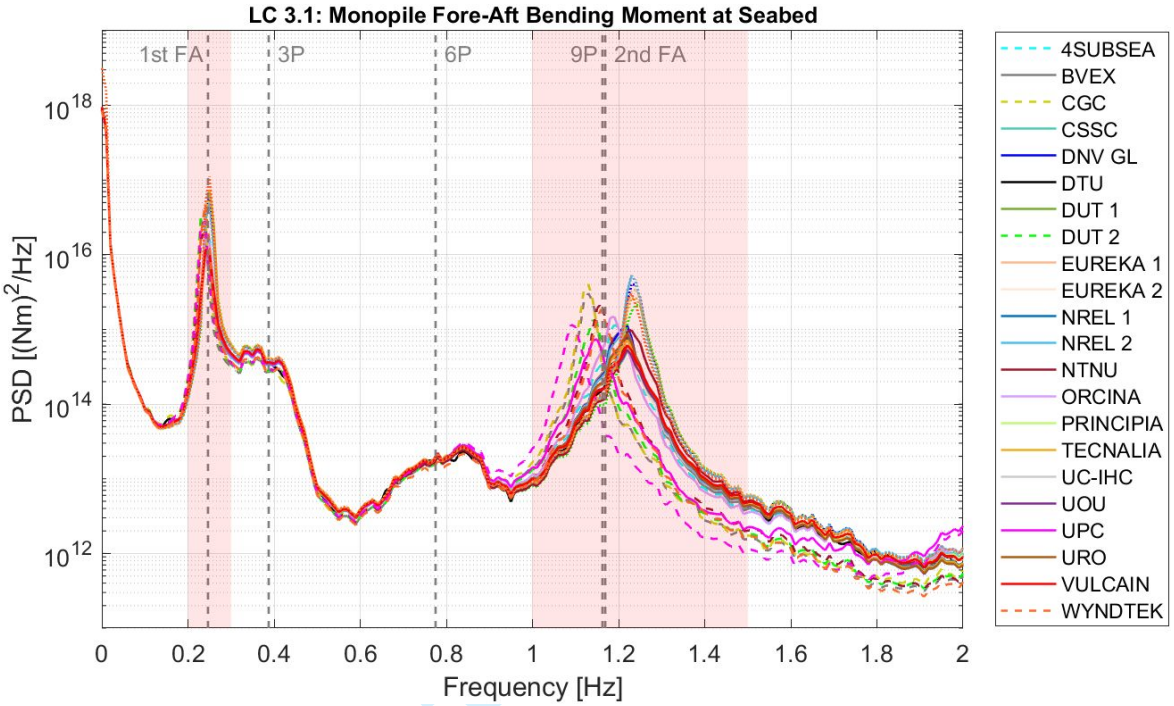

Figure 11. Power spectral density (PSD) of the monopile fore-aft bending moment at the seabed in load case (LC) 3.1

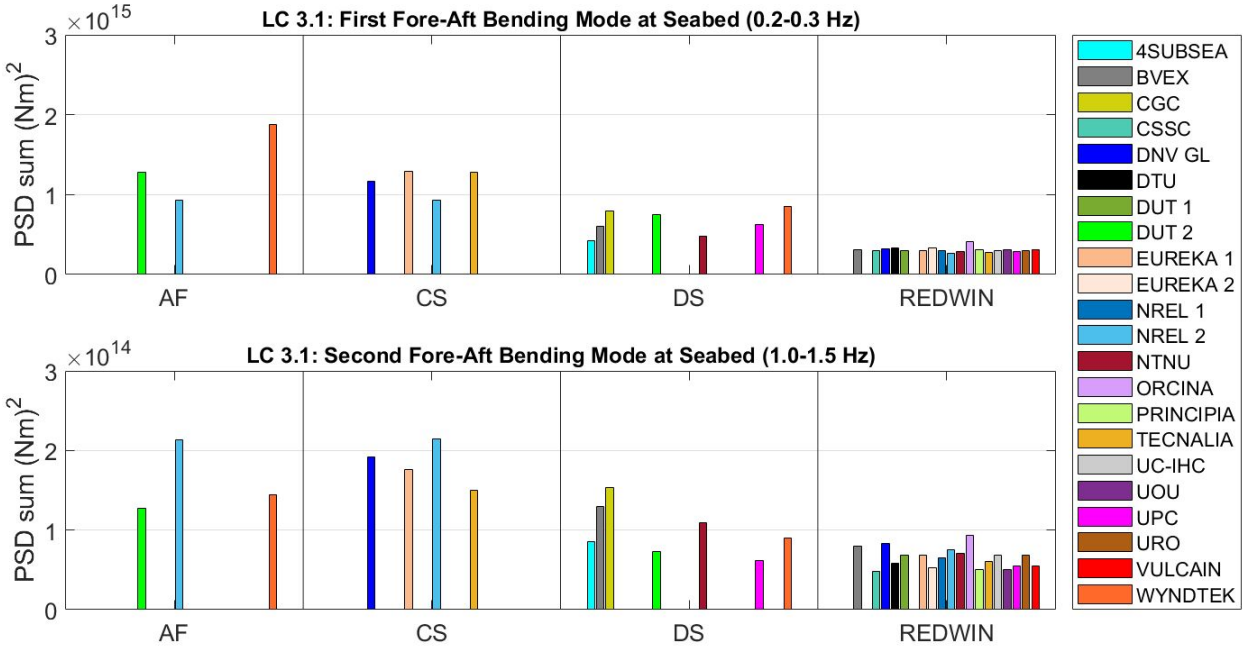

Figure 12. Power spectral density (PSD) sums of the fore-aft bending moment at the seabed in load case (LC) 3.1

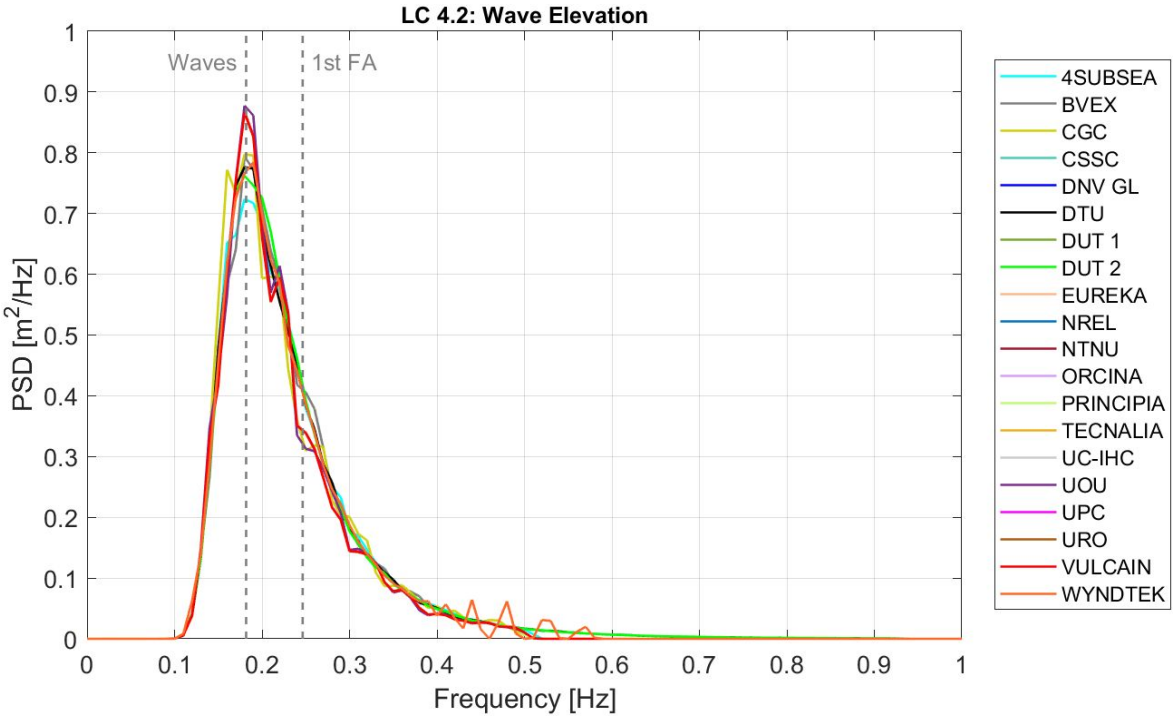

Figure 13. Power spectral density (PSD) of the wave elevation in load case (LC) 4.2 (H_s = 1.25 m, T_p = 5.5 s, γ = 1.0)

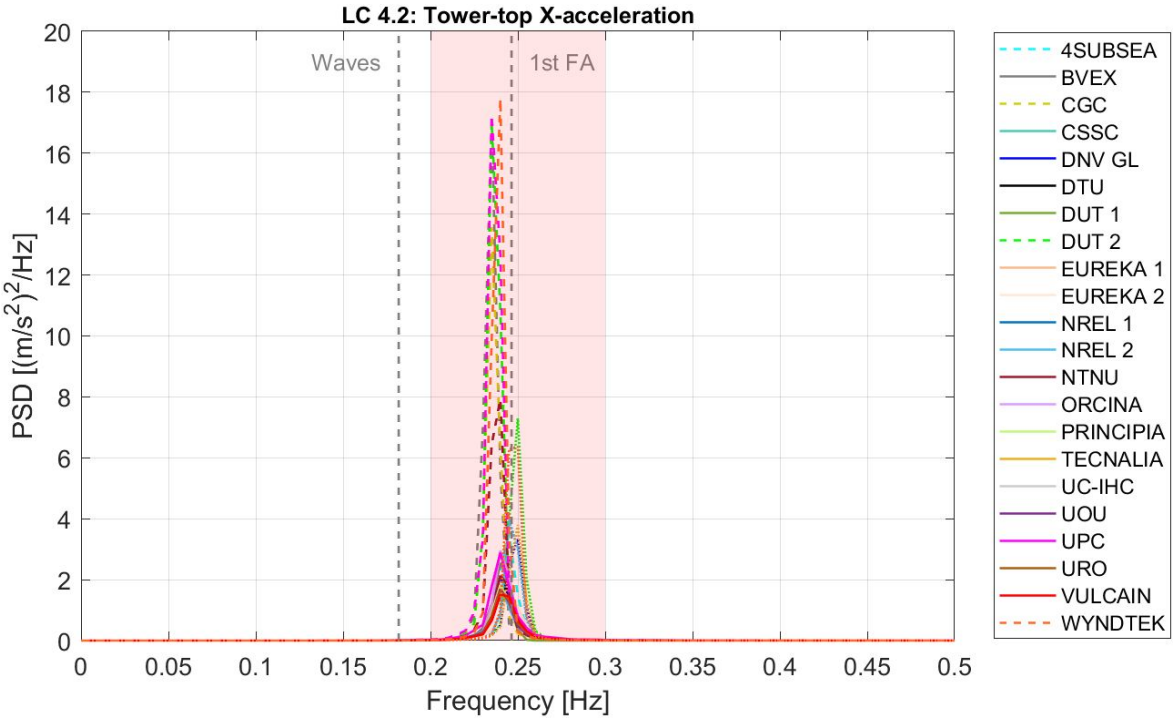

Figure 14. Power spectral density (PSD) of the tower-top X-acceleration in load case (LC) 4.2

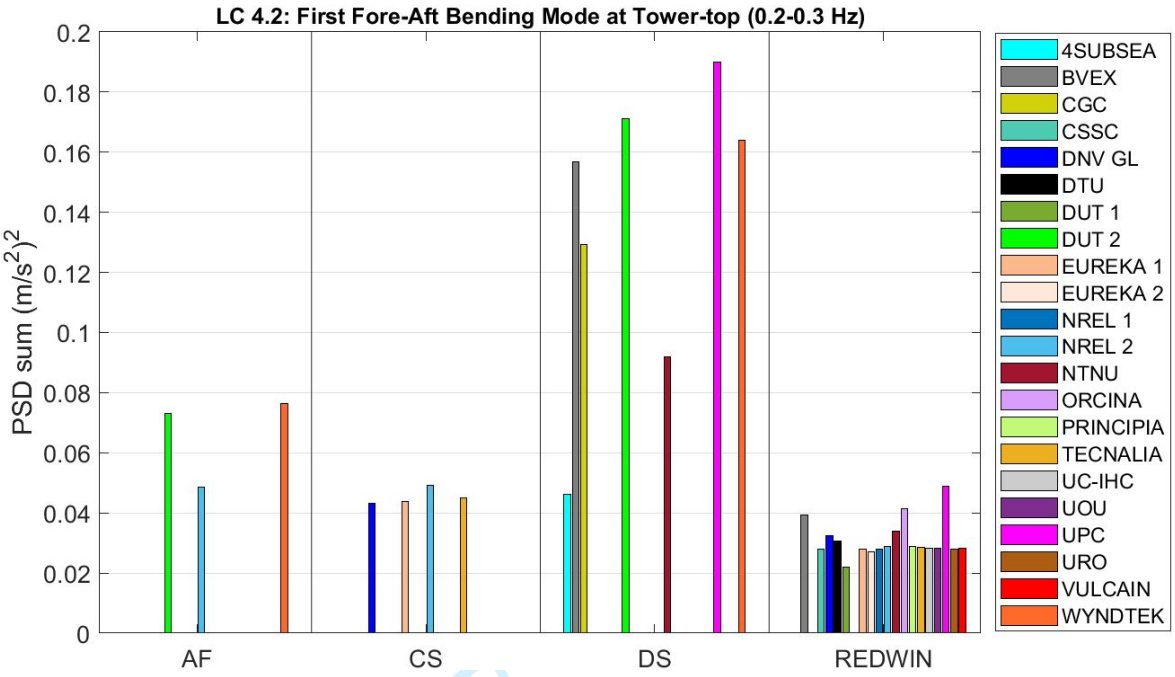

Figure 15. Power spectral density (PSD) sum of the tower-top X-acceleration in load case (LC) 4.2

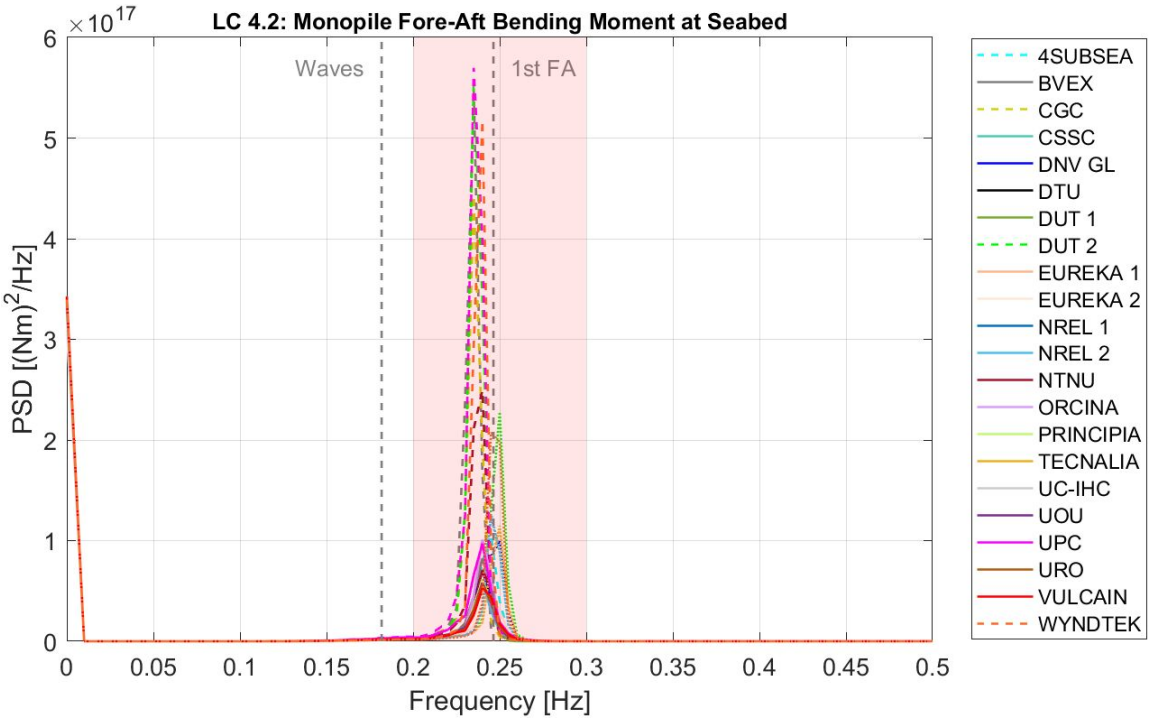

Figure 16. Power spectral density (PSD) of the monopile fore-aft bending moment at the seabed in load case (LC) 4.2

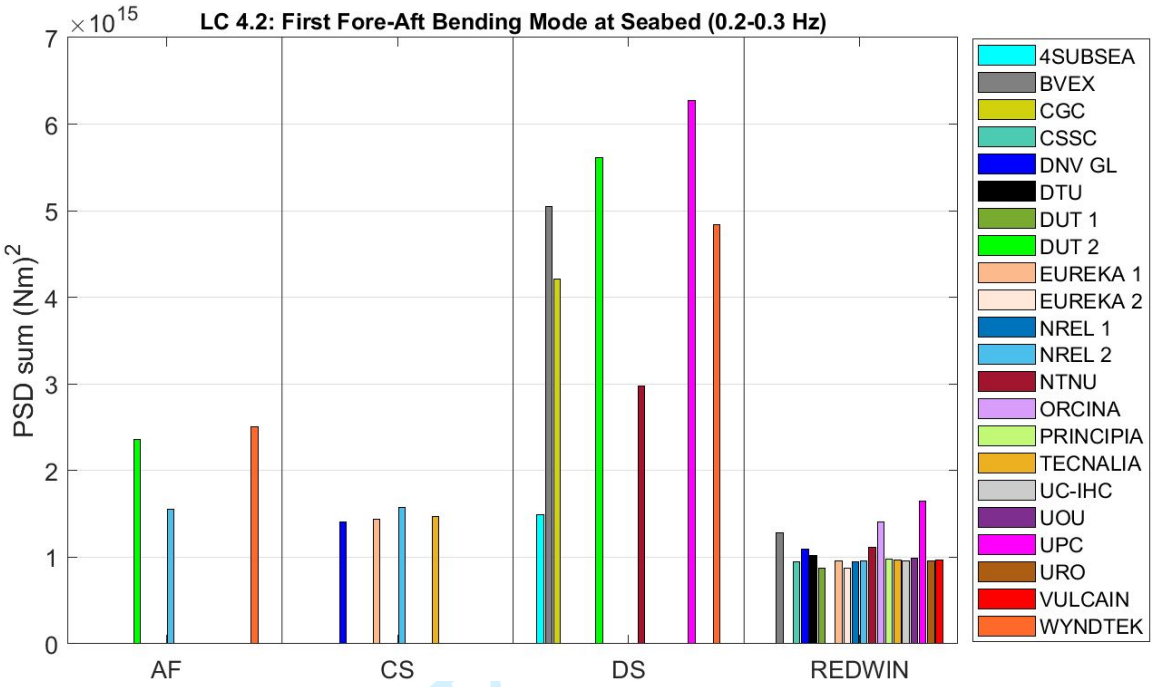

Figure 17. Power spectral density (PSD) sums of the fore-aft bending moment at the seabed in load case (LC) 4.2

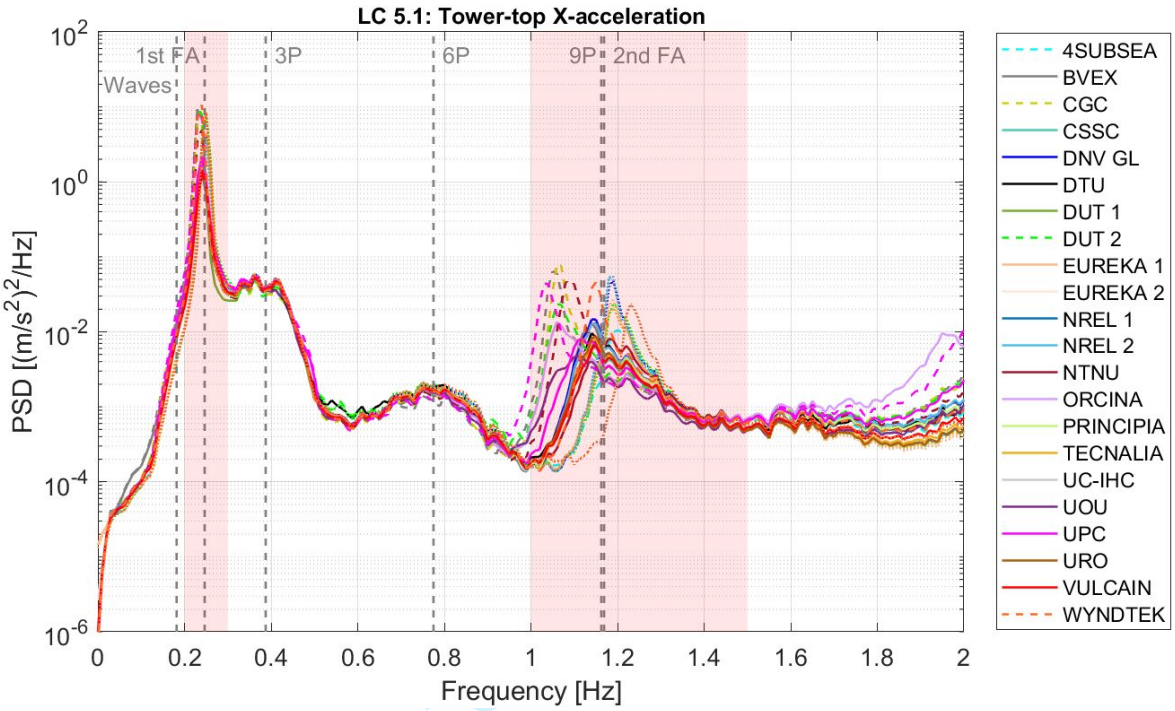

Figure 18. Power spectral density (PSD) of the tower-top X-acceleration in load case (LC) 5.1

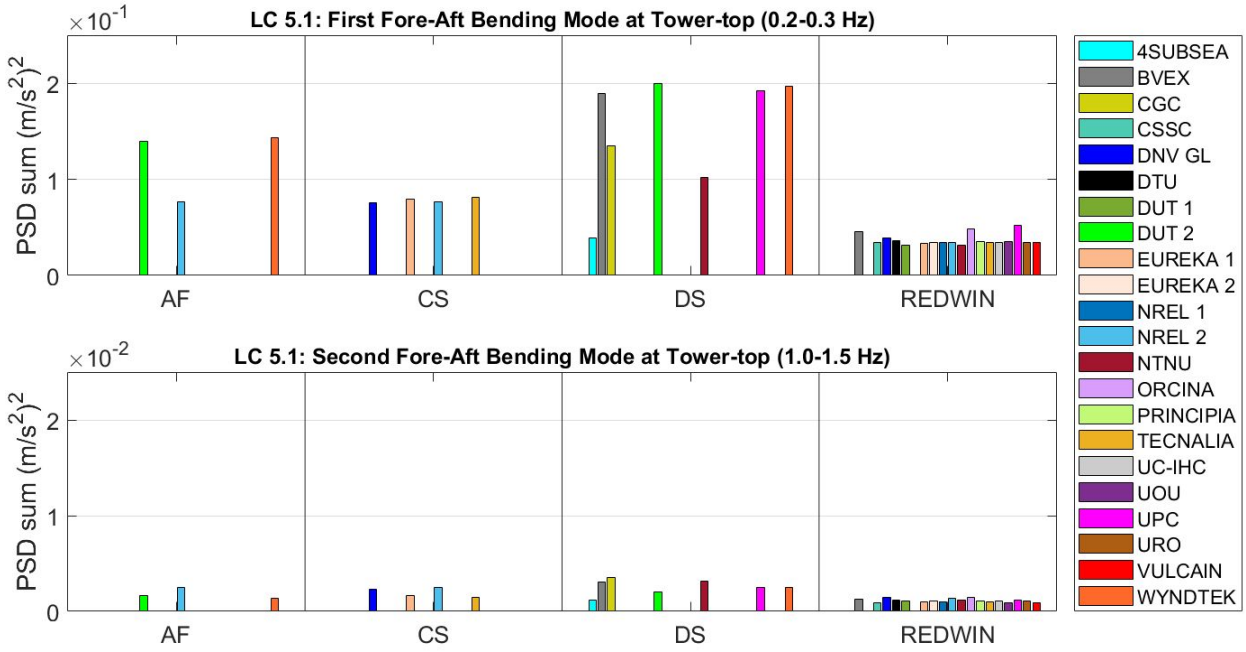

Figure 19. Power spectral density (PSD) sums of the tower-top X-acceleration in load case (LC) 5.1

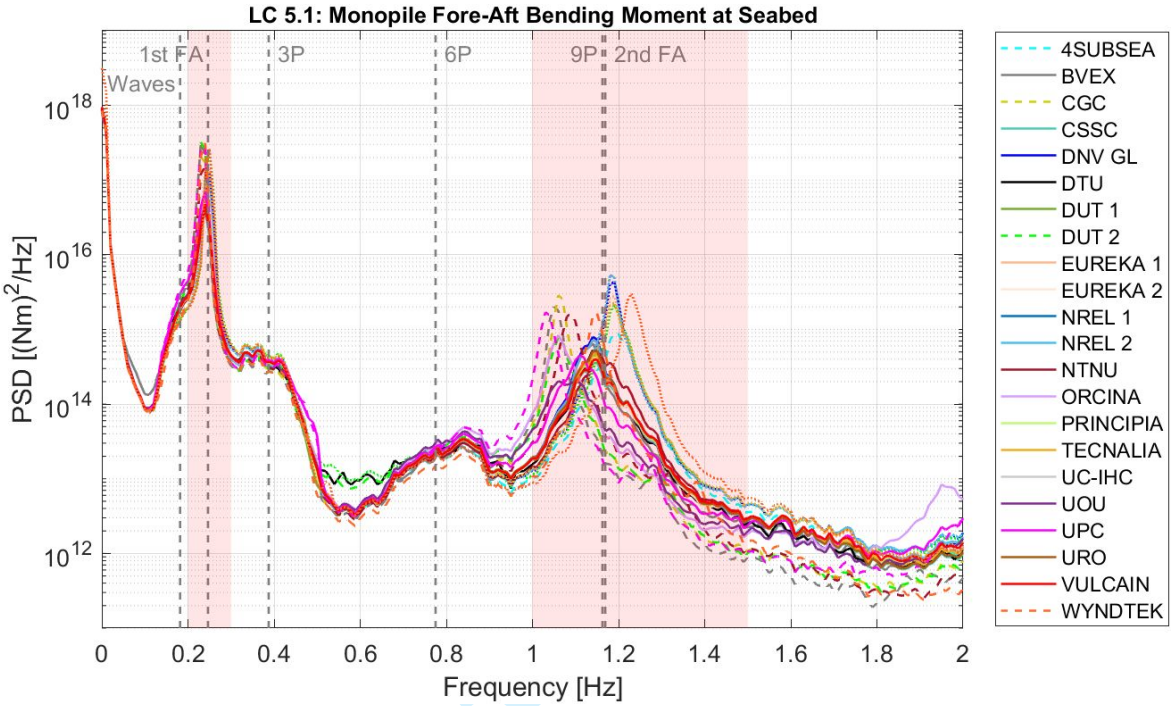

Figure 20. Power spectral density (PSD) of the monopile fore-aft bending moment at the seabed in load case (LC) 5.1

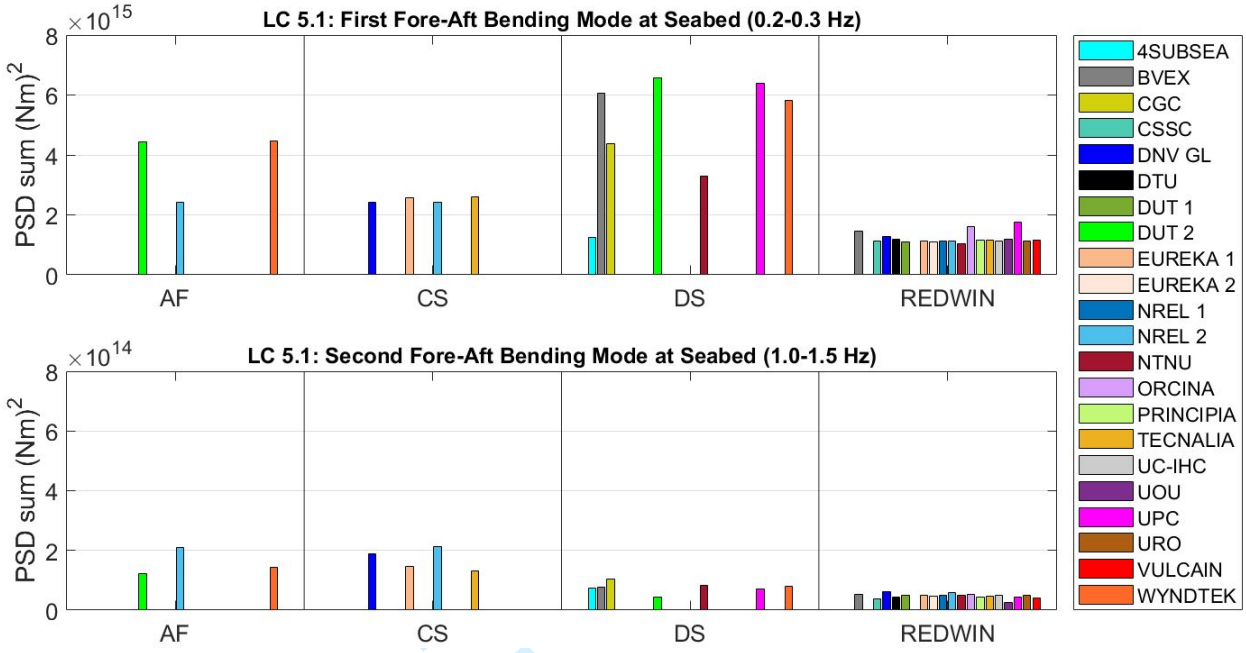

Figure 21. Power spectral density (PSD) sums of the fore-aft bending moment at the seabed in load case (LC) 5.1

Table 1. Rotor-nacelle assembly mass properties

CM: center of mass; I: moments of inertia

Parameter	Value	Description
Mass	839741 kg	Total tower-top mass
CM_x	-5.80 m	Center of mass in X direction from yaw bearing
CM_y	0 m	Center of mass in Y direction from yaw bearing
CM_z	3.19 m	Center of mass in Z direction from yaw bearing
I_{xx}	1.84E8 kg m^2	Moment of inertia around X axis at the center of mass
I_{yy}	9.61E7 kg m^2	Moment of inertia around Y axis at the center of mass
I_{zz}	1.06E8 kg m^2	Moment of inertia around Z axis at the center of mass
$I_{xy} = I_{yx}$	0 kg m^2	XY product of inertia at the center of mass
$I_{xz} = I_{zx}$	-7.11E6 kg m^2	XZ product of inertia at the center of mass
$I_{yz} = I_{zy}$	0 kg m^2	YZ product of inertia at the center of mass

Table 2. Tower and monopile dimensions

Location	Elevation (h) [m]	Outer diameter ($\emptyset_{ext}$) [m]	Wall thickness (t) [mm]
Yaw Bearing	145.63	5.50	30
	134.55	5.79	30
	124.04	6.07	35
	113.54	6.35	45
	103.03	6.63	50
	92.53	6.91	55
	82.02	7.19	60
	71.52	7.46	60
	61.01	7.74	65
	50.51	8.02	70
Tower Base	40.00	8.30	70
Monopile Top	40.00	9.00	110
Mean Sea Level (MSL)	30.00	9.00	110
Seabed	0.00	9.00	110
Monopile Base	-45.00	9.00	110

Table 3. Tower and monopile material properties

Parameter	Value
Young's modulus (E)	210 GPa
Shear modulus (G)	80.8 GPa
Density (ρ)	8,500 kg/m^3
Damping ratio (ζ_1) first bending mode	0.005
Damping ratio (ζ_2) second bending mode	0.010

Table 4. Approximate eigenfrequencies up to 2 Hz for the system clamped at seabed without water

Mode shape	Eigenfrequency [Hz]
First fore-aft bending mode	0.28
First side-side bending mode	0.28
Second fore-aft bending mode	1.44
Second side-side bending mode	1.33
First torsional mode	1.27

Table 5. Summary of participants, codes, and modeling approach used for the soil-structure interaction

Participant	Code	Soil-Structure Interaction Approach			
		AF	CS	DS	REDWIN
4SUBSEA	OrcaFlex			X	
BVEX	Samcef WT			X	X
CGC	Bladed			X	
CSSC	OpenFAST				X
DNV GL	Bladed		X		X
DUT 1	OpenFAST				X
DUT 2	HAWC2	X		X	
DTU	HAWC2				X
EUREKA 1	OpenFAST		X		X
EUREKA 2	OpenFAST				X
NREL 1	OpenFAST				X
NREL 2	OpenFAST	X	X		X
NTNU	SIMA			X	X
ORCINA	OrcaFlex				X[a]
PRINCIPIA	DeepLines Wind				X
TECNALIA	OpenFAST		X		X
UC-IHC	OpenFAST				X
URO	OpenFAST				X
UOU	OpenFAST				X
UPC	FloaWDyn			X	X
VULCAIN	OpenFAST				X
WYNDTEK	Ashes	X		X	

[a]Orcina uses a built-in capability in OrcaFlex with some of the inputs from the REDWIN approach.

Table 6. Offshore Code Comparison Collaboration, Continued, with Correlation and unCertainty (OC6) Phase II load case simulations (summary)

Analysis Type	Load Case	Enabled Degrees of Freedom	Wind Conditions	Marine Conditions	Comparison Type
Static	1.2	Tower, substructure, foundation	None	None	Static response
Eigenanalysis	2.3	Tower, substructure, foundation	None	Still water	Frequencies, damping, and mode shapes
Wind-Only	3.1	Tower, substructure, foundation	Prescribed load time series at yaw bearing V_{hub} = 9.06 m/s	None	Time series (t = 3600 s)
Wave-Only	4.2	Tower, substructure, foundation	None	Irregular waves: Pierson-Moskowitz wave spectrum H_s = 1.25 m, T_p = 5.5 s	Time series (t = 3600 s)
Wind + Waves	5.1	Tower, substructure, foundation	Prescribed load time series at yaw bearing V_{hub} = 9.06 m/s	Irregular waves: Pierson-Moskowitz wave spectrum H_s = 1.25 m, T_p = 5.5 s	Time series (t = 3600 s)

H_s: significant wave height
T_p: peak-spectral wave period
V_{hub}: average hub height wind speed
t: time

Table 7. Prescribed settings for marine conditions

Hydrodynamic forces	Wave kinematics	Seawater density
Relative form of Morison equation (without corrections) Drag coefficient (C_D) = 1 Inertia coefficient (C_M) = 2	Linear (first order) waves No wave stretching No directional spreading	1025 kg/m^3 [8]

OC6 Phase II: Verification of an Advanced Soil-Structure Interaction Model for Offshore Wind Turbines

***Roger Bergua**, *, **Amy Robertson**, **Jason Jonkman**, **Andy Platt**—National Renewable Energy Laboratory, —United States
***Ana Page**—Norwegian Geotechnical Institute, —Norway
***Jacob Qvist**—4Subsea, —Norway
***Ervin Amet**—Bureau Veritas, —France
***Zhisong Cai**—China General Certification Center, —China
***Han Huali**—CSIC Haizhuang Windpower Co., Ltd., —China
***Alec Beardsell**—DNV GL, —United Kingdom
***Wei Shi**—Dalian University of Technology, —China
***Josean Galván**—eureka!, —Spain
***Erin Bachynski-Polić**—Norwegian University of Science and Technology, —Norway
***Gill McKinnon**—Orcina, —United Kingdom
***Violette Harnois**—PRINCIPIA, —France
***Paul Bonnet**—Siemens Industry Software, —Spain
***Loup Suja-Thauvin**—Simis AS, —Norway
***Anders Melchior Hansen**—Technical University of Denmark, —Denmark
***Iñigo Mendikoa Alonso, Ander Aristondo**—Tecnalia, —Spain
***Tommaso Battistella, Raúl Guanche**—Universidad de Cantabria, —Spain
***Paul Schünemann**—University of Rostock, —Germany
***Pham Thanh Dam**—University of Ulsan, —Korea
***Pau Trubat, Daniel Alarcón**—Universitat Politècnica de Catalunya, —Spain
***Florence Haudin, Minh Quan Nguyen**—Vulcain Engineering, —France
***Akhilesh Goveas**—WyndTek, —The Netherlands

*Corresponding author. E-mail address: roger.bergua@nrel.gov
Tel: +1-303-384-7960
15013 Denver West Parkway, Golden, CO 80401, United States.

Abstract

This paper provides a summary of the work done within the OC6 Phase II project, which was focused on the implementation and verification of an advanced soil-structure interaction model for offshore wind system design and analysis. The soil-structure interaction model comes from the REDWIN project, and uses an elasto-plastic, macro-element model with kinematic hardening, which captures the stiffness and damping characteristics of offshore wind foundations more accurately than more traditional and simplified soil-structure interaction modeling approaches. Participants in the OC6 project integrated this macro-element capability to coupled aero-hydro-servo-elastic offshore wind turbine modeling tools and verified the implementation by comparing simulation results across the modeling tools for an example monopile design. The simulation results were also compared to more traditional soil-structure interaction modeling approaches like apparent fixity, coupled springs, and distributed springs models. The macro-element approach resulted in smaller overall loading in the system due to both shifts in the system frequencies and increased energy dissipation. No validation work was performed, but the macro-element approach has shown increased accuracy within the REDWIN project, resulting in decreased uncertainty in

the design. For the monopile design investigated here, that implies a less conservative and thus more cost-effective offshore wind design.

Keywords

Offshore wind, monopile, soil-structure interaction, macro-element, hysteretic damping, OC6

1 Introduction

As the wind industry moves to increasingly larger offshore wind turbines (OWTs) to lower cost, the associated support structures must similarly increase in size. One of the main challenges in designing fixed-bottom systems with large support structures is accurately representing the soil-structure interaction (SSI). The soil reaction is dependent on the foundation movement, and the foundation movement is dependent on the soil reaction. Thus, the SSI directly affects the dynamic response of the OWT system.

The foundation models traditionally used in integrated analysis of OWTs are simplistic and based on several assumptions. Most engineering tools model the foundation according to one of the following approaches: apparent fixity (AF), coupled springs (CS), or distributed springs (DS). The Norwegian Geotechnical Institute (NGI) has developed new macro-element models [1] for the soil-structure interaction in offshore wind turbines that address some of the limitations in these previous models, allowing for a more accurate assessment of the dynamic response for OWTs. This development was done as part of the REDWIN (REDucing cost of offshore WINd by integrated structural and geotechnical design) project [1].

The OC6 (Offshore Code Comparison Collaboration, Continued, with Correlation and unCertainty) Phase II project focuses on integrating the new REDWIN SSI modeling capability into coupled aero-hydro-servo-elastic modeling tools used to design offshore wind systems and verifying the new capability. OC6 is part of an on-going effort under Wind Task 30 of the International Energy Agency (IEA) to verify and validate OWT modeling tools, which originated back in 2005 with the foundational OC3 project (Offshore Code Comparison Collaboration). In the current extension, OC6 is focused on examining specific physical phenomena that are not well represented in present modeling approaches and have a significant impact on their ability to accurately represent OWT loads and performance.

To verify the integration of the new REDWIN SSI capability, participants in OC6 Phase II modeled a monopile offshore wind system examined in the WAS-XL (Wave loads And Soil support for eXtra Large monopiles) project [2], ran a series of simulations, including wind and wave loading, and compared the resulting system loads across different modeling tools. The resulting system loads were also compared to more traditional SSI modeling approaches to assess the level of difference that the macro-element modeling approach has on the global loads of the system. This paper summarizes the work of the OC6 Phase II project, including findings on the improvements the REDWIN model provides.

The organization of the remainder of the paper is as follows. In Section 2, an overview summarizes of the different soil-structure interaction models considered in the project, including the new REDWIN model, are summarized. In Section 3, provides athe definition of the example model that was used to verify the implementation of the new SSI modeling capability is provided. Section

4 provides a description of the active participants involved in OC6 Phase II and the modeling approach used. Section 5 then summarizes the load cases that were performed for the verification study. Finally, Sections 6 and 7 provide some example results from the project~~,~~ and the conclusions drawn.

The modeling information and simulation results from this project will be made available to the public by the end of 2021 through the U.S. Department of Energy Data Archive and Portal, https://a2e.energy.gov/projects/oc6.

2 Soil-Structure Interaction Models

In this section, an overview of the traditional methods for modeling SSI is given, and then the new REDWIN modeling capability is introduced.

2.1 Traditional Methods

The traditional approaches presently used within the offshore wind industry to model SSI rely on the AF, CS, or DS methods. The ~~apparent fixity~~AF method assumes that the substructure is fixed (cantilevered, without surrounding soil) at a depth below the original seabed, with a fixity depth and beam properties determined such that it matches the same lateral displacement and rotation at the seabed as the one resulting from the pile embedded in the true soil profile. The fixity depth and beam properties are dependent on the beam theory used (e.g., Euler-Bernoulli or Timoshenko). However, due to the nonlinear nature of the actual foundation, the response can only be identical under a particular set of conditions. The damping properties of the beams used in the AF method can also be modified to account for the energy dissipation provided by the soil-structure interaction. Using the same structural damping as for the substructure may result in an underestimation of the fatigue lifetime.

The ~~coupled springs~~CS approach replaces the soil with one linear stiffness matrix located at the seabed that accounts for the six rigid-body degrees of freedom (DOFs) (or fewer) of the base of the monopile. This approach can reproduce the same results as the ~~apparent fixit~~AF~~y~~ model and can be extended with a viscous damping matrix to account for the energy dissipated by the foundation.

The ~~distributed springs~~DS approach is the most sophisticated of the three approaches and can be considered the current practice in the wind industry to model soil-pile interaction. This approach was originally developed by the oil and gas industry and it is recommended in many offshore design standards (e.g., Det Norske Veritas (DNV) [3] and the American Petroleum Institute (API) [4]). The method is based on the Winkler modeling approach. It employs uncoupled nonlinear springs represented by *p*-*y* curves to support the pile along the embedded depth. These springs relate the local lateral soil resistance (p) to the local lateral displacement of the pile (y). This relationship is commonly specified as semi-empirical functions based on experimental tests. This approach characterizes four monopile DOFs (radial and bending directions). The vertical and torsional DOFs are usually fixed at the monopile base. It is also possible to add *t*-*z* curves in the vertical direction and torsional springs to define the six DOFs. Dashpot elements in parallel with the springs could be included to account for the foundation damping. This method was originally intended for static analysis, where the foundation response can be captured reasonably well with a non-linear elastic curve, ~~while~~ although the offshore wind industry takes advantage of the approach

to perform dynamic analysis~~,~~ in situations where elastic models might not accurately capture the foundation response.

2.2 REDWIN Macro-Element

The primary objective of the REDWIN project [1] was to develop soil-foundation models that better account for key geotechnical issues such as stiffness, damping, drainage, and degradation. Three soil-foundation models were developed. The models cover the most common foundation types for OWTs and are intended to be used in integrated time-domain simulation tools, where the wind turbine structure itself is the main focus of the analysis.

REDWIN model 1 was developed primarily for piles that are intended to be analyzed by the traditional *p-y* approach. It can be used to model the distributed soil response along a monopile structure, a piled jacket, or the lumped response of a caisson foundation. REDWIN model 2 is a single macro-element intended for monopile foundations. The third model, REDWIN model 3, is a macro-element developed for shallow foundations such as gravity-based and caisson foundations (e.g., for suction bucket jackets).

OC6 Phase II focuses on verifying implementation of the REDWIN capability in participant modeling tools by investigating REDWIN model 2 to describe the response of a pile foundation supporting a monopile-based OWT. The REDWIN model 2 is an elasto-plastic macro-element model with kinematic hardening formulated within the multi-surface plasticity framework [5]. It reduces the foundation and surrounding soil to a set of linear and nonlinear load-displacement relationships in the six DOFs of the interface point (the seabed), separating the foundation and the rest of the structure (see Figure 1). It can represent the nonlinear hysteretic load-displacement response observed in experimental tests and in the field, including the coupled response between horizontal loads and bending moments. The model has been demonstrated to give good agreement with results from finite element analyses of the soil and monopile, results from large-scale pile tests, and results from full-scale field measurements of an OWT installed in the North Sea [5–7].

Aero-hydro-servo-elastic simulation tools are used during the design and certification of wind turbines [8]. During this process, thousands of load cases must be computed and analyzed. This requires these tools to be computationally efficient. In general, these simulation tools use relatively few DOFs, taking advantage of a combined modal and multibody dynamics formulation. Modeling the SSI in the time domain with a 3D finite-element model would require thousands of additional DOFs, which would substantially increase the simulation time of the aero-elastic solver. The REDWIN approach is a CPU efficient way to couple the SSI capability into these tools, using as few degrees of freedom as possible [1], leading to a minimal increase in computational time while providing higher fidelity than the traditional methods (AF, CS, or DS). The macro-element communicates with the wind turbine model through a DLL [~~(~~dynamic link library~~)~~] in a Windows environment or through a shared object in a Linux environment. In each calculation step, the OWT simulation tool provides the displacements and rotations at the seabed to the foundation model, which transfers back the computed forces and moments. The soil-foundation model is solved following an explicit integration algorithm with correction. The model also includes a sub-stepping algorithm, which should help the convergence when the input displacement and/or rotation increment is large.

The macro-element allows for an accurate ~~and computationally efficient~~ representation of the foundation stiffness and hysteretic damping (see Figure 2)~~,~~ crucial to performing reliable fatigue analysis. It is important to note that aerodynamic damping provides the highest contribution to the overall system damping in the fore-aft direction when the wind turbine is operating, ~~however~~ but the aerodynamic damping importance decreases in idling and wind-wave misalignment situations, resulting in increased importance of soil damping [~~8~~9,10].

Figure 2 illustrates how the macro-element model provides different stiffness values during loading (segment O-A-B and B-D), unloading (segment B-C and D-E), and reloading (segment C-B) conditions, as observed in pile tests [~~10~~12]. The area of the loops described by the load-displacement trajectories is indicative of the energy dissipated. It is important to note that the macro-element provides foundation stiffness and energy dissipation independently of the applied loading frequency. The remaining displacement after the cycling loading (distance O-E) is due to the plastic~~ity~~ nature of the system.

REDWIN model 2 requires two inputs from the user from which the macro-element behavior is derived: (1) the coefficients of the elastic stiffness matrix at the seabed, and (2) two load-displacement curves at the seabed from a nonlinear pushover analysis. In addition, a few numerical parameters must be specified. In OC6 Phase II, this information was supplied to the participants [~~11~~13].

3 Verification Model Definition

To verify the integration of the REDWIN SSI approach into coupled OWT modeling tools, an example offshore wind system was modeled from the WAS-XL project [2]. WAS-XL is a project funded by the Norwegian Research Council that aims to reduce the uncertainties in large-diameter monopile design by improving hydrodynamic models for critical design loads and load history-consistent soil support model~~l~~ing procedures.

Aerodynamic models are known to be an important source of differences in wind turbine code-to-code comparisons. In an effort to focus the verification work on the soil-structure interaction behavior, only the support structure was modeled, a lumped mass and inertia were used to represent the rotor-nacelle assembly (RNA), and time histories of lumped forces and moments were applied at the yaw bearing to represent rotor aerodynamics.

The global coordinate system used for defining the OWT design and outputting results is given in Figure 3. The x-axis of the global Cartesian coordinate system points downwind with respect to the main wind and wave direction. The z-axis points upwards and the y-axis forms a right-hand system.

3.1 Rotor-Nacelle Assembly

The RNA is modeled as a lumped mass and inertia at the location indicated in Table 1, which uses the standard wind turbine convention of Figure 3. The properties used can be considered representative of the ones from the IEA-10.0-198-RWT. This reference wind turbine (RWT) is a 10-MW, 198-m rotor diameter, direct-drive design developed as part of IEA Wind Task 37 [1~~2~~4].

On ~~the~~ one hand, the products of inertia I_{xy} and I_{yz} equal to zero reported in Table 1 denote the symmetry about the XZ plane in the system. On the other hand, the product of inertia I_{xz} being different than 0 denotes that the X and Z principal axes of inertia have a different orientation than the global coordinate system (Figure 3).

3.2 Tower

The tower is based on the offshore DTU 10-MW wind turbine design [13~~3~~5]. The tower has a length of 105.63 m, a base outer diameter of 8.30 m with a thickness of 70 mm, and a top outer diameter of 5.50 m with a thickness of 30 mm. The tower base begins at an elevation of 40 m above the seabed (10 m above the mean sea level [~~(~~MSL]~~)~~). The water depth considered is 30 m.

3.3 Monopile

The monopile extends from the tower base with a constant outer diameter of 9 m, a constant thickness of 110 mm, and a penetration depth of 45 m, resulting in a length-to-diameter ratio of 5. The dimensions for the tower and monopile are included in Table 2, the material properties can be found in Table 3, and a schematic representation of the system can be seen in Figure 4. The outer diameter and wall thickness varies linearly between the elevations given in Table 2.

The material density used for the tower and monopile in Table 3 was increased from the default value of 7,850 kg/m^3 to account for mass of secondary structures not otherwise accounted for in the wall thickness. The eigenfrequencies of the system, assuming that the monopile is clamped at the seabed and there is no water, can be found in Table 4. The structural damping considered for the first bending mode ~~-~~when the system is clamped at the seabed and the rigid RNA is placed atop ~~of~~ the tower ~~-~~is 0.5% critical damping. One percent~~1%~~ critical damping is assumed for higher modes (e.g., second bending mode and torsion).

3.4 Soil-Structure Interaction

This section provides the inputs used for the REDWIN macro-element model 2 explained in section 2. The information provided in this section corresponds to the model used in the WAS-XL project [2]. The foundation model was calibrated by NGI [14~~3~~6]. Models for the ~~apparent fixity~~AF ~~method~~, ~~coupled springs~~CS, and ~~distributed springs~~DS methods can be found in the project definition document [11~~3~~3].

The coefficients of the elastic stiffness matrix at the seabed used as an input for the REDWIN macro-element model 2 are provided in Eq. 1.

$$[K_{seabed\ 6x6}] = \begin{bmatrix} 6.336198E9 & 0 & 0 & 0 & -5.015421E10 & 0 \\ 0 & 6.336198E9 & 0 & 5.015421E10 & 0 & 0 \\ 0 & 0 & 1.119691E10 & 0 & 0 & 0 \\ 0 & 5.015421E10 & 0 & 8.111942E11 & 0 & 0 \\ -5.015421E10 & 0 & 0 & 0 & 8.111942E11 & 0 \\ 0 & 0 & 0 & 0 & 0 & 2.552673E11 \end{bmatrix} \quad (1)$$

The stiffness matrix in Eq. 1 accounts for the six DOFs at the seabed and is expressed according to the coordinate system shown in Figure 3. The stiffness matrix includes all diagonal coefficients (K_{11},K_{22}, K_{33}, K_{44}, K_{55}, K_{66}) and horizontal-rotational (K_{15},K_{24}, K_{42}, K_{51}) coupling coefficients. The vertical (K_{33}) and torsional (K_{66}) directions are uncoupled from the other DOFs. The

coefficients are expressed according to the international system of units (N, m, rad). The stiffness matrix is symmetric, which denotes the reciprocity in the system.

The load-displacement curves used as input for the REDWIN macro-element model can also be found in the project definition document [1~~1~~3]. These values were obtained from a nonlinear pushover analyses performed with a quasi-static, three-dimensional FEA [~~(~~finite-element analysis]~~)~~.

4 Participants and Modeling Approach

A total of ~~nineteen~~ 19 academic and industrial partners from 10~~ten~~ different countries actively participated in OC6 Phase II. Those actively involved are: the National Renewable Energy Laboratory (NREL, ~~(~~USA), 4Subsea (Norway), Bureau Veritas (BVEX~~–~~, France), China General Certification Center (CGC~~–~~, China), CSIC Haizhuang Windpower Co., Ltd (CSSC~~–~~, China), DNV GL (United Kingdom), Dalian University of Technology (DUT, ~~–~~China), eureka! (Spain), Norwegian University of Science and Technology (NTNU, ~~–~~Norway), Orcina (United Kingdom), PRINCIPIA (France), Technical University of Denmark (DTU~~–~~, Denmark), Tecnalia (Spain), Universidad de Cantabria (UC-IHC~~–~~, Spain), University of Rostock (URO~~–~~, Germany), University of Ulsan (UOU, ~~–~~Korea), Universitat Politècnica de Catalunya (UPC, ~~–~~Spain), Vulcain Engineering (France), and WyndTek (The Netherlands).

A list of the participants and the tools used in this study is provided in Table 5, which also shows the modeling approach employed.

As ~~it can be observed in~~ Table 5 shows, some participants decided to use more than one modeling approach and some used different codes. NREL used two different OpenFAST models (NREL 1 and NREL 2). NREL 1 models the tower by means of Euler-Bernoulli beams that account for the bending DOFs (ElastoDyn module) while NREL 2 models the tower by means of Timoshenko beams that account for axial, shear, bending, and torsion DOFs (SubDyn [1~~5~~7] module). A similar approach was adopted by eureka!. The EUREKA 1 model is equivalent to NREL 1 and ~~the~~ EUREKA 2 is equivalent to ~~the~~ NREL 2. The rest of the participants using OpenFAST adopted the same modeling approach as ~~the~~ NREL 1 ~~model~~.

There are three participants using the ~~apparent fixity~~AF method: DUT 2, NREL 2, and WyndTek. The fixity depth and beam properties for this approach must be determined according to the beam theory used. NREL 2 and DUT 2 use Timoshenko beam elements ~~while~~ and WyndTek uses Euler-Bernoulli beams. Accordingly, NREL 2 and DUT 2 use the ~~apparent fixity~~AF properties specified in the project definition document [1~~1~~3], and WyndTek uses the properties corresponding to the improved ~~apparent fixity~~AF method.

The participants modeling the SSI by means of the ~~coupled springs~~CS method use the stiffness matrix from Eq. 1 and the participants using the ~~distributed springs~~DS approach use 61 discrete nonlinear springs defined every 0.75 m along the monopile. Each spring is defined by 22 pairs of *p-y* points. The numerical values of these *p-y* curves are available in the project definition document [1~~1~~3].

The ~~apparent fixity~~AF, ~~coupled springs~~CS, and ~~distributed springs~~DS approaches do not account for the SSI damping by default. To inform these methods, the equivalent SSI damping from the

REDWIN approach was characterized at different loading levels by means of free-decay tests [11~~3~~]. 4Subsea is the only participant using a traditional method (AF, CS, or DS) that includes damping for the SSI. 4Subsea includes viscous damping in the ~~distributed springs~~DS approach through dashpots with a constant damping coefficient in parallel with the springs. The damping coefficient is the same for all the dashpots and the same regardless of the loading condition. It is important to note that this viscous damping is proportional to the velocity while the hysteretic damping in the REDWIN approach is dependent on the displacement time history. The hysteretic damping of the REDWIN approach is also nonlinear; larger amplitudes translate into larger energy dissipated [11~~3~~].

Some participants decided to use some built-in capabilities in their codes to study the system. For example, Orcina uses a nonlinear hysteretic stiffness model available in OrcaFlex. In this case, only the diagonal positions of the stiffness matrix are populated. The nonlinear horizontal (K_{11},K_{22}) and rotational (K_{44}, K_{55}) DOFs are defined according to the two load-displacement curves at the seabed from the nonlinear pushover analyses used as input for the REDWIN approach. The vertical (K_{33}) and torsional (K_{66}) DOFs are characterized based on the elastic stiffness matrix (see Eq. 1). Although this approach results in a hysteretic behavior in the horizontal and rotational DOFs, these directions are uncoupled because the stiffness matrix used does not include cross-coupling coefficients. To avoid this, the location of the stiffness matrix is placed at a point along the monopile longitudinal axis below the seabed that induces a coupling between the horizontal and rotational directions.

5 Verification Methodology

Similar to the OC3 [1~~6~~8], OC4 [1~~7~~9,~~18~~20], and OC5 [~~19~~21–~~23~~5] projects, a stepwise verification procedure was performed in the OC6 Phase II project. The model complexity is increased one step at a time to facilitate the identification of modeling discrepancies introduced by different theories and/or model implementations in the various codes. Table ~~7~~6 provides a summary of the simulations that are presented in section 6~~were performed~~, ~~which includes~~including static simulations (1.X), eigen-analyses (2.X), wind-only simulations (3.X), wave-only simulations (4.X), and combined wind/wave simulations (5.X). The complete list of load cases studied can be found in the project definition document [13].

~~5.1 Load Case 1.X – Static Simulations~~

~~Load caseC 1.1 and load case LC 1.2 focus on ensuring that the structural model was implemented correctly by examining the static loads and deflections of the system with the gravity acceleration as the only external loading. Load caseC 1.3 includes one horizontal force (= 1500 kN) at the yaw bearing (tower-top) representative of the mean thrust force at rated wind speed for the IEA-10.0-198-RWT [12].~~

~~5.2 Load Case 2.X – Eigena-Analyses~~

~~Load caseC 2.X furthers the examination of the structural model by assessing the system eigenfrequencies, damping values, and mode shapes for three configurations: including/excluding the foundation, and also including/excluding still water. The method for assessing the eigen-properties around the static equilibrium was up to the participant, and can be accomplished using~~

a linearization methodology in the modeling tool, through a free-decay simulation, or through a broad-band wind or wave excitation.

5.3 Load Case 3.X — Wind-Only Simulations

Load caseC 3 – 5 then focus on assessing the response loads and motions of the full monopile-based OWT when considering wind and wave loading separately, and then in combination. The environmental conditions are representative of a 30-m water depth site at the Norwegian Continental Shelf [8].

As commented noted in section 3, the computational models account for the support structure and a lumped mass and inertia for the RNA. The wind loading for load cases 3 and 5 (see Table 7) was computed beforehand, and was applied as external force and moment time histories by participants at the yaw bearing. The force was calculated by NREL using an aeroelastic model of the IEA-10.0-198-RWT with turbulent wind. The IEA-10.0-198-RWT is an IEC [(International Electrotechnical Commission]) class IA [12] wind turbine. Accordingly, the turbulent winds use the IEC Kaimal wind spectrum [24] with turbulence according to the normal turbulence model (NTM) for Class A turbines. The wind shear power law exponent used is $\alpha = 0.14$ [24]. The loads at the yaw bearing location are obtained by means of simulations that consider the structural components of the wind turbine (i.e., support structure, drivetrain, and blades) as rigid and do not account for the gravity acceleration. In this way, the inertial and gravity loads are disregarded and the computed loads can be considered as externally applied loads. The participants can then account for the gravity and inertia loading in their simulation tools and prescribe these time series of loads as non-follower loads at the yaw bearing location.

Load caseC 3.X focuses on wind-only load cases. Load caseC 3.1 considers a mean wind speed at hub height () of 9.06 m/s. This wind speed is below the rated wind speed of 10.75 m/s [12] for the IEA-10.0-198-RWT. Load caseC 3.2 examines the system response for a mean wind speed of 20.90 m/s.

It is important to note that the responses from load cases that involve wind (i.e., load caseLC 3.1X and load caseLC 5.X1) are used for verification purposes, but cannot be considered representative of a real wind turbine in operating conditions due to the lack of aerodynamic damping in the models used in this code-to-code verification.

5.4 Load Case 4.X — – Wave-Only Simulations

Load caseC 4.X focuses on wave-only load cases. With a focus on the soil-structure interactionSSI model, a simple modeling approach was used for the hydrodynamic forces. Table 6 provides the settings that were used for the load cases that involve marine conditions to try to replicate the same input loading across participants and simulation tools.

Load caseC 4.1 analyzes the response of the system under regular wave conditions, whereas LC load cases 4.2 and 4.3 focus on irregular waves with the latter focused on a storm condition in the North Sea [25].

~~5.5 Load Case 5.X — – Combined Wind and Waves~~

~~Load caseC 5.1 combines the wind conditions proposed in load caseLC 3.1 with the Pierson-Moskowitz wave spectrum analyzed in LC load case 4.2. Load caseC 5.2 combines the wind conditions proposed in load caseLC 3.2 with a JONSWAP wave spectrum.~~

6 Selected Results

In this section, a comprehensive overview ~~of some~~ of the studied load cases shown in Table ~~7~~6 is presented and explained.

6.1 Static Simulations Results: Load Case 1.2

Load case 1.2 focus on ensuring that the structural model was implemented correctly by examining the static loads and deflections of the system with the gravity acceleration as the only external loading.

Figure 5 shows the tower-top (yaw bearing) displacement along the *x*-axis (fore-aft direction) under gravity-only conditions (load case~~LC~~ 1.2). This displacement is the result of the overhanging weight of the RNA (see Table 1) and it is affected by the SSI stiffness. The dashed black line shows the average displacement from all participants and it can be used as a reference to compare the different solutions.

As ~~it can be observed~~Figure 5 shows, the linear SSI approaches (AF and CS) result in smaller tower-top displacements. These linear approaches were characterized based on the unloaded state (see Eq. 1) and behave slightly stiffer than the nonlinear SSI approaches. Interestingly, WyndTek AF using the improved ~~apparent fixity~~AF method (Euler-Bernoulli beams) and NREL 2 AF using the ~~apparent fixity~~AF method (Timoshenko beams) produce the same displacement. The tower-top displacements for the DS approach are slightly bigger due to the nonlinearity of the *p-y* curves. Finally, the REDWIN shows slightly larger displacements than the DS approach because it accounts for the nonlinear stiffness and plasticity. Not all the simulation tools are able to perform a static analysis or gradually apply the gravity acceleration in a quasi-static fashion. Accordingly, some participants perform a transient analysis where the gravity acceleration is suddenly applied over the system at the beginning of the simulation. This results in an initial transient loading that can induce a small level of plasticity. ~~This plasticity depends on the initial transient in the simulation.~~ Therefore, REDWIN solutions using an initial static computation or a gradual loading result in slightly smaller displacements closer to the DS approach.

6.2 Eigena-Analysis Results: Load Case 2.3

Load case 2.3 furthers the examination of the structural model by assessing the system eigenfrequencies, damping values, and mode shapes. Figure 6 and Figure 7 show the system eigenfrequencies for the first and second bending modes in the fore-aft direction. These outputs are from ~~LC~~ load case 2.3, which includes foundation flexibility and still water conditions. For reference, the plots include a grey dashed line with the average result when the foundation is considered rigid (i.e., clamp at seabed) and there are no marine conditions (i.e., no water). These average results were obtained from the results provided by the participants in load case~~LC~~ 2.1 (see the project definition document [13] for reference) and are aligned with the numerical values from

Table 4. The black dashed line denotes the average solution when accounting for the foundation flexibility and marine conditions (i.e., still water).

As ~~it can be observed in~~ Figure 6 shows, the first bending mode drops around 10% in frequency due to the flexible foundation. The water does not have a significant impact for the first bending mode in this system. For the second bending mode (Figure 7), the drop in frequency is around 20% on average. The main reason for this drop in frequency is also the foundation flexibility, but the added mass from the still water is also noticeable. In the studied system and for all load cases, the monopile does not have water inside. Having the monopile filled with water would decrease these eigenfrequencies further.

There is a good agreement between participants for the first bending mode in the fore-aft direction. The linear approaches (AF and CS) behave slightly stiffer than the DS approach as expected and observed during the static analysis (i.e., load case~~LC~~ 1.2). A similar trend can be observed in Figure 7 for the second bending mode. It is also interesting to note that in this second bending mode, the agreement between participants is not as good as for the first bending mode. One of the reasons for the dispersion in the eigenfrequencies between participants using the same SSI approach is the method used to extract the eigen-properties around the static equilibrium. Some simulation tools used by the participants include a linearization capability, while other participants without this functionality tried to obtain these properties from time-domain simulations (e.g., by means of a free-decay test or a broad-band wind or wave excitation). For example, Figure 7 shows some significant differences between some of the participants using the REDWIN approach. However, when post-processing the time-domain results of load case~~LC~~ 5.X in the frequency domain, these differences were not observed (see, e.g., Figure 18 and Figure 20). Extracting the eigen-properties of a model using the REDWIN approach can be challenging due to the nonlinear nature of the system.

Figure 8 shows the associated eigenvectors of the first and second bending modes in the fore-aft direction. The eigenvectors are normalized by their maximum amplitude to allow the comparison between participants.

As expected, the largest amplitude for the first bending mode is located at the tower--top. As seen in ~~it can be observed~~Figure 8, the agreement between the participants is very good regardless of the SSI approach used. For the second bending mode, the maximum amplitude occurs at ~~around~~ about two--thirds of the support structure height. In this case, all the participants using the DS approach have slightly more deflections at the seabed (h = 0 m).

6.3 Wind-Only Simulations Results: Load Case 3.1

After analyzing the static cases and the eigen-properties of the system, the response under wind-only conditions was studied. The environmental conditions in load cases 3-5 are representative of a 30-m water depth site at the Norwegian Continental Shelf [10].

As noted in section 3, the computational models account for the support structure and a lumped mass and inertia for the RNA. The wind loading in the six DOFs for load cases 3.1 and 5.1 (see Table 6) was computed beforehand by NREL, and was applied as external force and moment time histories by participants at the yaw bearing (see the project definition document [13] for further details).

~~The wind loading in the six DOFs was computed beforehand by NREL and applied as an external load by participants at the yaw bearing.~~

Load case~~C~~ 3.1 is a wind-only load case and considers a mean wind speed at hub height (V_{hub}) of 9.06 m/s. This wind speed is below the rated wind speed of 10.75 m/s [14] for the IEA-10.0-198-RWT. ~~(~~Under these conditions, the wind turbine is rotating ~~around~~ at about 7.75 rpm ~~(below rated speed)~~. The aeroelastic model used to compute the externally applied loads did not include any rotor imbalance (e.g., no mass nor aerodynamic imbalance). Accordingly, the only excitations present in the computed loads correspond to the blade passing frequency (3P for a three-bladed wind turbine) and the corresponding harmonics (e.g., 6P and 9P), where P is the rotor speed.

The power spectral density (PSD) of the tower-top acceleration along the *x*-axis (fore-aft direction) is shown in Figure 9. The main excitations (i.e., 3P, 6P, and 9P) as well as the eigenfrequencies (i.e., first and second fore-aft bending modes) are also included with vertical dashed lines in the figure. The eigenfrequencies are marked according to the average solution from all participants in load case~~LC~~ 2.3 (Figure 6 and Figure 7). It is important to note that load case~~LC~~ 2.3 includes the marine conditions ~~while~~ but load case~~LC~~ 3.1 does not. However, the same vertical lines were used for the eigenfrequencies for an easier comparison against the results from load case~~LC~~ 5.~~X~~1.

Different line styles are used in the spectrum to compare the different approaches. The solutions using a linear SSI approach (AF or CS) are denoted with a dotted line, the ones using the DS approach are denoted with a dashed line, and the ones using the REDWIN approach are denoted with a solid line. In the legend, participants using different modeling approaches appear with the line style associated with~~to~~ its highest model fidelity used (REDWIN ~~>~~ DS ~~>~~ AF ~~|~~ CS).

For this loading condition, the 9P excitation is virtually at the same frequency as the second fore-aft bending mode. This resonance can lead to increased levels of structural activity at this frequency.

The agreement between participants for the first fore-aft bending mode eigenfrequency is very good with only some differences in terms of amplitude. For the second fore-aft bending mode, some differences in terms of frequency can be observed. The linear SSI approaches (AF and CS) show the stiffest behavior and the DS approach the softest. For this second bending mode, the DS approach also has the largest amplitude.

To more systematically compare the response between participants and modeling approaches, the PSD sum (Eq. 2) is computed based on the one-sided, unsmoothed, discrete power density functions~~:~~.

$$S_{sum} = \sum_{i=j}^{k} S_{resp}(f_i)\Delta f \quad (2)$$

where $S_{resp}(f_i)$ is the discrete PSD amplitude at frequency f_i, Δf is the frequency resolution, j and k are the indices of the first and last frequency of interest. This PSD sum is equivalent to the integral of the PSD for a given frequency range. For reference, the square root of this PSD sum is equivalent to the root mean square (RMS) for the frequency range of interest.

Two PSD sum magnitudes are computed to analyze the results in more detail: one for the frequency range between 0.2 and 0.3 Hz and the other between 1.0 and 1.5 Hz. These two frequency ranges are marked with two red rectangles in Figure 9 and can be considered indicative of the first and second fore-aft bending mode responses. Figure 10 shows the PSD sums for the different participants according to the SSI approach used. ~~t~~The y-axis scale for the first frequency range (0.2~~–~~0.3 Hz) is one order of magnitude higher than for the second frequency range (1.0~~–~~1.5 Hz) to highlight the relative importance of the first bending mode response compared to the second bending mode.

For the first fore-aft bending mode, the largest response corresponds to the linear SSI approaches. These linear approaches result in a slightly stiffer system, which places the first structural mode closer to the 3P excitation. The DS approach has a smaller response than the linear SSI approaches, but a larger response than the REDWIN due to the lack of damping. For the second fore-aft bending mode, the smallest response also corresponds to the REDWIN approach. 4Subsea also uses the DS approach, but it includes SSI damping. By including this damping, the response is the smallest ~~between~~ of the DS solutions for the first and second fore-aft bending modes and is at a level that is quite similar to the REDWIN approach. The results across the REDWIN solutions are very similar, showing~~;~~ comparable trends ~~are seen~~ for the remaining load cases.

Figure 11 shows the monopile fore-aft bending moment at the seabed and Figure 12 the associated PSD sums. The main difference in this case is the behavior at 0 Hz. This amplitude is indicative of the signal average; the mean fore-aft bending moment at the seabed in this case. This mean value is mainly driven by the aerodynamic thrust force acting over the system. For the acceleration, the mean value will always be zero.

6.4 Wave-Only Simulations Results: Load Case 4.2

Load case 4.2 analyzes the response of the system under irregular waves. Load case 4.2 is a wave-only load case. With a focus on the SSI model, a simple modeling approach was used for the hydrodynamic forces. Table 7 provides the settings that were used for the load cases that involve marine conditions to try to replicate the same input loading across participants and simulation tools.

Figure 13 shows the wave elevation spectrum in load case~~LC~~ 4.2. The peak-spectral wave frequency ($1/T_p$), as well as the first fore-aft bending mode~~,~~ are also included in the figure with vertical dashed lines. The frequency range between 0.1 and 0.5 Hz contains most of the energy in the wave spectrum. This wave-only condition can only excite the first bending mode of the structure.

Figure 14 and Figure 16 show the PSD of the tower-top acceleration along the x-axis and the monopile fore-aft bending moment at the seabed. Figure 15 and Figure 17 show the associated PSD sums for the frequency range between 0.2 and 0.3 Hz, representative of the first fore-aft bending mode response. The line styles, output locations, and ~~the~~ post-processing in terms of PSD sums are the same as the one presented for the wind-only conditions. In this case, the largest response occurs for the DS approach and it is likely due to the slightly lower frequency compared to the other solutions. This lower frequency locates the structural mode in a region where the wave energy is higher. As already observed in the wind-only condition, 4Subsea also uses the DS approach but the response is more aligned with the REDWIN solution. For this participant, the

first bending mode is slightly higher in terms of frequency than the other DS solutions (observed in Figure 14) and the SSI accounts for damping.

6.5 Combined Wind and Waves: Load Case 5.1

~~LC~~ Load case 5.1 combines the wind conditions studied and presented in load case~~LC~~ 3.1 with the Pierson-Moskowitz wave spectrum analyzed in load case~~LC~~ 4.2. Figure 18 shows the PSD of the tower-top acceleration along the *x*-axis and Figure 19 the corresponding PSD sums. Figure 18 can be compared to the one from the wind-only condition (Figure 9). As it ~~can be observed~~shows, the two main differences between the wind-only and the wind/wave conditions are the response amplitude for the first fore-aft bending mode and the slight frequency shift for the second fore-aft bending mode. The amplitude of the first fore-aft bending mode is higher due to the wave excitation. The drop in frequency for the second fore-aft bending mode is due to the added mass term from the water. The PSD sums for this load case are mainly the result of the superposition of the PSD sums from the wind-only and wave-only conditions.

Figure 20 shows the monopile fore-aft bending moment at the seabed and Figure 21 the associated PSD sums. Similar to the wind-only and wave-only conditions, the response of the REDWIN approach is the smallest for the first and second fore-aft bending modes. Also, the response of the DS with damping (4Subsea) is quite similar to the one from the REDWIN approach.

7 Conclusions

During the OC6 Phase II project, the REDWIN modeling capability was coupled to a variety of offshore wind modeling tools. The new capability was verified across different tools and against industry standard methods for an example monopile offshore wind system (DTU 10-MW wind turbine). Two linear (~~apparent fixity~~AF and ~~coupled springs~~CS) and two nonlinear (~~distributed springs~~DS and REDWIN) soil-structure interaction approaches were used during this code-to-code verification.

The REDWIN macro-element approach differs from traditional methods in the inclusion of plasticity and hysteretic damping. It requires more elaborate inputs (e.g., stiffness matrix and load-displacement curves at the seabed) to characterize the ~~soil-structure interaction~~SSI. However, it models the hysteretic damping internally. This is a great advantage because the energy dissipated by the ~~soil-structure interaction~~SSI is not easy to quantify and include in a numerical model. On the one hand, traditional methods have often employed a viscous damping matrix at the seabed or dashpot elements along the monopile with viscous damping. In these cases, the damping forces are proportional to the velocity. On the other hand, the hysteretic damping included in the REDWIN macro-element is dependent on the displacement trajectories. This hysteretic damping is inherently nonlinear: larger displacement loops result in ~~larger~~ more energy dissipated. The differences between these two damping approaches would be especially noticeable at high frequency ranges, where the displacements are relatively small, but the velocities are high. The proper characterization of this soil damping is especially important in idling and wind-wave misalignment conditions.

The support structure loads at the first and second bending mode are the smallest when using the REDWIN macro-element compared to the other modeling approaches, for all load cases analyzed. This would mean a lower fatigue estimate using the REDWIN model. ~~While~~ Although no

validation was done here to assess the accuracy of the REDWIN capability, this validation was achieved within the REDWIN project and the lower fatigue estimate would mean that OWT designs could remove some conservancy. The differences observed in the loads between the REDWIN and the traditional methods are mainly due to small differences in terms of system eigenfrequencies because of the foundation flexibility and the lack of damping defined in the traditional approaches.

Across the different tools that have integrated in the REDWIN modeling approach, very similar results were seen for all load cases. This verifies the accurate implementation of the REDWIN capability in these tools, making them ready for use in the design of future OWT systems.

Acknowledgments

The authors would like to thank the Norwegian Geotechnical Institute for their work in the REDWIN project to develop the capability being incorporated in OC6 Phase II and, to provide the data to model the foundation, and as well as for their ongoing support. We would also like to thank the Norwegian University of Science and Technology for their support in developing the model for this project.

This work was authored in part by the National Renewable Energy Laboratory, operated by Alliance for Sustainable Energy, LLC, for the U.S. Department of Energy (DOE) under Contract No. DE-AC36-08GO28308. Funding provided by the U.S. Department of Energy Office of Energy Efficiency and Renewable Energy Wind Energy Technologies Office. The views expressed in the article do not necessarily represent the views of the DOE or the U.S. Government. The U.S. Government retains and the publisher, by accepting the article for publication, acknowledges that the U.S. Government retains a nonexclusive, paid-up, irrevocable, worldwide license to publish or reproduce the published form of this work, or allow others to do so, for U.S. Government purposes.

References

1. REDWIN (–Reducing cost of offshore wind by integrated structural and geotechnical design). 3D Foundation Model Library. https://www.ngi.no/eng/Projects/REDWIN-reduce-wind-energy-cost/#Reports-and-publications. Accessed: 2020-03-23.
2. Velarde, J., and Bachynski, E.E., 2017. Design and fatigue analysis of monopile foundations to support the DTU 10 MW offshore wind turbine. *Energy Procedia*. 2017;–137:, pp.3––13. https://doi.org/10.1016/j.egypro.2017.10.330.
3. DNV (Det Norske Veritas). 2014.–DNV-OS-J101 - Design of Offshore Wind Turbine Structures. Oslo: Det Norske Veritas. 2014. https://rules.dnv.com/docs/pdf/dnvpm/codes/docs/2014-05/Os-J101.pdf.
4. API (American Petroleum Institute). 2010.–RP 2A-WSD - Recommended Practice for Planning, Designing and Constructing Fixed Offshore Platforms. 20104.– Washington, D.C.: American Petroleum Institute.
5. Page, A.M., Grimstad, G., Eiksund, G.R., and Jostad, H.P., 2019. A macro-element model for multidirectional cyclic lateral loading of monopiles in clay. *Comput Geotech*Computers and Geotechnics. 2019;–106:, pp.314––326. https://doi.org/10.1016/j.compgeo.2018.11.007.

6. Page, A.M., Grimstad, G., Eiksund, G.R., and Jostad, H.P., 2018. A macro-element pile foundation model for integrated analyses of monopile-based offshore wind turbines. *Ocean Eng Ocean Engineering*. 2018; , 167:, pp.23–35. https://doi.org/10.1016/j.oceaneng.2018.08.019.

7. Page, A.M., Næss, V., De Vaal, J.B., Eiksund, G.R., and Nygaard, T.A., 2019. Impact of foundation modelling in offshore wind turbines: Comparison between simulations and field data. *Mar Struct.* Marine Structures, 2019; 64, pp.:379–400. https://doi.org/10.1016/j.marstruc.2018.11.010.

8. IEC (International Electrotechnical Commission)., 2009. Wind energy generation systems – Part 3-1: Design requirements for offshore wind turbines. International Electrotechnical Commission, Geneva, Switzerland. 20019.

9. Malekjafarian, A., Jalilvand, S., Doherty, P., and Igoe, D., 2021. Foundation damping for monopile supported offshore wind turbines: A review. 2021. *Mar Struct.* 2021; Marine Structures, 77, p.:102937. https://doi.org/10.1016/j.marstruc.2021.102937.

9.10. Katsikogiannis, G., Bachynski, E.E. and , Page, A.M., 2019, October. Fatigue sensitivity to foundation modelling in different operational states for the DTU 10MW monopile-based offshore wind turbine. *In J Phys Conf Ser* Journal of Physics: Conference Series. 2019; (Vol. 1356, No. (1):, p. 012019). IOP Publishing. October. DOI:10.1088/1742-6596/1356/1/012019.

10.11. Page, A.M., Grimstad, G., Eiksund, G.R., and Jostad, H.P., 2018. A macro-element pile foundation model for integrated analyses of monopile-based offshore wind turbines. *Ocean Eng.* Ocean Engineering, 2018; 167:, pp.23–35. https://doi.org/10.1016/j.oceaneng.2018.08.019.

11.12. Byrne, B.W., McAdam, R., Burd, H.J., et al. Houlsby, G.T., Martin, C.M., Zdravkovic, L., Taborda, D.M.G., Potts, D.M., Jardine, R.J., Sideri, M. and Schroeder, F.C., 2015. New design methods for large diameter piles under lateral loading for offshore wind applications. In: *Frontiers in offshore geotechnics III*., 2015:, pp.705–710. 2015. June. DOI:10.1201/b18442-96.

12.13. TBDBergua, R., Robertson, A., Jonkman, J., and Platt, A., 2021. Specification Document for Offshore Code Comparison Collaboration, Continued, with Correlation and unCertainty (OC6) Phase II: Verification of an Advanced Soil-Structure Interaction Model for Offshore Wind Turbines (No. NREL/TP-5000-79938). National Renewable Energy Laboratory (NREL), Golden, CO (United States). 2021. https://www.nrel.gov/docs/fy21osti/79938.pdf.

13.14. Bortolotti, P., Canet Tarres, H. Canet., Dykes, K.L., Merz, K., Sethuraman, L., Verelst, D., and Zahle, F., 2019. IEA Wind TCP Task 37: Systems Engineering in Wind Energy-WP2. 1 Reference Wind Turbines. 2019. https://www.nrel.gov/docs/fy19osti/73492.pdf

14.15. Anaya-Lara, O., Tande, J.O., Uhlen, K., and Merz, K. (2020). Appendix. In: Anaya-Lara O, Tande JO, Uhlen K, Merz K, eds. *Offshore Wind Energy Technology* (eds O. Anaya-Lara, J.O. Tande, K. Uhlen and K. Merz). 2020. https://doi.org/10.1002/9781119097808.app. doi:10.1002/9781119097808.app

15.

16. Sivasithamparam, N., Misund, B., Page, A., and Løkke, A., 2020. Implementation of REDWIN models in OC6 [Offshore Code Comparison Collaboration, Continued, with Correlation and unCertainty] (Doc. 20190610-01-TN). 2020.

17. Damiani, R., Jonkman, J., and Hayman, G., 2015. SubDyn User's Guide and Theory Manual (No. NREL/TP-5000-63062). National Renewable Energy Laboratory (NREL), Golden, CO (United States). 2015. https://www.nrel.gov/wind/nwtc/assets/downloads/SubDyn/SubDyn_Manual.pdf.

18. Jonkman, J., and Musial, W., 2010. Offshore Ceode Ceomparison Ceollaboration (OC3) for IEA Wind Task 23 Ooffshore Wwind Ttechnology and Ddeployment (No. NREL/TP-5000-48191). National Renewable Energy Laboratory (NREL), Golden, CO (United States). 2010. https://www.nrel.gov/docs/fy11osti/48191.pdf.

19. Popko, W., Vorpahl, F., Zuga, A., et alKohlmeier, M., Jonkman, J., Robertson, A., Larsen, T.J., Yde, A., Saetertro, K., Okstad, K.M. and Nichols, J., 2012. Offshore Ceode Ceomparison Ceollaboration Ceontinuation (OC4), Phase I—R-results of Ceoupled Ssimulations of an Ooffshore Wwind Tturbine with Jjacket Ssupport Sstructure (No. NREL/CP-5000-54124). National Renewable Energy Laboratory (NREL), Golden, CO (United States). 2012. https://www.nrel.gov/docs/fy12osti/54124.pdf.

20. Robertson, A., Jonkman, J., Musial, W., Vorpahl, F., and Popko, W., 2013. Offshore code comparison collaboration, continuation: Phase II results of a floating semisubmersible wind system (No. NREL/CP-5000-60600). National Renewable Energy Laboratory (NREL), Golden, CO (United States). 2013. https://www.nrel.gov/docs/fy14osti/60600.pdf.

21. Robertson, A.N., Wendt, F.F., Jonkman, J.M., et al. Popko, W., Vorpahl, F., Stansberg, C.T., Bachynski, E.E., Bayati, I., Beyer, F., de Vaal, J.B. and Harries, R., 2015. OC5 project phase I: Validation of hydrodynamic loading on a fixed cylinder (No. NREL/CP-5000-63567). National Renewable Energy Lab(oratory (NREL), Golden, CO (United States). 2015. https://www.nrel.gov/docs/fy15osti/63567.pdf.

22. Robertson, A.N., Wendt, F., Jonkman, J.M, et al., Popko, W., Borg, M., Bredmose, H., Schlutter, F., Qvist, J., Bergua, R., Harries, R. and Yde, A., 2016. OC5 Project Phase Ib: validation of hydrodynamic loading on a fixed, flexible cylinder for offshore wind applications. (NREL/JA-5000-66648). National Renewable Energy Laboratory (NREL), Golden, CO (United States). 2016. https://doi.org/10.1016/j.egypro.2016.09.201.

23. Robertson, A.N., Wendt, F., Jonkman, J.M., et al. Popko, W., Dagher, H., Gueydon, S., Qvist, J., Vittori, F., Azcona, J., Uzunoglu, E. and Soares, C.G., 2017. OC5 project phase II: validation of global loads of the DeepCwind floating semisubmersible wind turbine. *Energy Procedia*. 2017;-137:, pp.38–57. https://doi.org/10.1016/j.egypro.2017.10.333.

24. Robertson, A.N., Jonkman, J., Wendt, F.F., et al. Popko, W., Huhn, M.L., Muller, K., Le Dreff, J.B., Gilbert, P., Auriac, B., Villora, F.N. and Schunemann, P., 2018. Verification of a Numerical Model of the Offshore Wind Turbine Ffrom the Alpha Ventus Wind Farm Within OC5 Phase III (No. NREL/CP-5000-70878). National Renewable Energy Laboratory (NREL), Golden, CO (United States). 2018. https://doi.org/10.1115/OMAE2018-77589.

25. Popko , W., Robertson, A., Jonkman, J., et al. Wendt, F., Thomas, P., Müller, K., Kretschmer, M., Ruud Hagen, T., Galinos, C., Le Dreff, J.B. and Gilbert, P., 2019, May. Validation of numerical models of the offshore wind turbine from the alpha ventus wind farm against full-scale measurements within OC5 Phase III. In: *ASME 2019 38th International Conference on Ocean, Offshore and Arctic Engineering*. American Society of Mechanical Engineers Digital Collection. 2019. May. https://doi.org/10.1115/OMAE2019-95429.

26. IEC, 2009. IEC 61400-3 Wind Turbines – Part 3: Design Requirements for Offshore Wind Turbines. International Electrotechnical Commission, Geneva, February.

27. Bachynski, E.E., Page, A., and Katsikogiannis, G., 2019, November. Dynamic Response of a Large-Diameter Monopile Considering 35-Hour Storm Conditions. In: *ASME 2019 38th International Conference on Ocean, Offshore and Arctic Engineering*. American Society of Mechanical Engineers Digital Collection. 2019. November. https://doi.org/10.1115/OMAE2019-95170.

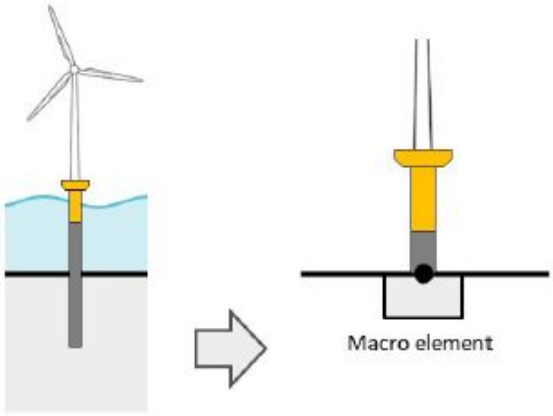

Figure 1. Illustration of the offshore wind turbine (left) and macro-element approach (right) [1]

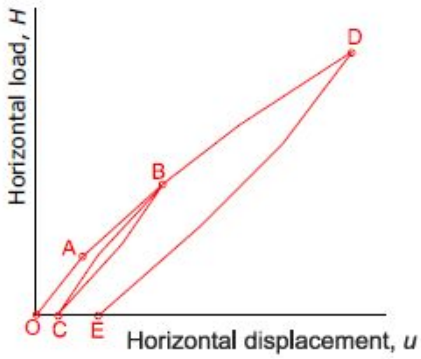

Figure 2. Nonlinear hysteretic pile foundation behavior [9~~,~~11]

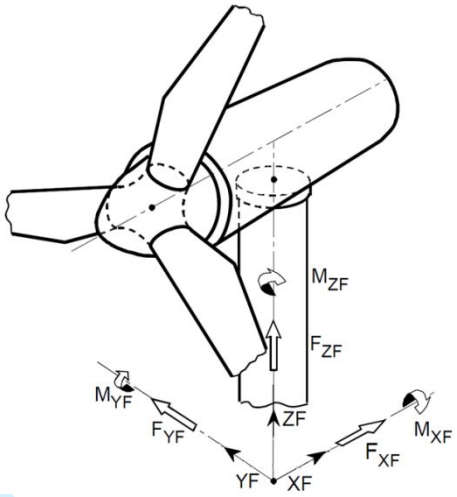

Figure 3. Global coordinate system

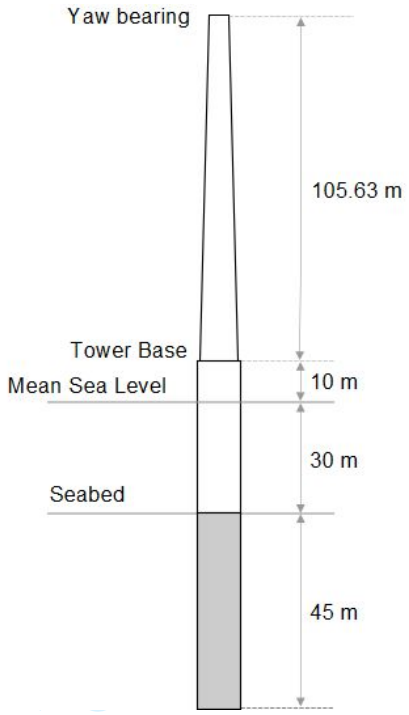

Figure 4. Schematic representation of the tower and monopile

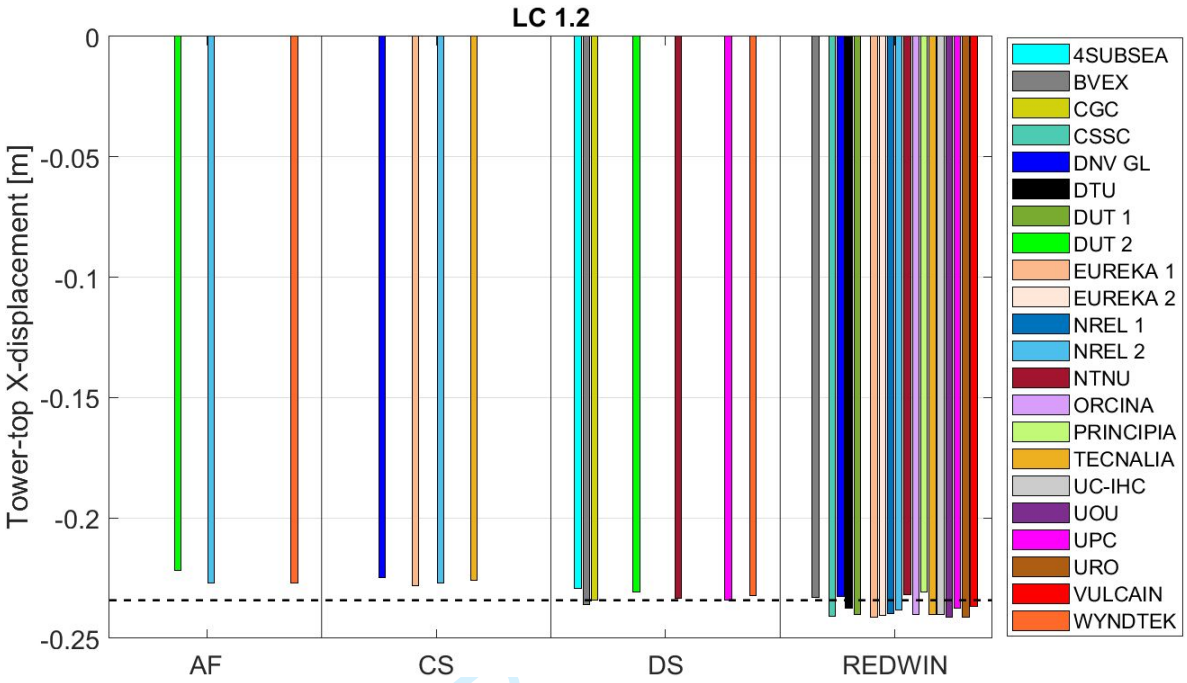

Figure 5. Tower-top X-displacement for gravity-only conditions in load case (LC) 1.2

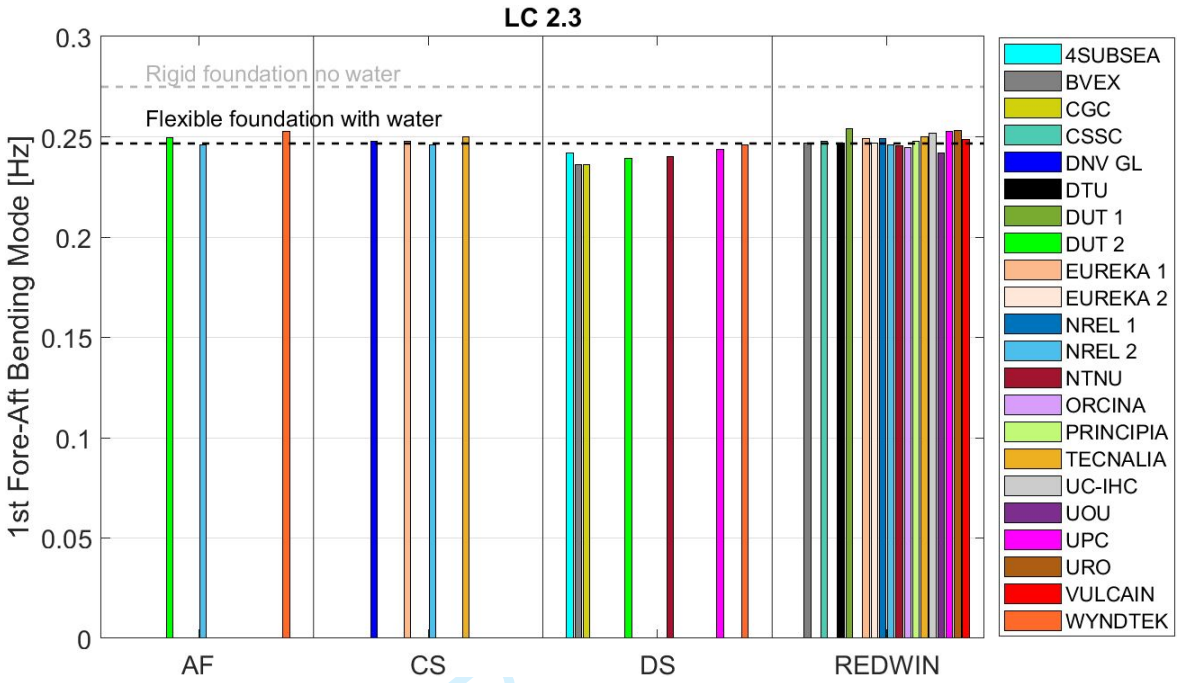

Figure 6. First fore-aft bending mode eigenfrequency depending on the soil-structure interaction~~SSI~~ approach in load case (LC) 2.3

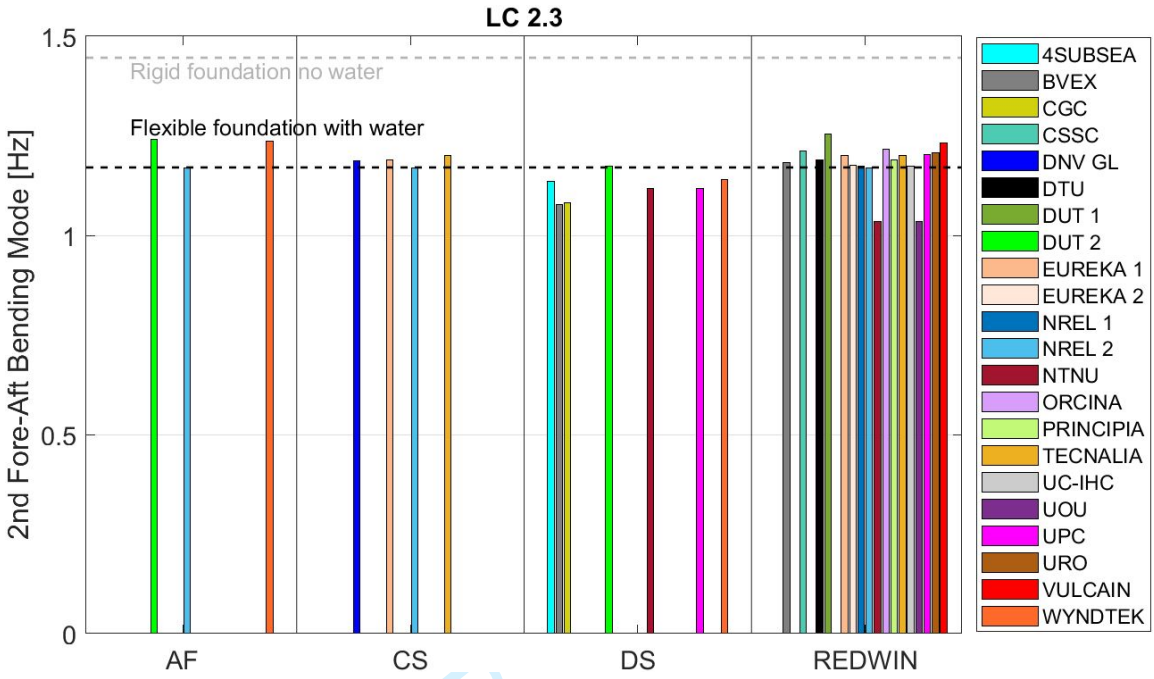

Figure 7. Second fore-aft bending mode eigenfrequency depending on the soil-structure interaction~~SSI~~ approach in load case (LC) 2.3

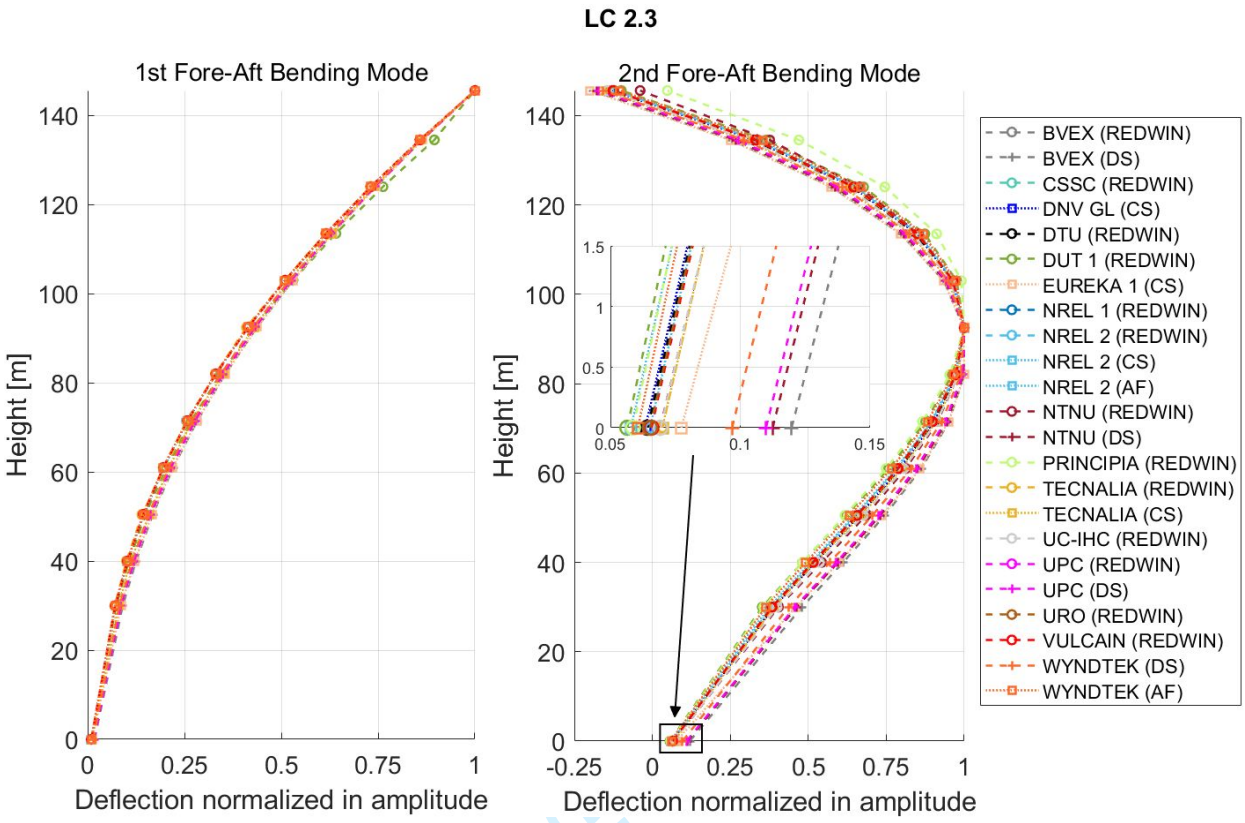

Figure 8. Eigenvectors of the first and second fore-aft bending modes in load case (LC) 2.3

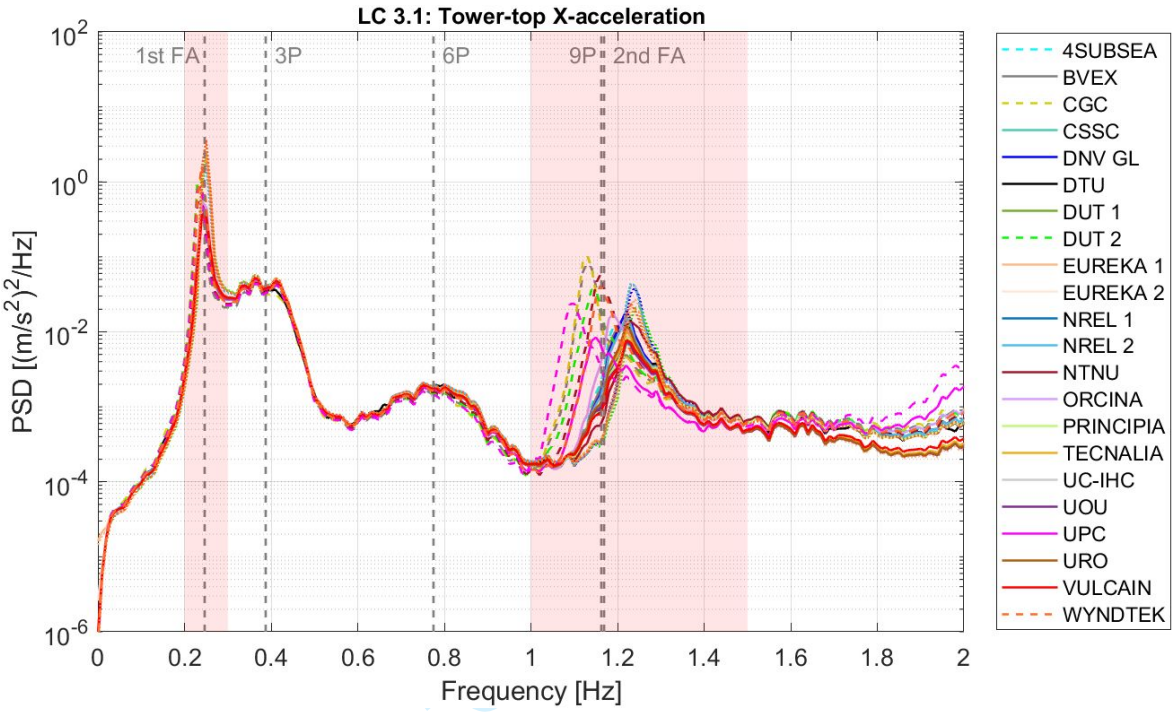

Figure 9. Power spectral density (PSD) of the tower-top X-acceleration in load case (LC) 3.1

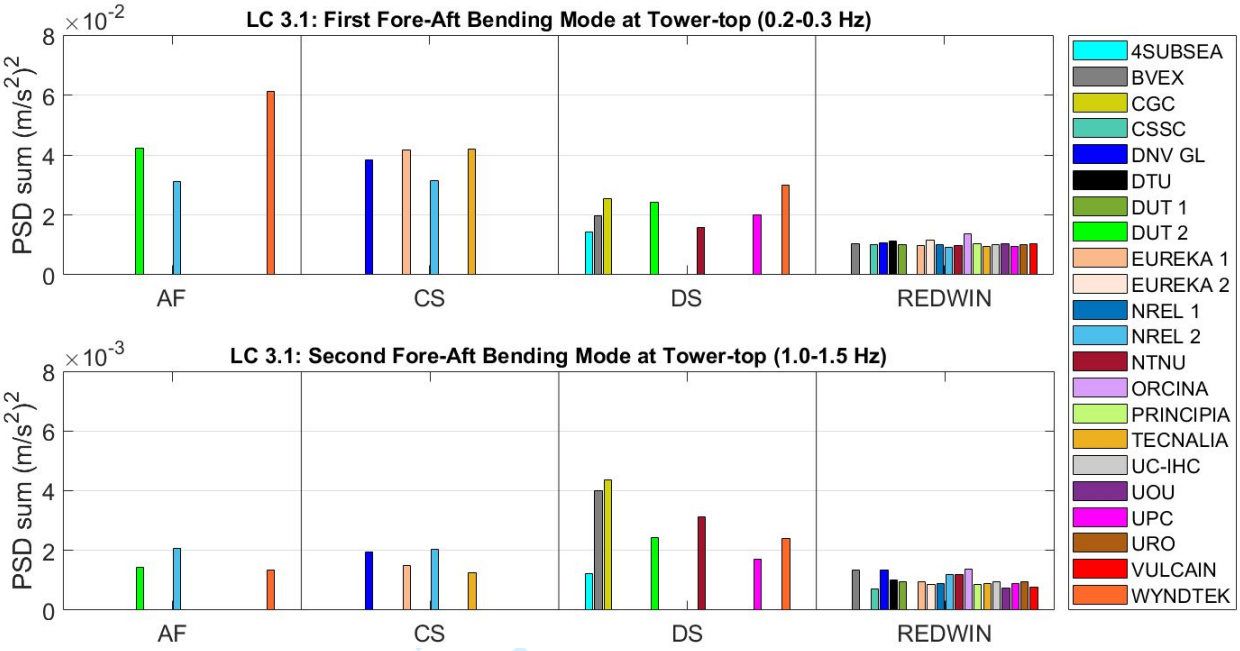

Figure 10. Power spectral density (PSD) sums of the tower-top X-acceleration in load case (LC) 3.1

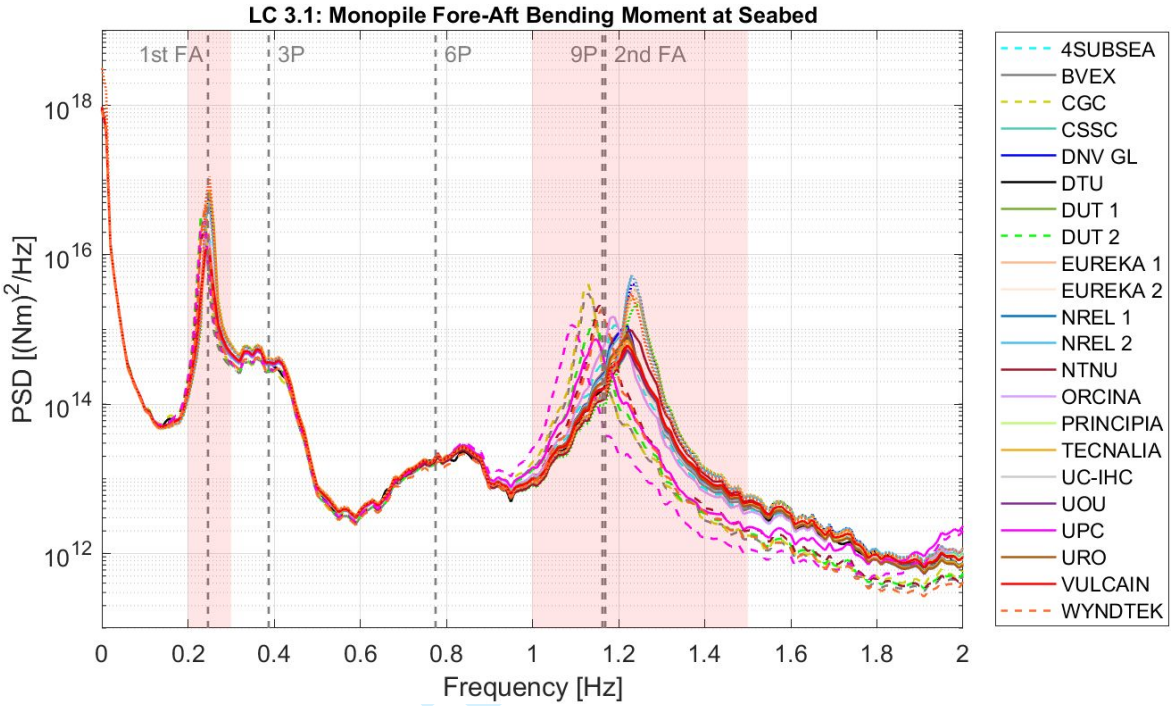

Figure 11. Power spectral density (PSD) of the monopile fore-aft bending moment at the seabed in load case (LC) 3.1

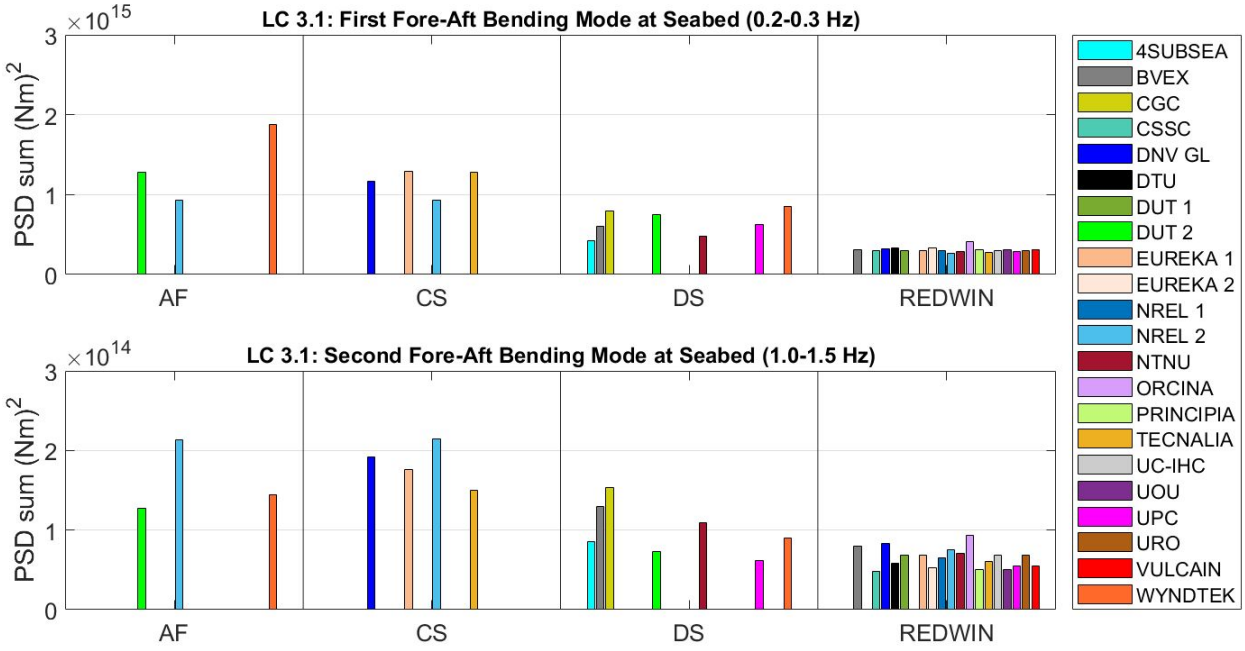

Figure 12. Power spectral density (PSD) sums of the fore-aft bending moment at the seabed in load case (LC) 3.1

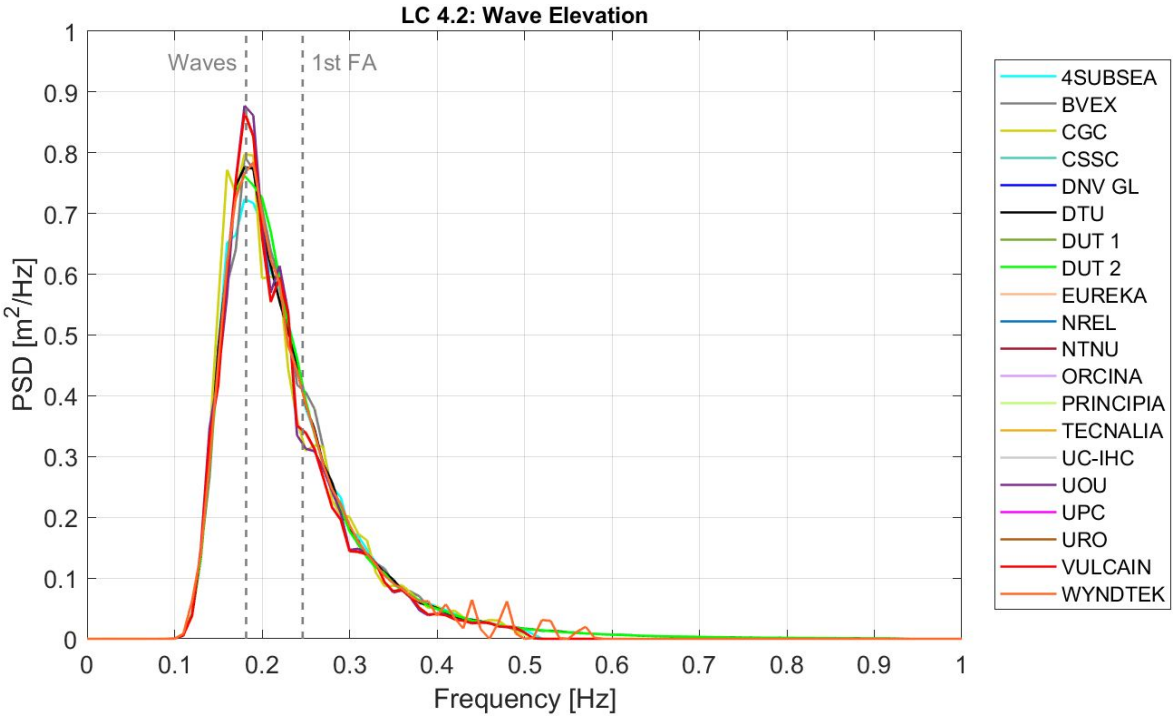

Figure 13. Power spectral density (PSD) of the wave elevation in load case (LC) 4.2 (H_s = 1.25 m, T_p = 5.5 s, γ = 1.0)

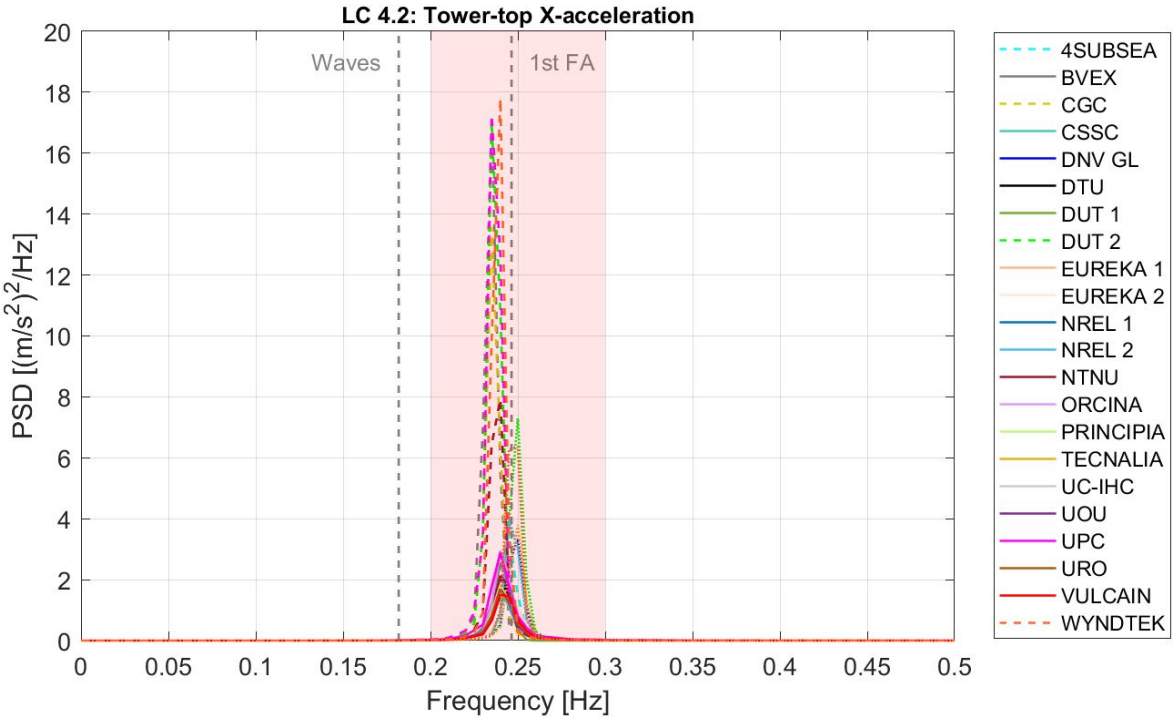

Figure 14. Power spectral density (PSD) of the tower-top X-acceleration in load case (LC) 4.2

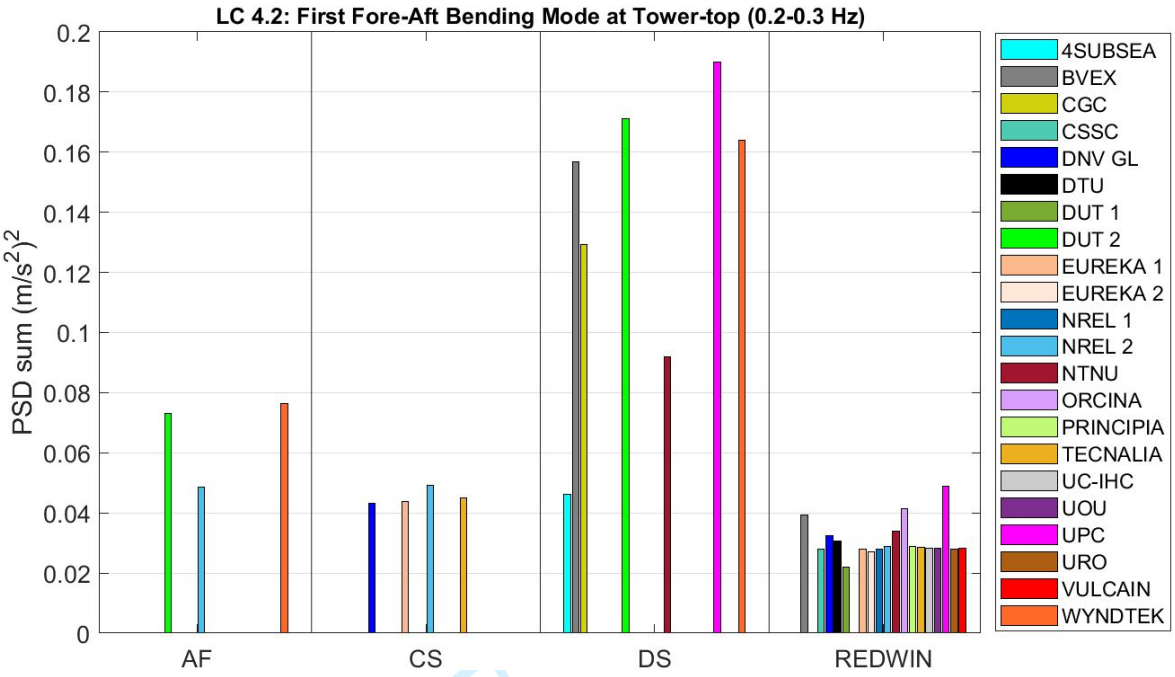

Figure 15. Power spectral density (PSD) sum of the tower-top X-acceleration in load case (LC) 4.2

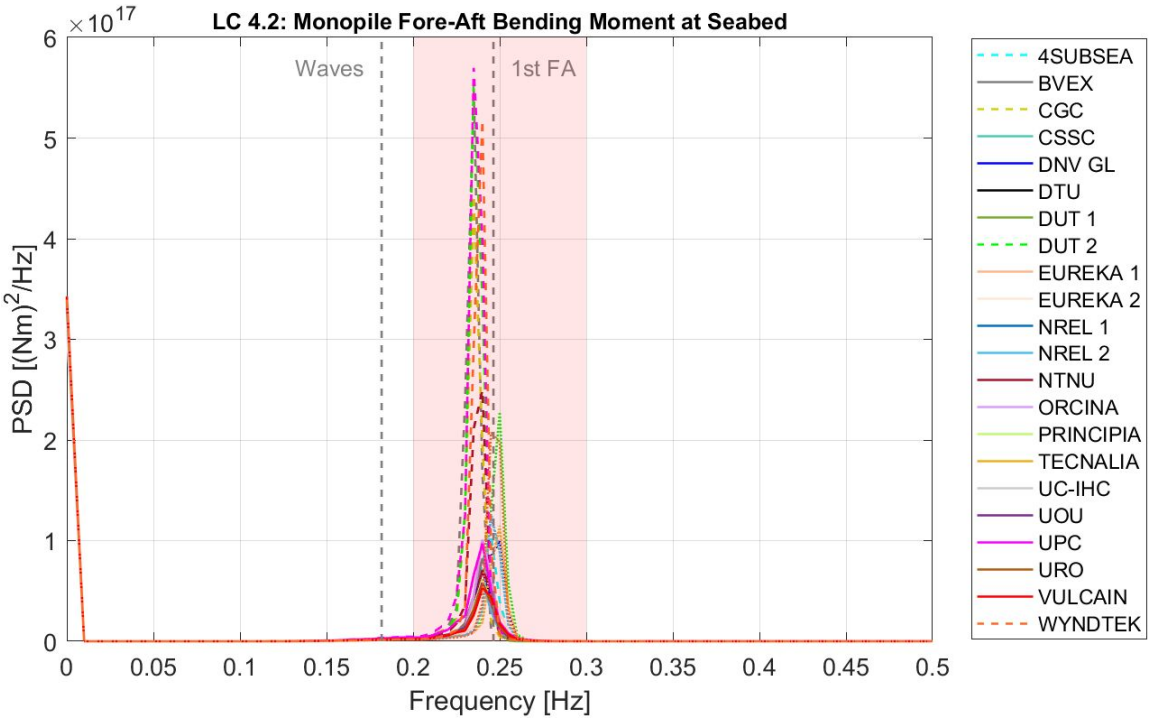

Figure 16. Power spectral density (PSD) of the monopile fore-aft bending moment at the seabed in load case (LC) 4.2

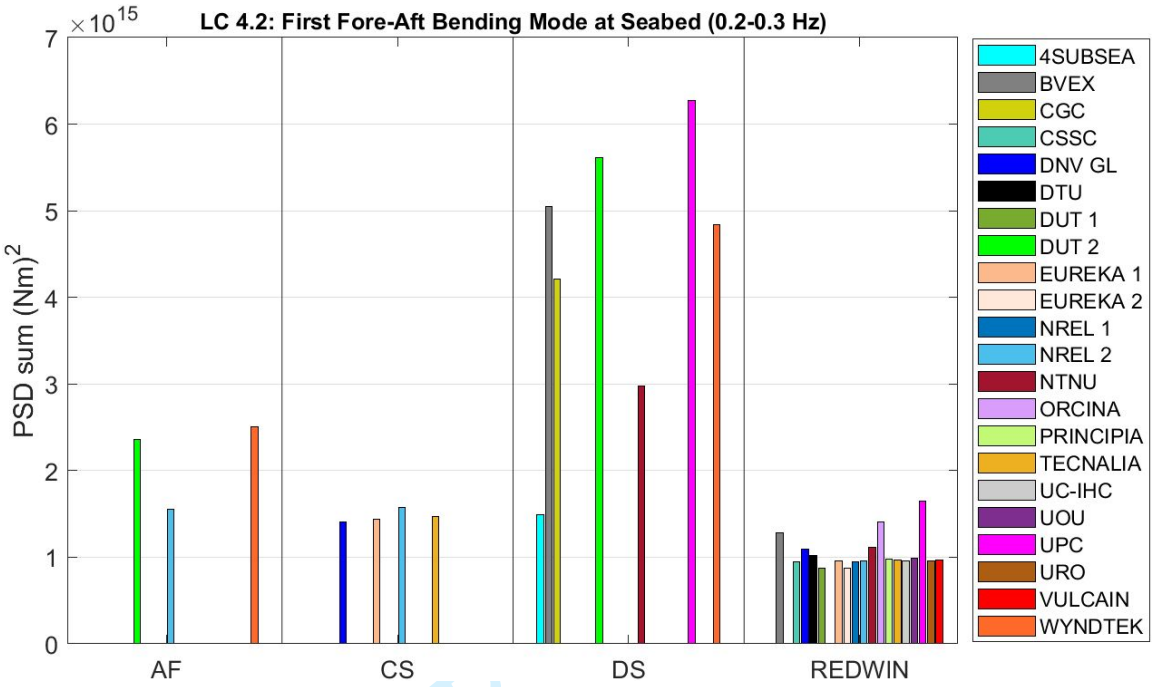

Figure 17. Power spectral density (PSD) sums of the fore-aft bending moment at the seabed in load case (LC) 4.2

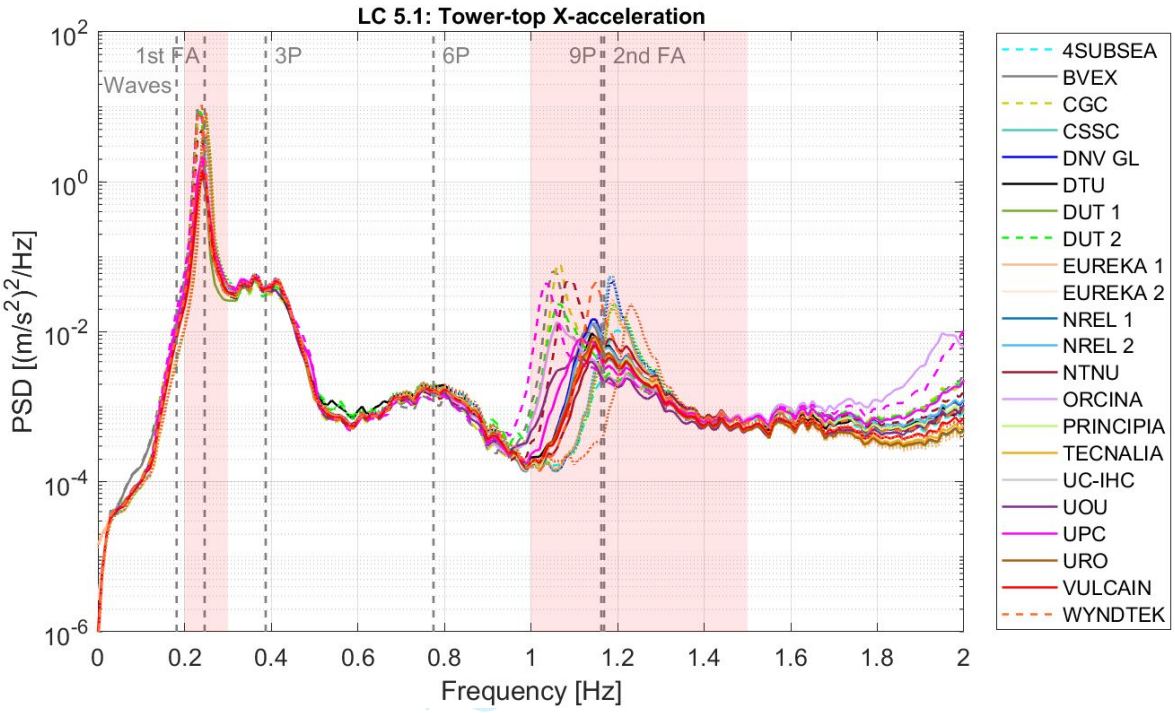

Figure 18. Power spectral density (PSD) of the tower-top X-acceleration in load case (LC) 5.1

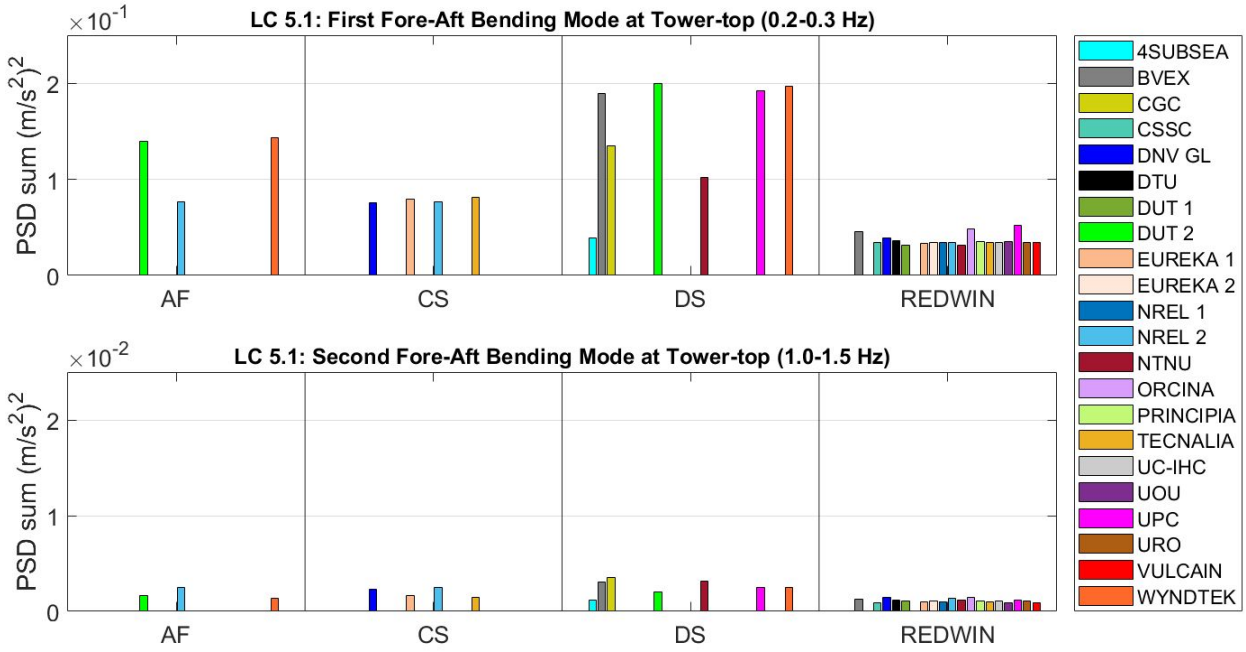

Figure 19. Power spectral density (PSD) sums of the tower-top X-acceleration in load case (LC) 5.1

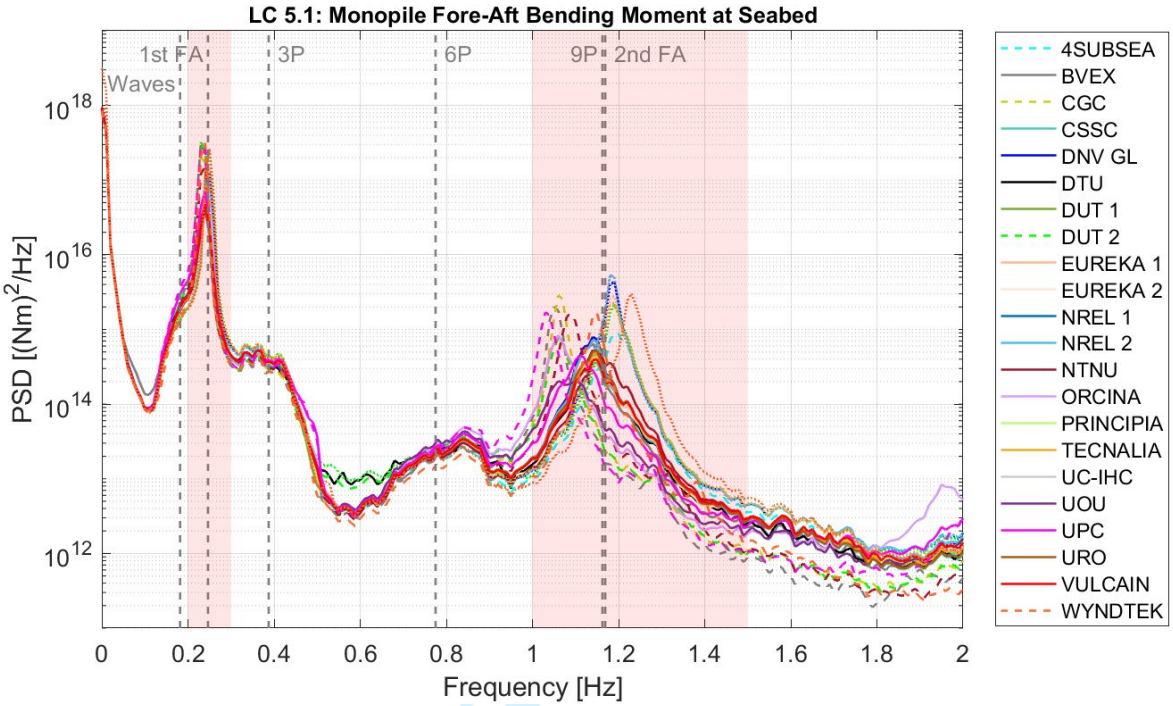

Figure 20. Power spectral density (PSD) of the monopile fore-aft bending moment at the seabed in load case (LC) 5.1

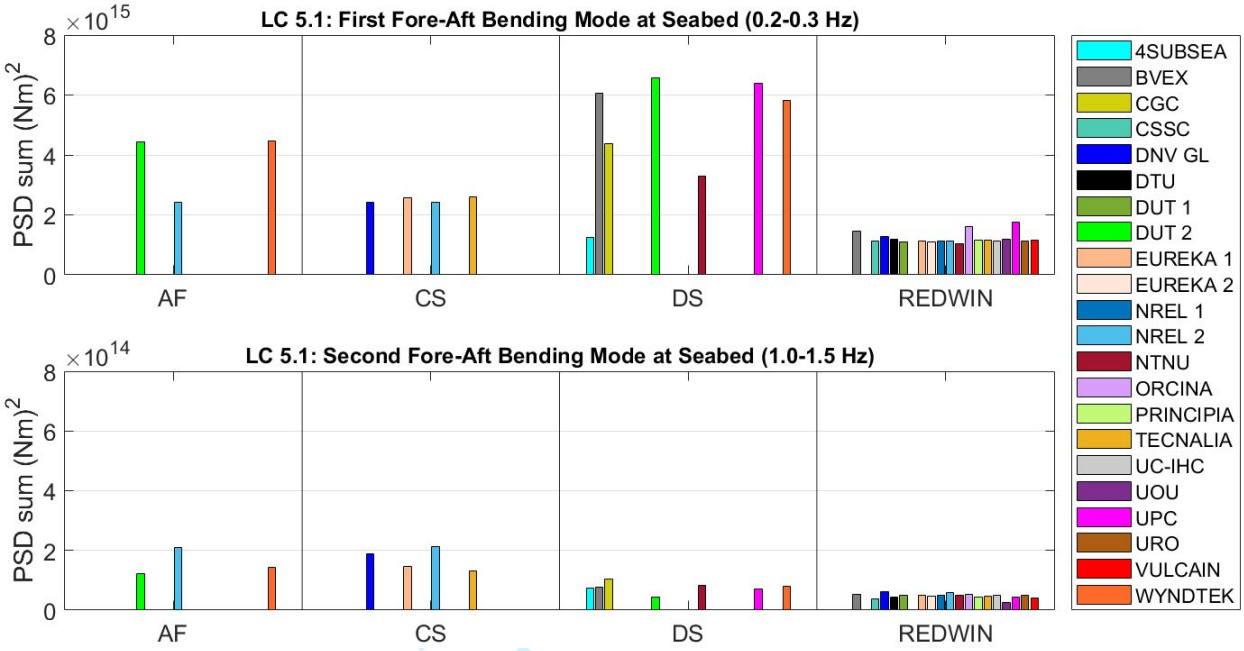

Figure 21. Power spectral density (PSD) sums of the fore-aft bending moment at the seabed in load case (LC) 5.1

Table 1. Rotor-nacelle assemblyNA mass properties

CM: stands for center of mass; and I for: moments of inertia

Parameter	Value	Description
Mass	839741 kg	Total tower-top mass
CM_x	-5.80 m	Center of mass in X direction from yaw bearing
CM_y	0 m	Center of mass in Y direction from yaw bearing
CM_z	3.19 m	Center of mass in Z direction from yaw bearing
I_{xx}	1.84E8 kg m^2	Moment of inertia around X axis at the center of mass
I_{yy}	9.61E7 kg m^2	Moment of inertia around Y axis at the center of mass
I_{zz}	1.06E8 kg m^2	Moment of inertia around Z axis at the center of mass
$I_{xy} = I_{yx}$	0 kg m^2	XY product of inertia at the center of mass
$I_{xz} = I_{zx}$	-7.11E6 kg m^2	XZ product of inertia at the center of mass
$I_{yz} = I_{zy}$	0 kg m^2	YZ product of inertia at the center of mass

Table 2. Tower and monopile dimensions

Location	Elevation (h) [m]	Outer diameter ($\emptyset_{ext}$) [m]	Wall thickness (t) [mm]
Yaw Bearing	145.63	5.50	30
	134.55	5.79	30
	124.04	6.07	35
	113.54	6.35	45
	103.03	6.63	50
	92.53	6.91	55
	82.02	7.19	60
	71.52	7.46	60
	61.01	7.74	65
	50.51	8.02	70
Tower Base	40.00	8.30	70
Monopile Top	40.00	9.00	110
Mean Sea Level (MSL)	30.00	9.00	110
Seabed	0.00	9.00	110
Monopile Base	-45.00	9.00	110

Table 3. Tower and monopile material properties

Parameter	Value
Young's modulus (E)	210 GPa
Shear modulus (G)	80.8 GPa
Density (ρ)	8,500 kg/m^3
Damping ratio (ζ_1) first bending mode	0.005
Damping ratio (ζ_2) second bending mode	0.010

Table 4. Approximate eigenfrequencies up to 2 Hz for the system clamped at seabed without water

Mode shape	Eigenfrequency [Hz]
First fore-aft bending mode	0.28
First side-side bending mode	0.28
Second fore-aft bending mode	1.44
Second side-side bending mode	1.33
First torsional mode	1.27

Table 5. Summary of participants, codes, and modeling approach used for the soil-structure interaction

Participant	Code	~~SSI~~ Soil-Structure Interaction Approach			
		AF	CS	DS	REDWIN
4SUBSEA	OrcaFlex			X	
BVEX	Samcef WT			X	X
CGC	Bladed			X	
CSSC	OpenFAST				X
DNV GL	Bladed		X		X
DUT 1	OpenFAST				X
DUT 2	HAWC2	X		X	
DTU	HAWC2				X
EUREKA 1	OpenFAST		X		X
EUREKA 2	OpenFAST				X
NREL 1	OpenFAST				X
NREL 2	OpenFAST	X	X		X
NTNU	SIMA			X	X
ORCINA	OrcaFlex				X[a*]
PRINCIPIA	DeepLines Wind				X
TECNALIA	OpenFAST		X		X
UC-IHC	OpenFAST				X
URO	OpenFAST				X
UOU	OpenFAST				X
UPC	FloaWDyn			X	X
VULCAIN	OpenFAST				X
WYNDTEK	Ashes	X		X	

[a*] Orca~~aFlex~~ina uses a built-in capability in OrcaFlex with some of the inputs from the REDWIN approach.

Table 6. Offshore Code Comparison Collaboration, Continued, with Correlation and unCertainty (OC6) Phase II load case simulations (summary)

Analysis Type	Load Case	Enabled Degrees of Freedom	Wind Conditions	Marine Conditions	Comparison Type
Static	1.2	Tower, substructure, foundation	None	None	Static response
Eigenanalysis	2.3	Tower, substructure, foundation	None	Still water	Frequencies, damping, and mode shapes
Wind-Only	3.1	Tower, substructure, foundation	Prescribed load time series at yaw bearing V_{hub} = 9.06 m/s	None	Time series (t = 3600 s)
Wave-Only	4.2	Tower, substructure, foundation	None	Irregular waves: Pierson-Moskowitz wave spectrum H_s = 1.25 m, T_p = 5.5 s	Time series (t = 3600 s)
Wind + Waves	5.1	Tower, substructure, foundation	Prescribed load time series at yaw bearing V_{hub} = 9.06 m/s	Irregular waves: Pierson-Moskowitz wave spectrum H_s = 1.25 m, T_p = 5.5 s	Time series (t = 3600 s)

H_s: significant wave height
T_p: peak-spectral wave period
V_{hub}: average hub height wind speed
t: time

Table 76. Prescribed settings for marine conditions

Hydrodynamic forces	Wave kinematics	Seawater density
Relative form of Morison equation (without corrections) Drag coefficient (C_D) = 1 Inertia coefficient (C_M) = 2	Linear (first order) waves No wave stretching No directional spreading	1025 kg/m^3 [248]

Table 7. Offshore Code Comparison Collaboration, Continued, with Correlation and unCertainty (OC6) Phase II load case simulations

	Load Case	Enabled Degrees OFsof Freedom	Wind Conditions	Marine Conditions	Comparison Type
	1.2	Tower, substructure, foundation	None	None	Static response
	2.3	Tower, substructure, foundation	None	Still water	Frequencies, damping, and mode shapes
Wind-Only	3.1	Tower, substructure, foundation	Prescribed load time series at yaw bearing = 9.06 m/s	None	Time series (t = 3600 s)
	4.2	Tower, substructure, foundation	None	Irregular waves: Pierson-Moskowitz wave spectrum = 1.25 m, = 5.5 s	Time series (t = 3600 s)
Wind + Waves	5.1	Tower, substructure, foundation	Prescribed load time series at yaw bearing = 9.06 m/s	Irregular waves: Pierson-Moskowitz wave spectrum = 1.25 m, = 5.5 s	Time series (t = 3600 s)

H: regular wave height
: significant wave height
T: regular wave period
: peak-spectral wave period
γ: peak-enhancement factor
: average hub height wind speed
t: time

Thank you very much for your time and effort reviewing the manuscript and providing feedback. It is very useful to us. Below we tried to address the different questions presented.

This is a useful paper describing a well-designed code validation study that is of use to the community. I recommend it for publication and have some comments that I trust the authors can address prior to publication.

1. I realize this is probably covered in the REDWIN publications, but it would be useful to include some information on how cumbersome (modeling difficulty and computation time) the FE SSI analyses are that are needed to seed the macro element information. Philosophically, I have wondered why, with the amount of desktop computational power available, tools such as FAST don't simply include an FE model of the soil volume. Perhaps such a model would be difficult to implement or would cause undue slowdown in simulation. Were I a geotechnical engineer I would wonder why I can't simply provide soil properties to FAST.

The main problem about including a FE model of the soil volume is that it would require a 3D finite-element model with thousands of additional DOFs. In general, aero-elastic tools take advantage of modal reductions to work with very few degrees of freedom. The paper has been modified as follows to try to provide a better understanding:

OC6 Phase II focuses on verifying implementation of the REDWIN capability in participant modeling tools by investigating REDWIN model 2 to describe the response of a pile foundation supporting a monopile-based OWT. The REDWIN model 2 is an elasto-plastic macro-element model with kinematic hardening formulated within the multi-surface plasticity framework [5]. It reduces the foundation and surrounding soil to a set of linear and nonlinear load-displacement relationships in the six DOFs of the interface point (the seabed), separating the foundation and the rest of the structure (see Figure 1). It can represent the nonlinear hysteretic load-displacement response observed in experimental tests and in the field, including the coupled response between horizontal loads and bending moments. The model has been demonstrated to give good agreement with results from finite element analyses of the soil and monopile, results from large-scale pile tests, and results from full-scale field measurements of an OWT installed in the North Sea [5–7].

Aero-hydro-servo-elastic simulation tools are used during the design and certification of wind turbines [8]. During this process, thousands of load cases must be computed and analyzed. This requires these tools to be computationally efficient. In general, these simulation tools use relatively few DOFs, taking advantage of a combined modal and multibody dynamics formulation. Modeling the SSI in the time domain with a 3D finite-element model would require thousands of additional DOFs, which would substantially increase the simulation time of the aero-elastic solver. The REDWIN approach is a CPU efficient way to couple the SSI capability into these tools, using as few degrees of freedom as possible [1], leading to a minimal increase in computational time while providing higher fidelity than the traditional methods (AF, CS, or DS). The macro-element communicates with the wind turbine model through a DLL [(dynamic link library)] in a Windows environment or through a shared object in a Linux environment. In each calculation step, the OWT simulation tool provides the displacements and rotations at the seabed to the foundation model, which transfers back the computed forces and moments. The soil-foundation model is solved following an explicit integration algorithm with correction. The model also includes a sub-stepping algorithm, which should help the convergence when the input displacement and/or rotation increment is large.

4

2. For the static case, the authors state, "Finally, the REDWIN shows slightly larger displacements than the DS approach because it accounts for the nonlinear stiffness and plasticity. This plasticity depends on the initial transient in the simulation." This comment is quite confusing. First, are the static loadings really large enough that plasticity is being induced in the soil? This seems highly unlikely to me. Second, What is meant by the 'initial transient'. A static analysis should not have 'transients'.

We agree that the 'transient' term can be confusing if a static analysis is being considered. This comes from the limitation of certain participants to perform a static analysis in their simulation tools. This has been clarified in the new revision of the paper (see below).

Regarding the plasticity itself, significant amounts of plasticity require large displacements. However, Figure 2 illustrates that any cyclic loading can induce *some* level of plasticity. It's also worth noting that the differences due to this cyclic loading resulting from the initial transient are lower than 0.01 m at the tower top location (and significantly smaller than that at the seabed location).

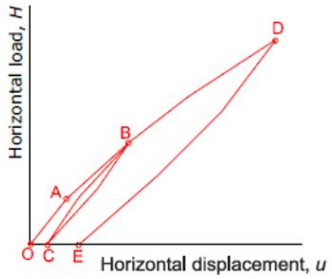

Figure 2. Nonlinear hysteretic pile foundation behavior

The paper has been modified as follows:

6.1 Static Simulations Results: Load Case 1.2

Figure 5 shows the tower-top (yaw bearing) displacement along the x-axis (fore-aft direction) under gravity-only conditions (load case~~LC~~ 1.2). This displacement is the result of the overhanging weight of the RNA (see Table 1) and it is affected by the SSI stiffness. The dashed black line shows the average displacement from all participants and it can be used as a reference to compare the different solutions.

As ~~it can be observed~~Figure 5 shows, the linear SSI approaches (AF and CS) result in smaller tower-top displacements. These linear approaches were characterized based on the unloaded state (see Eq. 1) and behave slightly stiffer than the nonlinear SSI approaches. Interestingly, WyndTek AF using the improved ~~apparent fixity~~AF method (Euler-Bernoulli beams) and NREL 2 AF using the ~~apparent fixity~~AF method (Timoshenko beams) produce the same displacement. The tower-top displacements for the DS approach are slightly bigger due to the nonlinearity of the p-y curves. Finally, the REDWIN shows slightly larger displacements than the DS approach because it accounts for the nonlinear stiffness and plasticity. Not all the simulation tools are able to perform a static analysis or gradually apply the gravity acceleration in a quasi-static fashion. Accordingly, some participants perform a transient analysis where the gravity acceleration is suddenly applied over the system at the beginning of the simulation. This results in an initial transient loading that can induce a small level of plasticity. ~~This plasticity depends on the initial transient in the simulation.~~ Therefore, REDWIN solutions using an initial static computation or a gradual loading result in slightly smaller displacements closer to the DS approach.

3. In discussing the eigenvalue analyses, the authors refer to the role of the water column in the solution. This requires more explanation. The eigenvalue analysis is based on the system stiffness and mass matrices. How does the water affect either matrix? Added mass? Something else?

The eigenvalue analysis consists of the extraction of the eigenvalues and eigenvectors from the mass and stiffness matrices of the system. When still water is included in the model the added mass is included in the mass matrix, which reduces the system eigenfrequencies.

> As it can be observed in Figure 6, the first bending mode drops around 10% in frequency due to the flexible foundation. The water does not have a significant impact for the first bending mode in this system. For the second bending mode (Figure 7), the drop in frequency is around 20% on average. The main reason for this drop in frequency is also the foundation flexibility, but the added mass from the still water is also noticeable. In the studied system and for all load cases, the monopile does not have water inside. Having the monopile filled with water would decrease these eigenfrequencies further.

4. Also regarding the eigen analysis, the authors write "Extracting the eigen-properties of a model using the REDWIN approach can be challenging due to the nonlinear nature of the system." This requires further explanation. The eigen problem is a linear problem. How does the nonlinearity of the REDWIN macro element affect things? Are the authors using an initial tangent stiffness? A secant stiffness at some prescribed set of displacements?

When linearizing the system, it's very important to account for the proper loading condition. In this case, the eigen-properties had to be extracted around the static equilibrium. Under these conditions, the tangent stiffness should be considered.

In a nonlinear system, the eigenfrequencies and eigenvectors will be different if the loading condition is not properly characterized. When trying to extract these properties from a time-domain simulation, special attention should be paid to ensure that the loading condition is around the working condition of interest. For example, in a free-decay test, the eigenfrequency would *slightly* increase over time because of the nonlinear stiffness (which is higher for lower load levels).

One of the participants that show these differences between the time domain and the frequency domain solution is NTNU. According to them, they obtained a frequency of 1.03 Hz for the second bending mode in the fore-aft direction (shown in Figure 7) when using the REDWIN approach and linearized the system. However, the frequency obtained by means of free-decay test when using the REDWIN approach was 1.19 Hz. They are trying to figure out why the eigen-solver that they use is returning this significantly lower frequency.

The paper has been modified as follows:

> observed during the static analysis (i.e., load case~~LC~~ 1.2). A similar trend can be observed in Figure 7 for the second bending mode. It is also interesting to note that in this second bending mode, the agreement between participants is not as good as for the first bending mode. One of the reasons for the dispersion in the eigenfrequencies between participants using the same SSI approach is the method used to extract the eigen-properties around the static equilibrium. Some simulation tools used by the participants include a linearization capability, while other participants without this functionality tried to obtain these properties from time-domain simulations (e.g., by means of a free-decay test or a broad-band excitation). For example, Figure 7 shows some significant differences between some of the participants using the REDWIN approach. However, when post-processing the time-domain results of load case~~LC~~ 5.X in the frequency domain, these differences were not observed (see, e.g., Figure 18 and Figure 20). Extracting the eigen-properties of a model using the REDWIN approach can be challenging due to the nonlinear nature of the system.

When linearizing the system, it's very important to account for the proper loading condition. In this case, the eigen-properties had to be extracted around the static equilibrium. Under these conditions, the tangent stiffness should be considered.
In a nonlinear system, the eigenfrequencies and eigenvectors will be different if the loading condition is not properly characterized. When trying to extract these properties from a time-domain simulation, special attention should be paid to ensure that the loading condition is around the working condition of interest. For example, in a free-decay test, the eigenfrequency would *slightly* increase over time because of the nonlinear stiffness (which is higher for lower load levels).
One of the participants that show these differences between the time domain and the frequency domain solution is NTNU. According to them, they obtained a frequency of 1.03 Hz for the second bending mode in the fore-aft direction (shown in Figure 7) when using the REDWIN approach and linearized the system. However, the frequency obtained by means of free-decay test when using the REDWIN approach was 1.19 Hz. They are trying to figure out why the eigen-solver that they use is returning this significantly lower frequency.

5. Some of the static solutions show large variability within the REDWIN group (e.g Fig. 7). This is deserving of some further comment. Is this related to the claim that extracting the eigen-properties is difficult for the REDWIN simulations?
That's correct. There are two participants that show clearly lower frequencies than the other REDWIN solutions. This could denote a problem in the algorithm used for the linearization (in case they used one) or the wrong boundary conditions (e.g., the system is loaded with a large external load that makes the foundation behave softer compared to the gravity-only condition).

6. The authors identify foundation damping as an important consideration, but reference only a single paper on this topic (by one of the co-authors). Although the research area is not deep with literature, a cursory google scholar search identifies several related papers on foundation damping and offshore wind. I suggest the authors augment the reference list in this area.
We thank the referee for pointing this out. One comprehensive paper providing insights on the contribution of soil damping to the total damping of OWTs and its importance to the OWTs fatigue life has been added to the references.

[9] Malekjafarian A, Jalilvand S, Doherty P, Igoe D. Foundation damping for monopile supported offshore wind turbines: A review. *Mar Struct.* 2021;77:102937.

https://doi.org/10.1016/j.marstruc.2021.102937.

> The macro-element allows for an accurate ~~and computationally efficient~~ representation of the foundation stiffness and hysteretic damping (see Figure 2)~~,~~ crucial to performing reliable fatigue analysis. It is important to note that aerodynamic damping provides the highest contribution to the overall system damping in the fore-aft direction when the wind turbine is operating, ~~however~~ but the aerodynamic damping importance decreases in idling and wind-wave misalignment situations, resulting in increased importance of soil damping [~~8~~9,10].

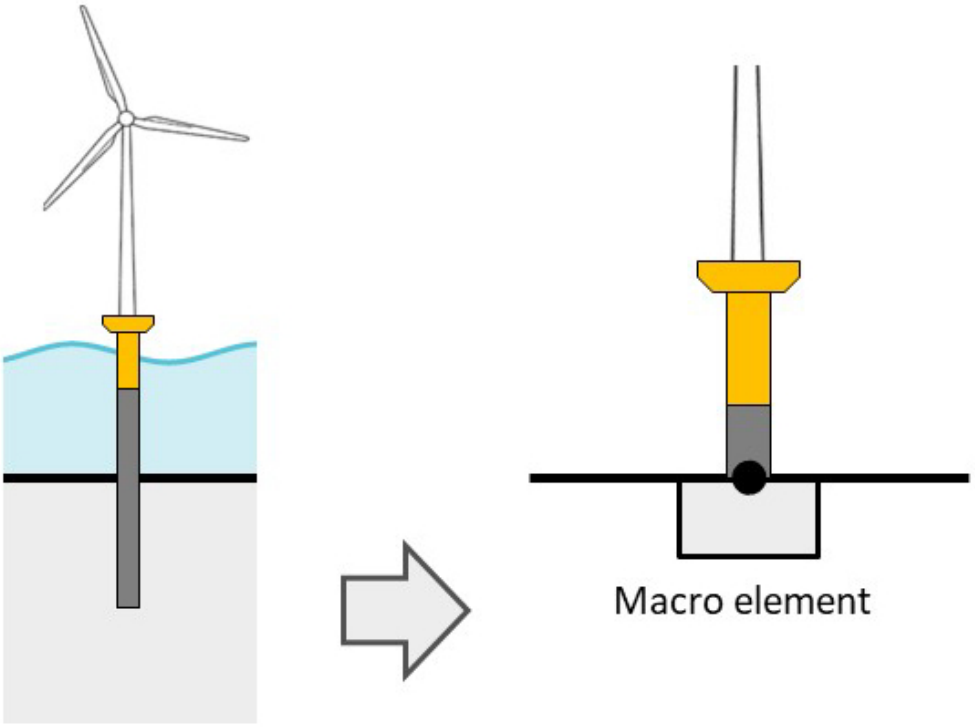

Figure 1. Illustration of the offshore wind turbine (left) and macro-element approach (right) [1]

96x72mm (144 x 144 DPI)

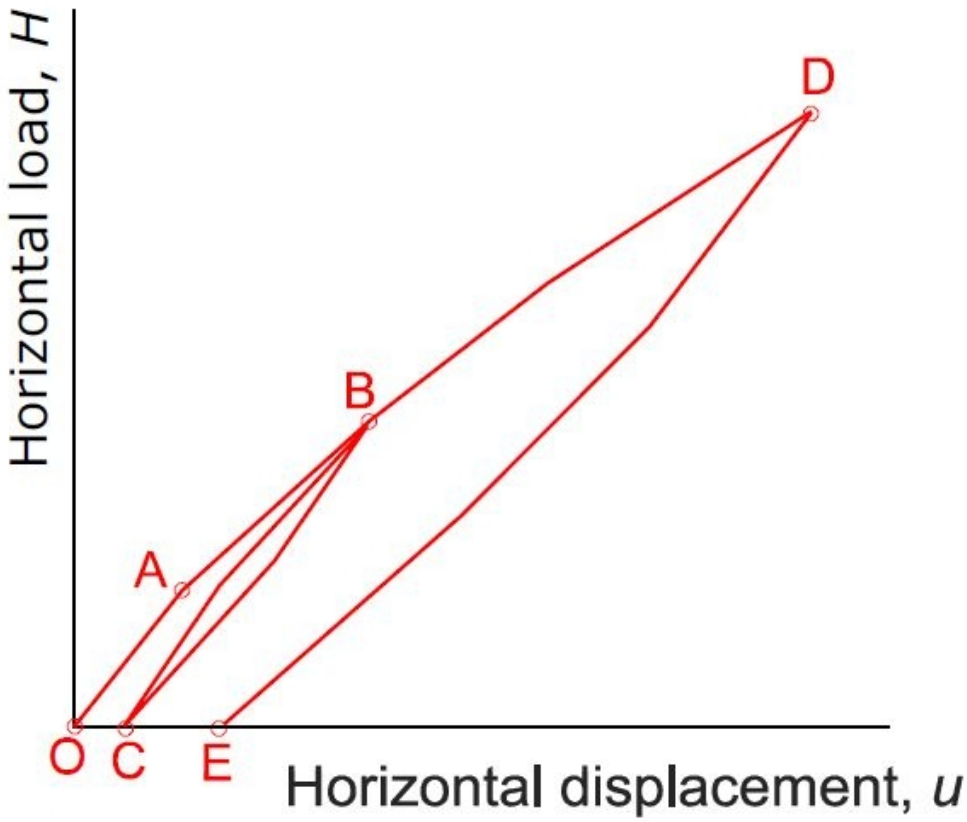

Figure 2. Nonlinear hysteretic pile foundation behavior [11]

103x89mm (144 x 144 DPI)

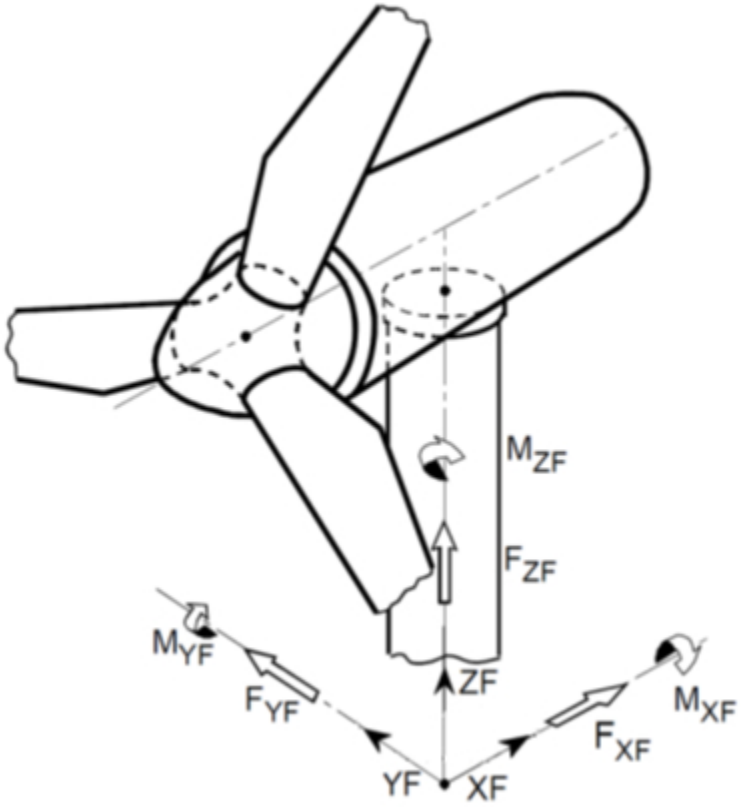

Figure 2. Global coordinate system

67x71mm (144 x 144 DPI)

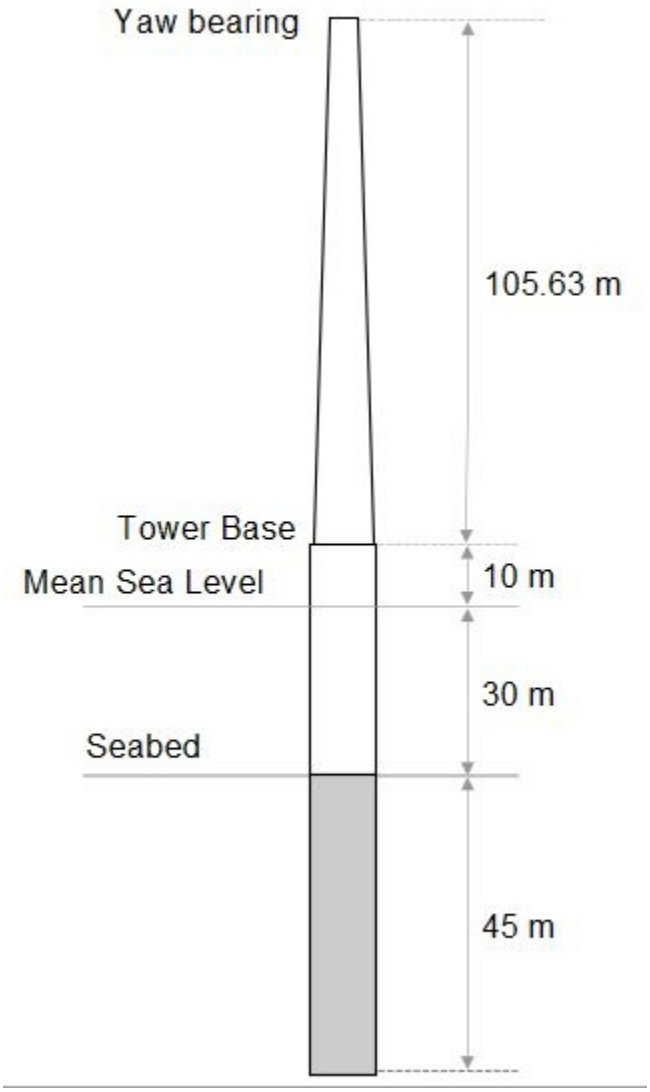

Figure 3. Schematic representation of the tower and monopile

56x96mm (144 x 144 DPI)

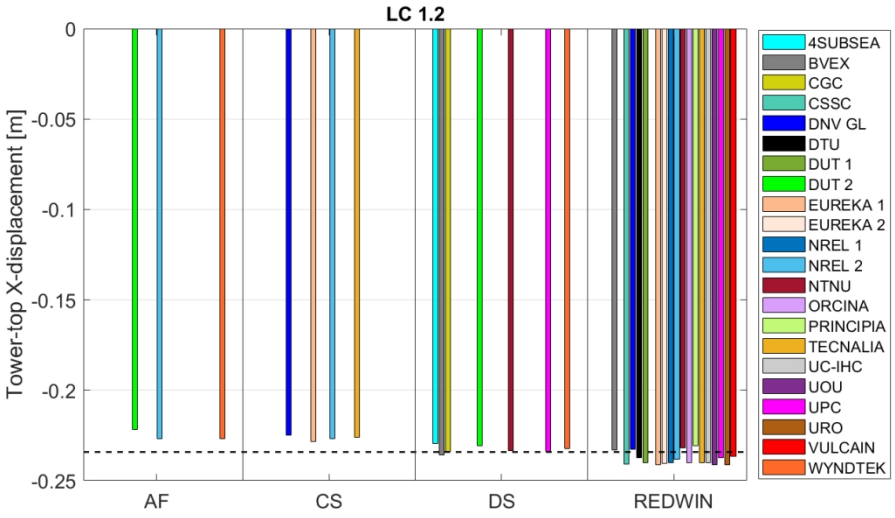

Figure 4. Tower-top X-displacement for gravity-only conditions in load case (LC) 1.2

375x208mm (96 x 96 DPI)

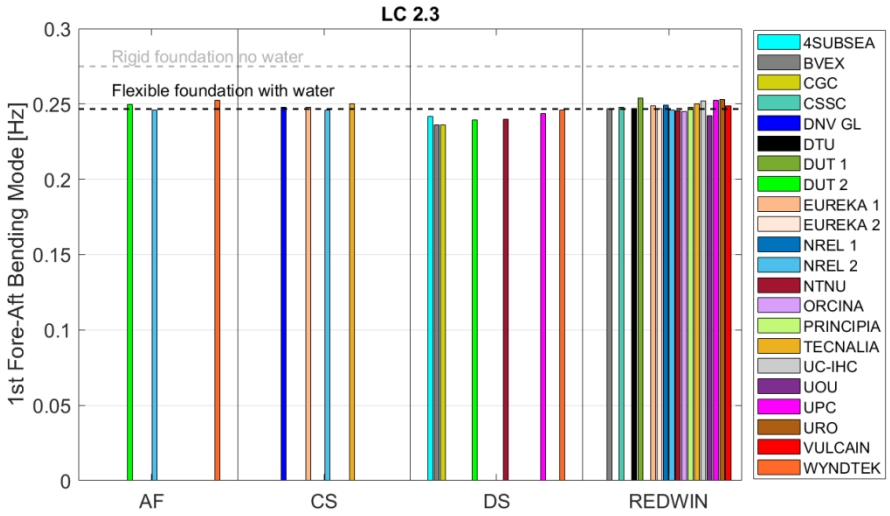

Figure 5. First fore-aft bending mode eigenfrequency depending on the soil-structure interaction approach in load case (LC) 2.3

375x208mm (96 x 96 DPI)

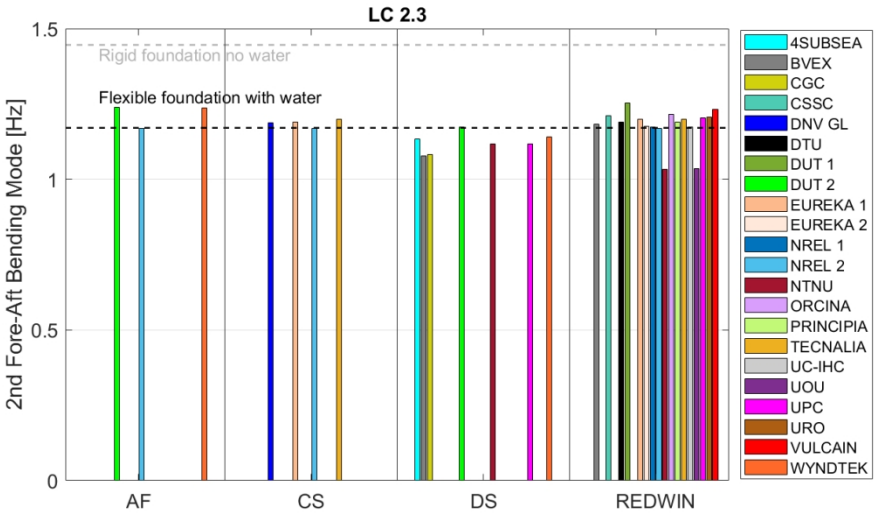

Figure 6. Second fore-aft bending mode eigenfrequency depending on the soil-structure interaction approach in load case (LC) 2.3

375x208mm (96 x 96 DPI)

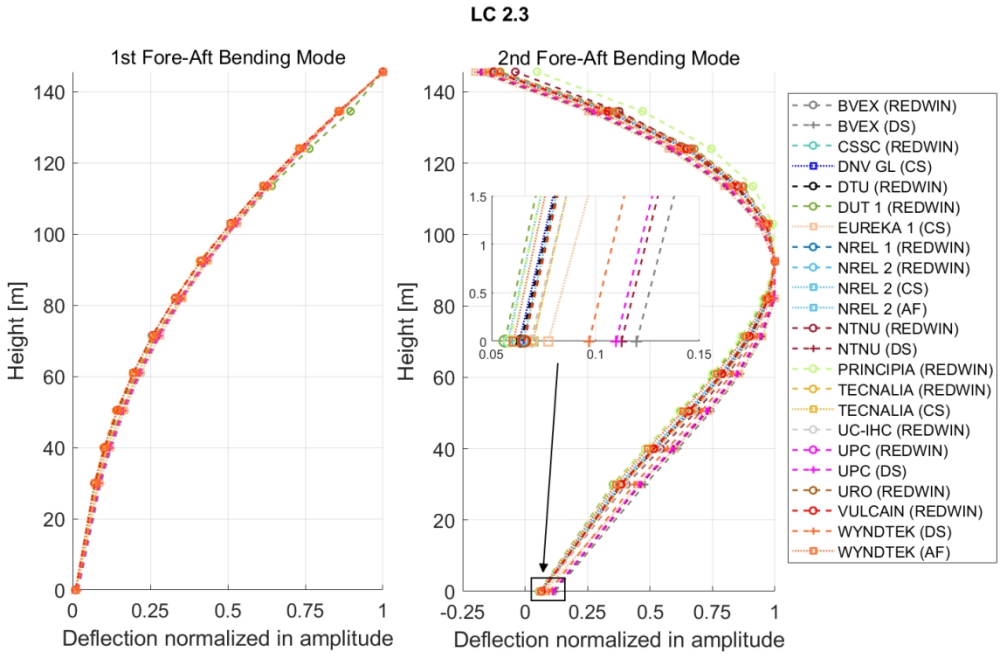

Figure 7. Eigenvectors of the first and second fore-aft bending modes in load case (LC) 2.3

375x251mm (96 x 96 DPI)

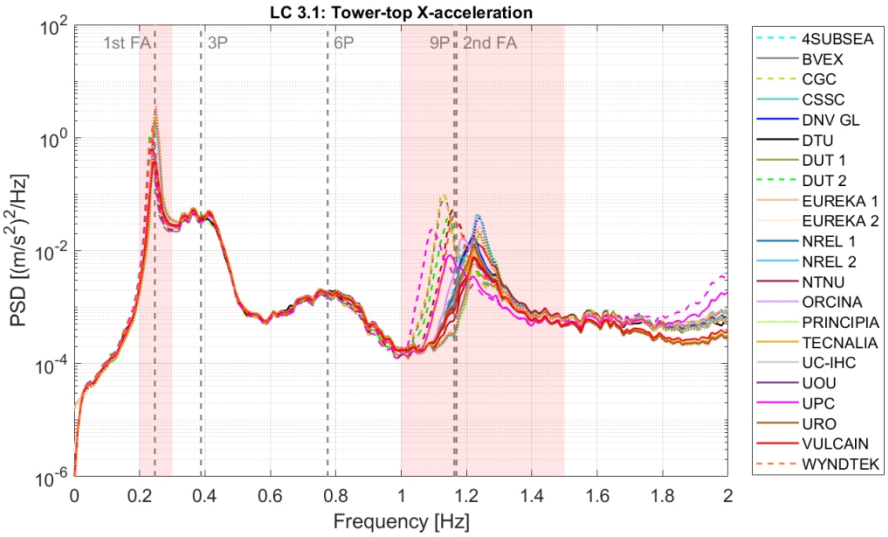

Figure 8. Power spectral density (PSD) of the tower-top X-acceleration in load case (LC) 3.1

375x208mm (96 x 96 DPI)

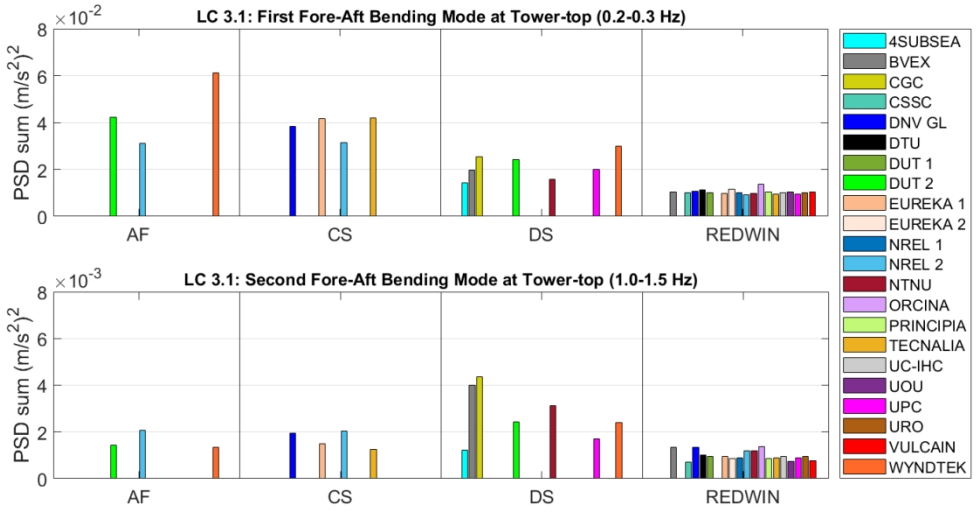

Figure 9. Power spectral density (PSD) sums of the tower-top X-acceleration in load case (LC) 3.1

375x208mm (96 x 96 DPI)

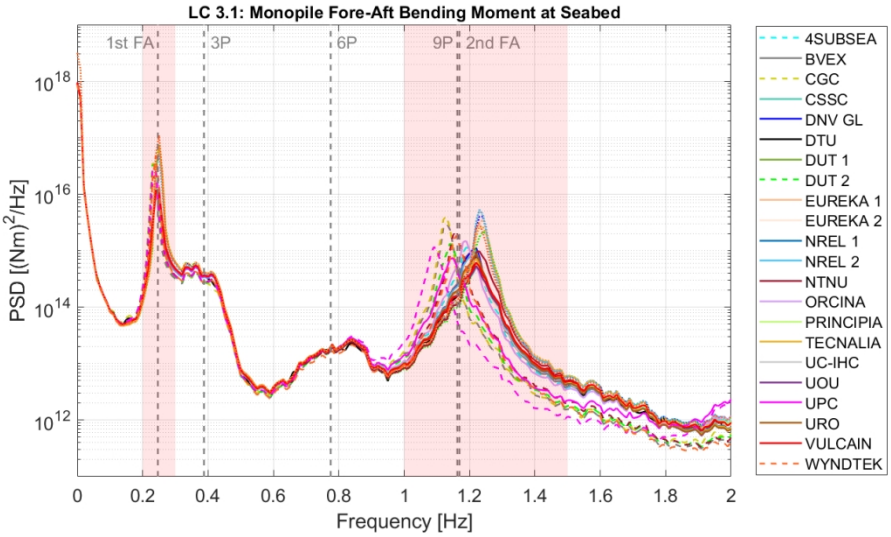

Figure 10. Power spectral density (PSD) of the monopile fore-aft bending moment at the seabed in load case (LC) 3.1

375x208mm (96 x 96 DPI)

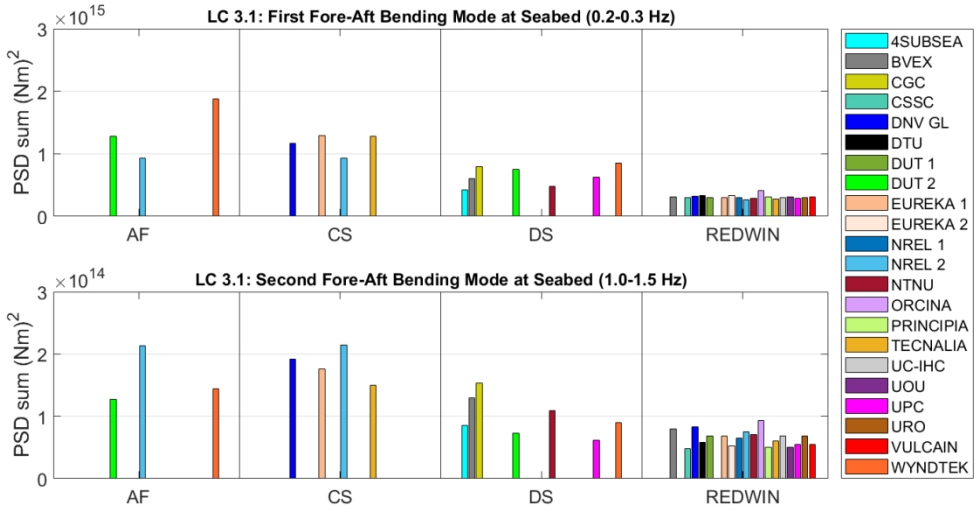

Figure 11. Power spectral density (PSD) sums of the fore-aft bending moment at the seabed in load case (LC) 3.1

375x208mm (96 x 96 DPI)

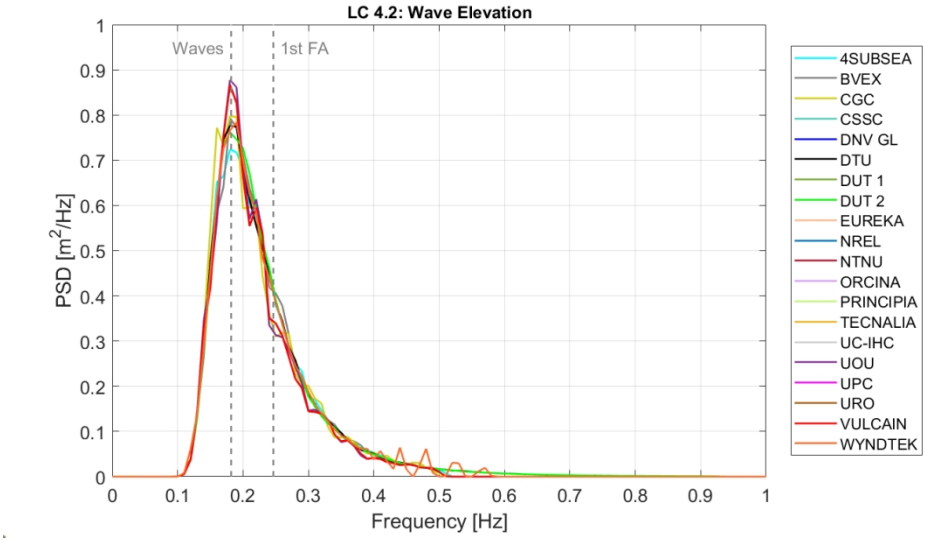

Figure 12. Power spectral density (PSD) of the wave elevation in load case (LC) 4.2 (H_s = 1.25 m, T_p = 5.5 s, γ = 1.0)

375x208mm (96 x 96 DPI)

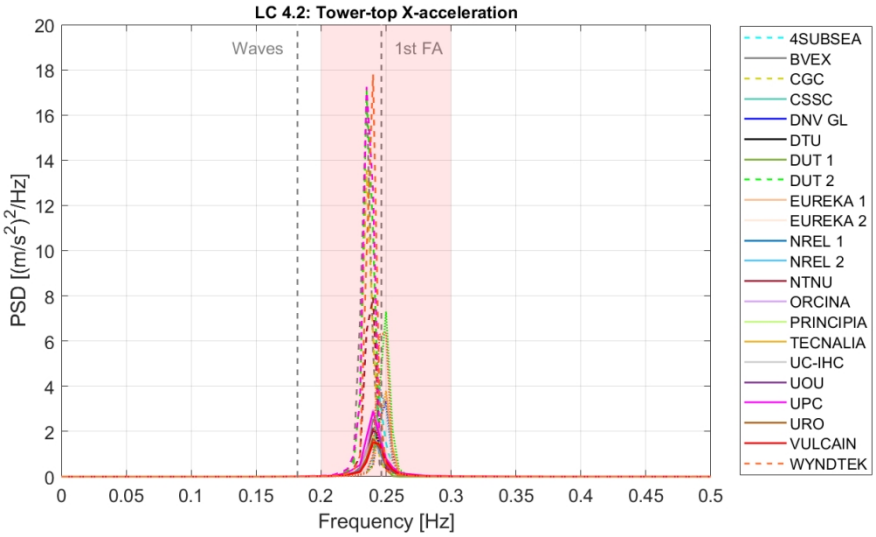

Figure 13. Power spectral density (PSD) of the tower-top X-acceleration in load case (LC) 4.2

375x208mm (96 x 96 DPI)

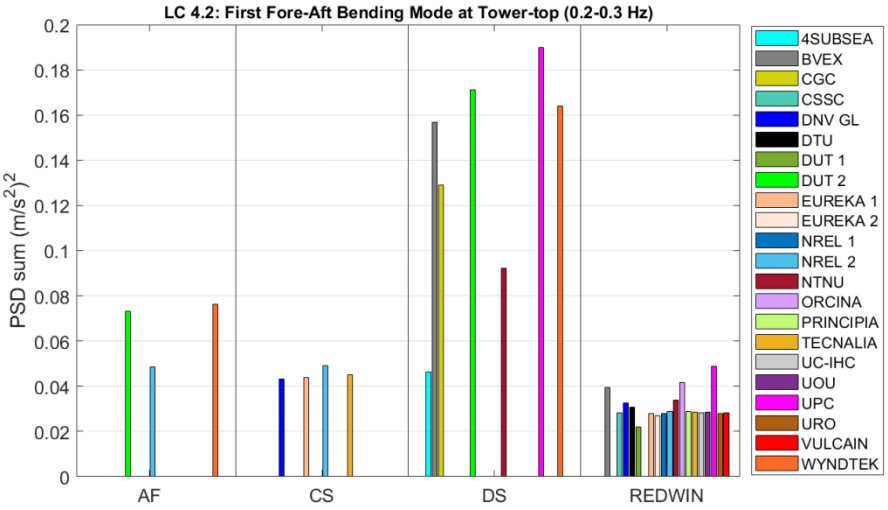

Figure 14. Power spectral density (PSD) sum of the tower-top X-acceleration in load case (LC) 4.2

375x208mm (96 x 96 DPI)

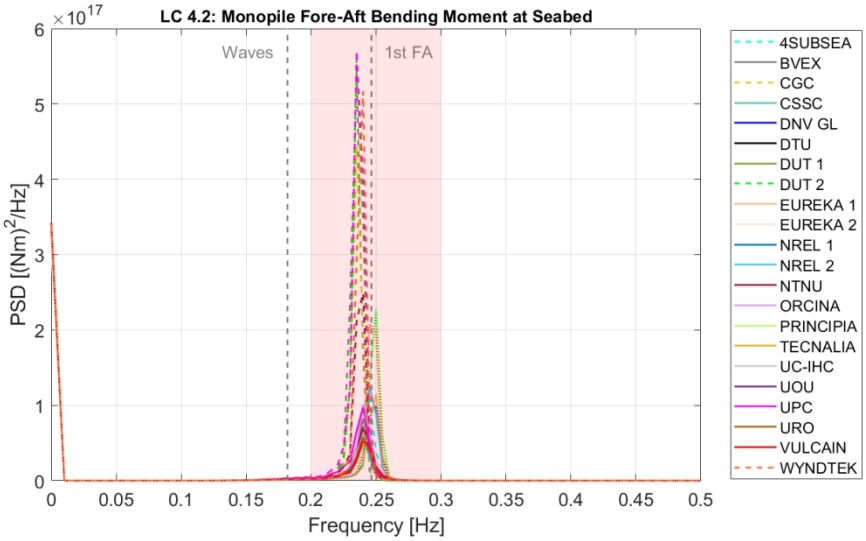

Figure 15. Power spectral density (PSD) of the monopile fore-aft bending moment at the seabed in load case (LC) 4.2

375x208mm (96 x 96 DPI)

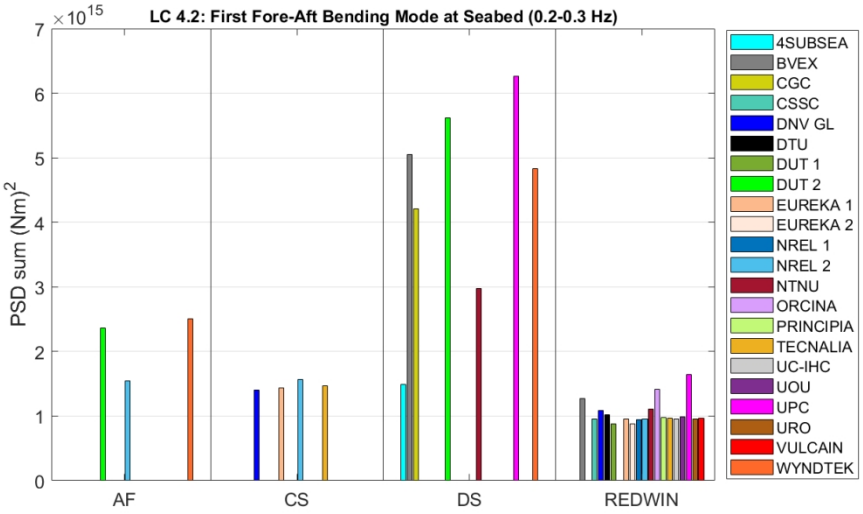

Figure 16. Power spectral density (PSD) sums of the fore-aft bending moment at the seabed in load case (LC) 4.2

375x208mm (96 x 96 DPI)

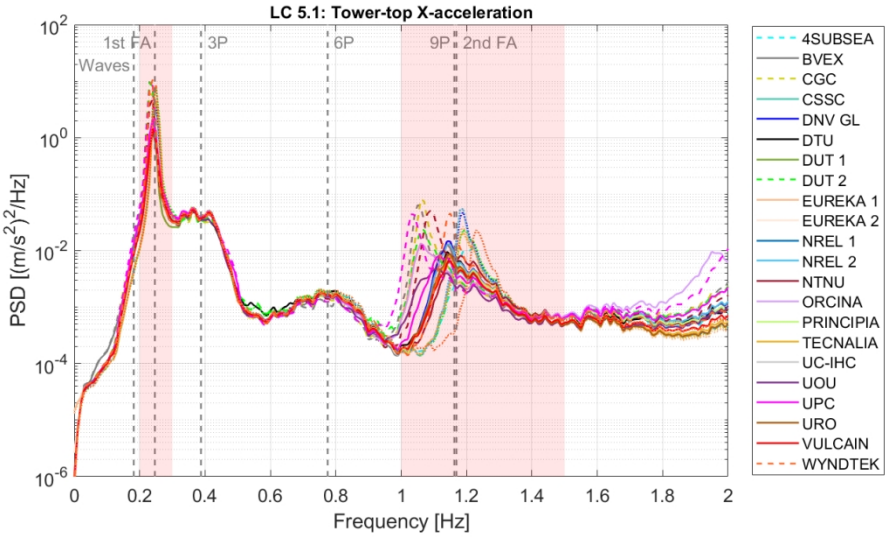

Figure 17. Power spectral density (PSD) of the tower-top X-acceleration in load case (LC) 5.1

375x208mm (96 x 96 DPI)

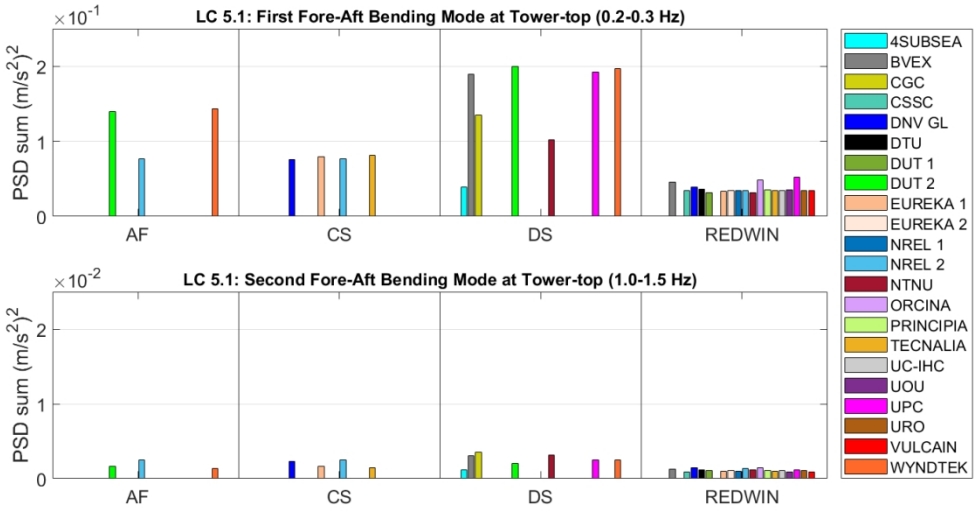

Figure 18. Power spectral density (PSD) sums of the tower-top X-acceleration in load case (LC) 5.1

375x208mm (96 x 96 DPI)

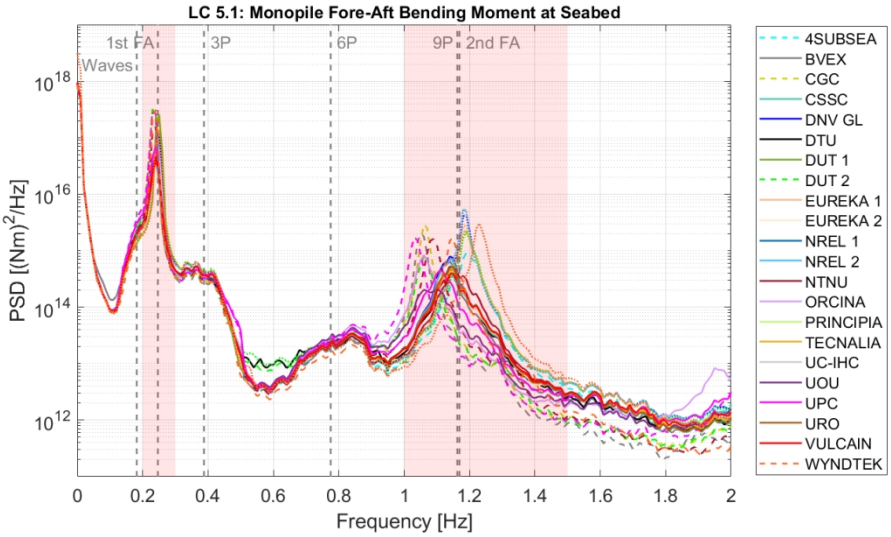

Figure 19. Power spectral density (PSD) of the monopile fore-aft bending moment at the seabed in load case (LC) 5.1

375x208mm (96 x 96 DPI)

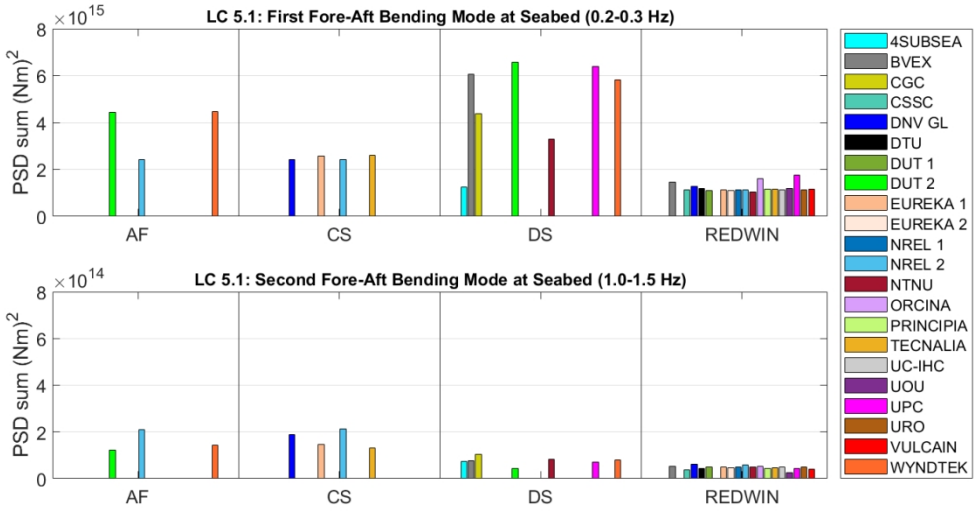

Figure 20. Power spectral density (PSD) sums of the fore-aft bending moment at the seabed in load case (LC) 5.1

375x208mm (96 x 96 DPI)